01 Aug 1983

Design of automotive structural components using high strength sheet steels - mechanical properties of materials

Wei-Wen Yu
Missouri University of Science and Technology, wwy4@mst.edu

M. Brad Parks

Civil Engineering Study 83-3
Structural Series

Second Progress Report

DESIGN OF AUTOMOTIVE STRUCTURAL COMPONENTS USING HIGH STRENGTH SHEET STEELS

MECHANICAL PROPERTIES OF MATERIALS

by

M.B. Parks
Research Assistant

Wei-Wen Yu
Project Director

A Research Project Sponsored by American Iron and Steel Institute

August 1983

Department of Civil Engineering
University of Missouri-Rolla
Rolla, Missouri

PREFACE

This report is based on a thesis presented to the Faculty of the Graduate School of the University of Missouri-Rolla (UMR) in partial fulfillment of the requirements for the degree of Master of Science in Civil Engineering.

The financial assistance granted by the American Iron and Steel Institute and the technical guidance provided by members of the AISI Task Force on Structural Research of the Transportation Department and the AISI staff are gratefully acknowledged. These members are: Messrs. S. J. Errera, D. M. Bench, A. E. Cornford, Jim Davidson, Emil Hanburg, B. S. Levy, D. J. Meuleman, W. J. Riffe, M. S. Rashid, M. T. Vecchio, Hickmat Mahmood, Charles Haddad, T. L. Treece, Don Malen, Joe Rice, R. J. Traficanti, David Whitaker, Kuanh-Heui Lin, Brian Taylor, Al Houchens, L. J. Howell, R. G. Lang, and A. L. Johnson.

All materials used for the experimental study were donated by Bethlehem Steel Corporation, DOFASCO Inc., Inland Steel Company, and National Steel Corporation.

Thanks are extended to Messrs. K. Haas, J. A. Tucker, and R. Haselhorst of the Department of Civil Engineering for developing the testing equipment. Appreciation is expressed to C. Hagan, Supervisor of the UMR Machine Shop, for preparing the test specimens. Thanks are due to Mr. Chiravut Santuputra for his valuable assistance in conducting the tests and evaluating the test data. Mr. Terry Leads also helped in some of the experimental work.

Special thanks are extended to Mrs. DeAnne Larson for the typing that she did in this publication.

ABSTRACT

In recent years fuel economy has become one of the major criteria for the the design of automobiles. In order to improve the efficiency of their vehicles many automotive designers are substituting high strength sheet steels for traditional materials of lower strength. This thesis discusses experimental work which was done to determine the representative mechanical properties and stress-strain relationships of a select group of high strength sheet steels with nominal yield strengths ranging from 80 to 140 ksi. The results show that high strength sheet steels are quite anisotropic with the variation in measured properties depending on the type of sheet steel, the direction of testing and the type of testing.

The literature was reviewed in depth to determine the effects of strain rate and fatigue on the design of automotive components using high strength sheet steels. It was found that increasing strain rates generally increased the strength of these steels while decreasing their ductility. The literature review of fatigue analysis revealed that even the most accurate fatigue analysis methods currently available to the automotive engineer predict fatigue lives that differ substantially from the actual lives obtained from tests.

TABLE OF CONTENTS

TABLE OF CONTENTS (Cont.)

TABLE OF CONTENTS (Cont.)

TABLE OF CONTENTS (Cont.)

LIST OF ILLUSTRATIONS

LIST OF ILLUSTRATIONS (Cont.)

LIST OF ILLUSTRATIONS (Cont.)

LIST OF ILLUSTRATIONS (Cont.)

LIST OF ILLUSTRATIONS (Cont.)

LIST OF TABLES

LIST OF TABLES (Cont.)

LIST OF TABLES (Cont.)

I. INTRODUCTION

A. GENERAL

During the past decade the automobile industry has been required to completely reverse their design philosophy from a fairly conservative design approach to one of ultra efficiency in order to increase the fuel economy of their vehicles and thus compete more favorably with foreign markets. The trend toward lighter, more efficient automobiles shows no sign of diminishing in the near future since the CAFE (corporate average fuel economy) requirement of 27.5 mpg becomes effective in 1985[1]. In order to meet the required gas mileage standards without sacrificing the safety of their vehicles many automotive designers are choosing high strength sheet steels to replace traditional materials of low to moderate strength. Other than being stronger than other materials, high strength sheet steels are also desirable because: (1) they offer favorable strength-to-cost ratios, (2) they are available in a wide range of strengths, and (3) they may be formed and assembled using existing production techniques and equipment[1,2].

This study primarily involved the determination of the material properties of a selected group of high strength sheet steels with nominal yield strengths ranging from 80 to 140 ksi as outlined in Phase I of a three phase research project entitled "Structural Design of Automobile Structural Components Using High Strength Sheet Steels." This project began in early 1982 at the University of Missouri-Rolla (UMR) under the sponsorship of the American Iron and Steel Institute

(AISI). The eventual goals of this three phase project are to (1) determine characteristics of high strength automotive sheet steels which influence their performance in structural applications, (2) determine if existing design procedures[3] are appropriate, and (3) develop new techniques if necessary.

B. PURPOSE OF INVESTIGATION

The primary purpose of this investigation was to establish the following typical mechanical properties for six different high strength sheet steels: modulus of elasticity, proportional limit, yield point, ultimate tensile strength, and ductility. The tested sheet steels were chosen to represent the broad range of commercially available high strength sheet steels that could possibly be used by the automobile industry. The mechanical properties determined in this study will be utilized not only for the analysis of structural strength of various automotive components using these materials but also for the development of design criteria at a later date.

An additional reason for this investigation was to determine the background information necessary to estimate the effects of strain rate and fatigue on the design of sheet steels both for this study and also for possible future research in this area. These subjects, strain rate and fatigue, were chosen because of their obvious importance to the automotive industry.

C. SCOPE OF INVESTIGATION

This study began with a thorough review of the literature in the following areas: (1) a detailed investigation of the stress-strain curves of high strength sheet steels and the necessary procedures to manipulate the stress-strain data to obtain the desired mechanical properties, (2) a thorough review of the strain rate effects on the mechanical properties of high strength sheet steels, and (3) a study of the history of fatigue analysis as well as the latest methods for predicting fatigue behavior. The literature review is presented in Section II.

The six sheet steels examined in this study were axially tested parallel to the direction of rolling (longitudinal direction) and perpendicular to the rolling direction (transverse direction) both in compression and tension. Included in Section III is a detailed description of the tested materials and the procedures employed to determine the desired mechanical properties. This Section also presents a representative sample of the resulting stress-strain curves as well as the mechanical properties of each material.

Section IV presents an evaluation of the results along with a discussion of the cold work effect on high strength sheet steels. Also included in Section IV are examples of the application of the information gained in the literature review on strain rate and fatigue to the longitudinal tension test data of the 80XF sheet steel. Finally, the research findings are summarized in Section V.

II. REVIEW OF LITERATURE

A. MECHANICAL PROPERTIES OF SHEET STEELS

1. Engineering Stress-Strain Curves. The information obtained from any type of stress-strain curve is the relationship between the load (or stress) and elongation (or strain). For engineering stress-strain curves, the stress, f, is measured by the load, P, divided by the original, unreduced area, A_o, of the specimen, i.e.

$$f = \frac{P}{A_o} \tag{2.1}$$

The engineering strain, ε, is the difference between the original, unreduced gage length, ℓ_o, and the deformed length, ℓ, divided by the original length, i.e.

$$\varepsilon = \frac{\ell - \ell_o}{\ell_o} \tag{2.2}$$

Typically the two basic types of engineering stress-strain (f-ε) curves for high strength sheet steels are gradual and sharp yielding as shown in Figure 2.1[4]. The classification of the f-ε curves obviously comes from the yielding behavior of the steel. As a general rule, hot-rolled sheet steels tend to be sharp yielding (Figure 2.1(a)) while those sheet steels that are cold-rolled or cold reduced in thickness are gradual yielding (Figure 2.1(b)).

Sharp yielding steels typically exhibit an upper and lower yield point (points A and B respectively, Figure 2.1(a)). Since the upper yield point is much more sensitive to strain rate, specimen alignment, and shape of the tested cross-section than the lower yield point, the

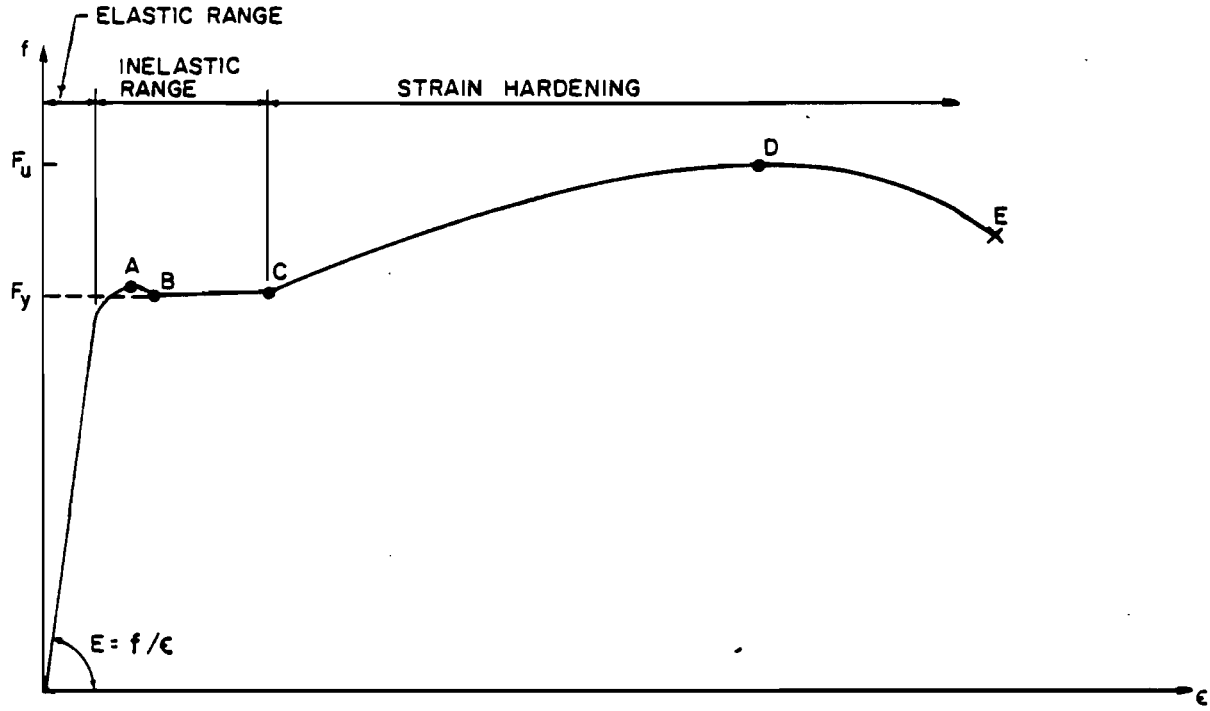

(a) SHARP-YIELDING STEEL

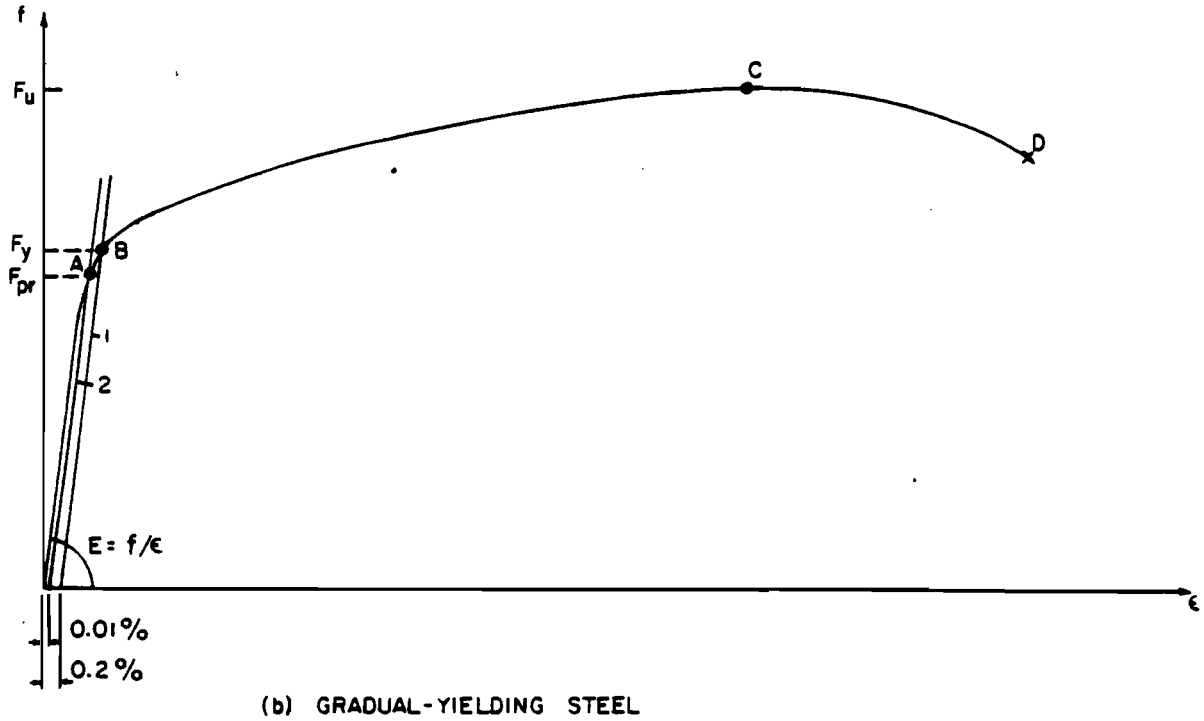

(b) GRADUAL-YIELDING STEEL

Fig. 2.1 Stress-Strain Curves of Carbon Steel Sheets[4]

lower yield point is customarily used to represent the yield stress of sharp yielding sheet steels subject to static loading.[5,6]

Since gradual yielding steels do not have such an obvious yield point, their yield strength is defined by either an offset method or the strain-under-load method. The offset method consists of drawing a straight line parallel to the initial linear portion of the f-ε curve at a given strain offset. For this study an offset of 0.2 percent strain was chosen. Using this method, the intersection of the straight line and the f-ε curve defines the yield strength as shown in Figure 2.2(a)[4]. The strain-under-load method defines the yield point as the stress corresponding to some fixed value of strain. The strain usually chosen is 0.5 percent as shown in Figure 2.2(b)[4].

The slope of the linear portion of the f-ε diagram is known as the modulus of elasticity, E. The point beyond which the f-ε curve becomes nonlinear is called the proportional limit (point A in Figure 2.1(b)). For sheet steels, whether they are gradual or sharp yielding, the proportional limit may be determined by the 0.01 percent offset method in exactly the same manner that the yield stress was defined for gradual yielding sheet steels except that the offset is now only 0.01 percent.

Once the specimen is strained beyond the yield point, the load carrying capacity of the steel continues to increase slightly in spite of the fact that the cross-sectional area of the specimen is continually decreasing. Since engineering stress is calculated based on the original area, there must be some other phenomenon occurring that causes the increase in load carrying capacity. This phenomenom is commomly referred to as work hardening or strain hardening and may be explained

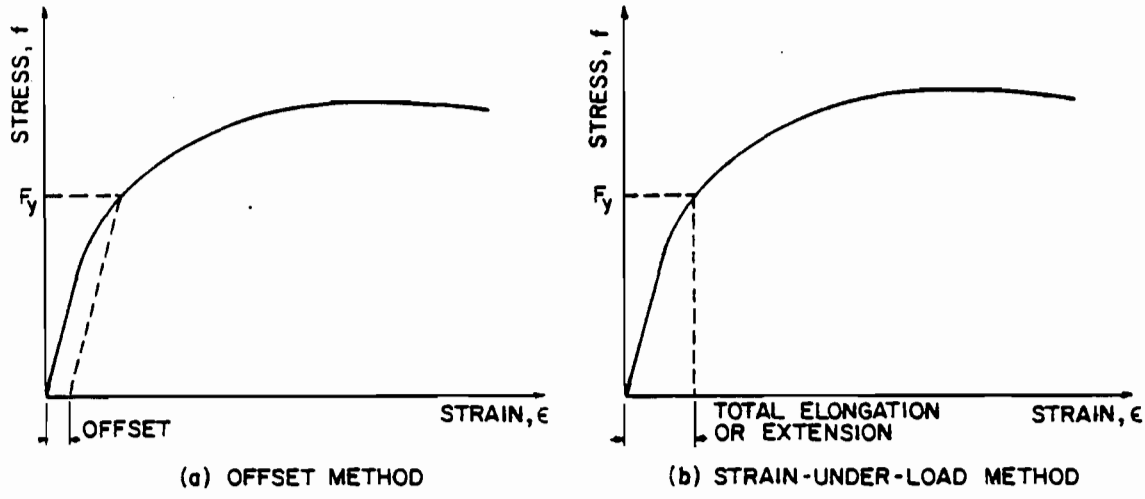

Fig. 2.2 Determination of Yield Point for Gradual-Yielding Steel[4]

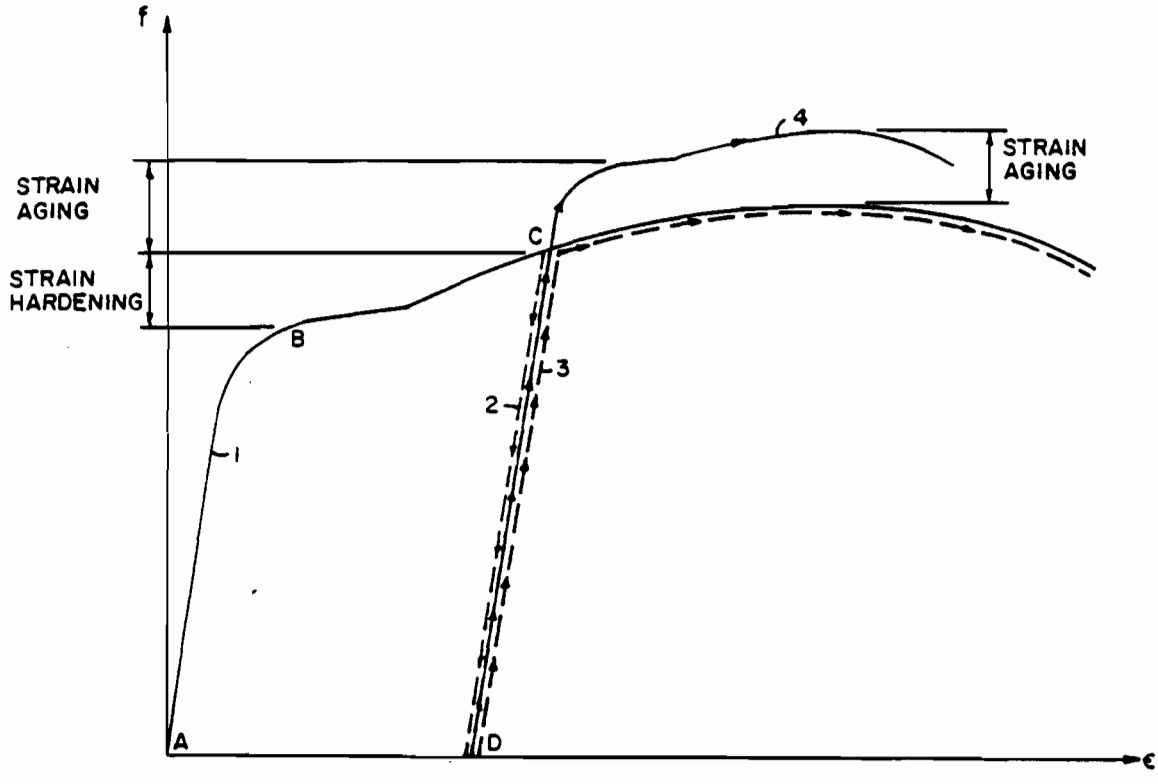

Fig. 2.3 Effects of Strain Hardening and Strain Aging on Stress-Strain Characteristics[4]

by dislocation theory[5]. The rate of strain hardening is high at the onset of yielding. However, as the strain is increased, the amount of strain hardening decreases to the point where it can no longer offset the continuous reduction of specimen area. At that point the maximum possible stress or ultimate strength, F_u, is reached in the steel. Further elongation of the tensile specimen results in localized straining of a small portion of the gage length known as necking[7]. The necked region continues to decrease in area at a faster pace than the strain hardening can keep up with which results in a decrease in the total load that the specimen can withstand. This unloading results in all areas of the specimen, other than the necked region, being unloaded back into the elastic range while the stress in the necked area continues to increase until fracture[5].

A material property that is dependent on the strain that a material can withstand up until fracture is ductility. Ductility is commonly defined by two methods. They are

$$\text{total elongation (percent)} = 100*(\ell_f-\ell_o)/\ell_o \qquad (2.3)$$

$$\text{and reduction in area (percent)} = 100*(A_o-A_f)/A_o \qquad (2.4)$$

In the above equations, the f subscripts denote the values at fracture. Although standard values are usually used for ℓ_o and A_o, it is important to realize that either method of measuring ductility will give varying results if non-standard values of ℓ_o and A_o are used[5].

Another important material property yet to be discussed is the capability of a material to absorb energy without fracture. Energy absorption is especially important in the design of structures such as automobile components, highway guard rails, and machinery guards[8]. For

a particular material the energy absorption is given by the area under the stress-strain curve from zero loading to fracture. Therefore the amount of absorption depends not only on the yield and ultimate strength but on the total elongation of the material as well.

Figure 2.3[4] illustrates the effect on the stress-strain curve of stressing a given sheet steel beyond the yield stress and then removing the load before failure. As shown by curve 2 of Figure 2.3, if the load is removed at point C along the stress-strain curve, then the unloading path follows a line very nearly the slope of the elastic portion of the stress-strain diagram. The elastic strain recovered upon unloading from point C, ε_e, is equal to the stress at C, f_c, divided by the modulus of elasticity , E, or $\varepsilon_e = f_c/E$. The permanent set or plastic strain, ε_p, is represented by the line AD[7]. Curve 3 represents the stress-strain curve if reloading occurs immediately and Curve 4 if reloading occurs after strain aging. It can be seen that, if the material is immediately reloaded (Curve 3), strain hardening produces an increase in apparent yield strength and a decrease in ductility as compared to the virgin material. If reloading occurs after a period of time a phenomenon known as strain aging occurs (Curve 4) which results in an even higher value of yield stress and tensile strength; however, the ductility decreases even more.

If the reloading from point D is opposite the original loading (e.g. compression instead of tension) as shown in Figure 2.4[8], the new value of the yield point G might be lower than the original yield point B. Also, if this load is reversed so that the load is now in the original direction, the yield point H may be lower than the original

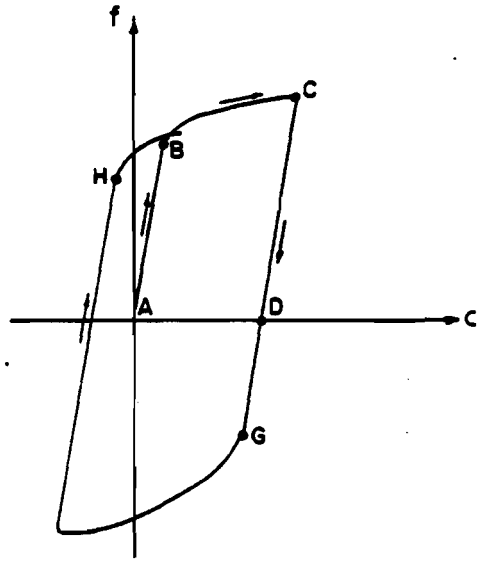

Fig. 2.4 Influence of Bauschinger Effect[8]

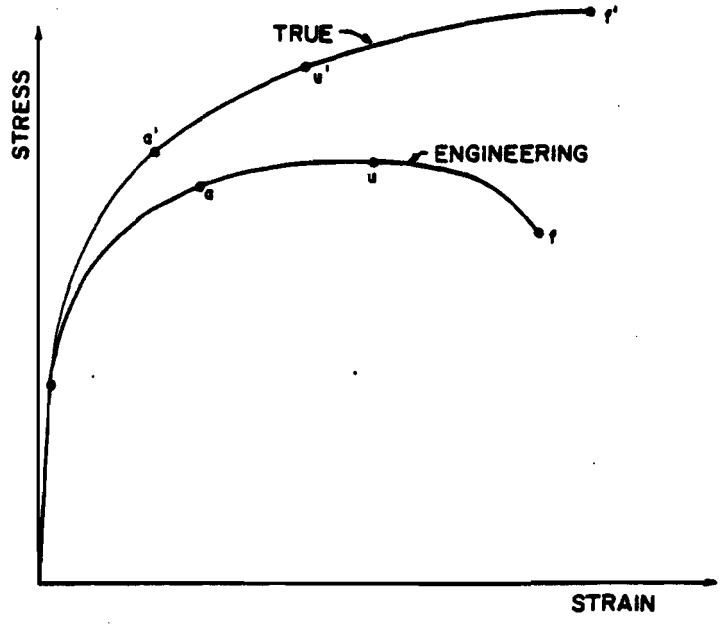

Fig. 2.5 Comparison of Engineering and True Stress-Strain Curves[5]

yield point B. This effect was first observed by Johann Bauschinger, of Germany, in 1886 and is commonly referred to as the Bauschinger Effect[8].

2. True Stress-Strain Curves. The exact or true stress, σ, in a tensile test is equal to the load, P, divided by the instantaneous area, A, or:

$$\sigma = \frac{P}{A} \quad (2.5)$$

As the load increases and thus the cross-sectional area decreases, the corresponding true stress will be greater than the engineering stress computed for the same loading. Since there is no appreciable change in area in the elastic range, the true and engineering stresses are practically identical. However, as the stress reaches the inelastic range, the strain increases and thus the area decreases much more for a given stress increase than in the elastic range. Therefore, the difference between true and engineering stresses become apparent in the inelastic range as can be seen in Figure 2.5[5]. Comparing the shape of the true and engineering stress-strain diagrams in the inelastic range, one can see that the difference between the two curves continually increases with increasing strain. It is also interesting to note that the true stress steadily increases up to fracture. This type of continuous increase of the f-ε curve seems much more logical than the engineering curve since it is difficult to imagine the stress actually decreasing in a material that is tested from zero load to fracture.

The true stress and strain may be related to the engineering stress and strain by assuming constancy of volume of the specimen. In other

words, the initial volume, $A_o \ell_o$, should equal the instantaneous volume, $A\ell$. Thus

$$A_o \ell_o = A\ell \tag{2.6}$$

$$A = A_o \ell_o / \ell = A_0 (\ell_o / (\ell_o (1 + \varepsilon))$$

$$A = A_o / (1 + \varepsilon) \tag{2.7}$$

Therefore the true stress, σ, may be given as

$$\sigma = P/A = P(1 + \varepsilon)/A_o = f(1 + \varepsilon) \tag{2.8}$$

The true or natural strain, ε', is derived from the differential increment of strain, $d\varepsilon'$, as

$$d\varepsilon' = d\ell/\ell, \tag{2.9}$$

where ℓ is the actual length to which $d\ell$ is added. The total unit elongation becomes

$$\varepsilon' = \int_{\ell_o}^{\ell} d\ell/\ell = \ln(\ell/\ell_o) = \ln(1 + \varepsilon) \tag{2.10}$$

Equations 2.8 and 2.10 obviously may be used in converting from engineering stress and strain to true stress and strain[6]. After necking, the above equations are not valid. Since the length changes within the gage length are now localized in the necked region, the engineering strain, which assumes a uniform strain over the gage length, cannot be used to calculate the true stress and natural strain. An alternate method for computing the true stress in the necked region is described by Hosford et al. on page 53 of Ref. 5.

From inspecting the above equations for stress and strain it can be seen that for very small strains, such as those occurring in the elastic

range, the engineering and true stresses and strains will be practically the same. Therefore, for properties such as yield stress and modulus of elasticity, the engineering values should be sufficiently accurate. However, for studies using stress-strain data in the plastic range, "the true stress and strain are more meaningful than engineering stress and strain[5]."

B. STRAIN RATE

With the new legislation requiring safer cars in the future, a good understanding of the effects of impact loading, controlled crush and energy absorption on automobile components is essential[9]. Since these design considerations involve dynamic loadings, a knowledge of the effects of changing strain rates on the mechanical properties of sheet steels must be known in order for the engineer to design a safe and efficient vehicle[9,10].

The fact that the strain rate influences metal properties has been known for some time. As early as the mid 1940's Manjoine[11] and Nadai[12] studied the relationship between strain rate, temperature and the material properties of mild steel. A summary of their findings is illustrated in Figure 2.6[11]. In 1959, Norris et al.[13] published Figure 2.7 which shows the effect of strain rate on the stress-strain curve of ordinary structural carbon steels. After analyzing these two figures, it seems that, based on a limited amount of data, the yield point of low to moderate strength steel is affected by changing strain rates much more than the ultimate strength or elongation. Since that time there have been several reports published on the influence of strain rate on

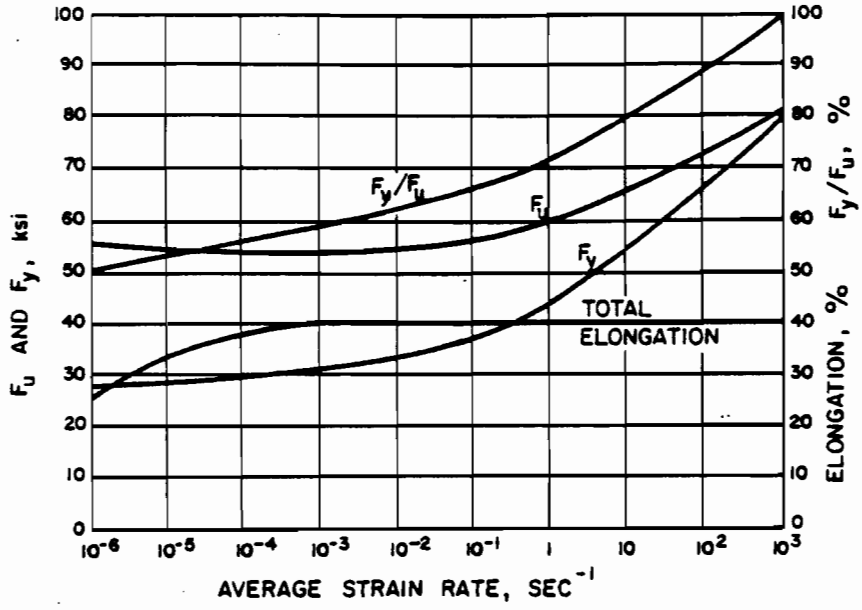

Fig. 2.6 Effect of Strain Rate on Tensile Properties of Mild Steel at Room Temperature[11]

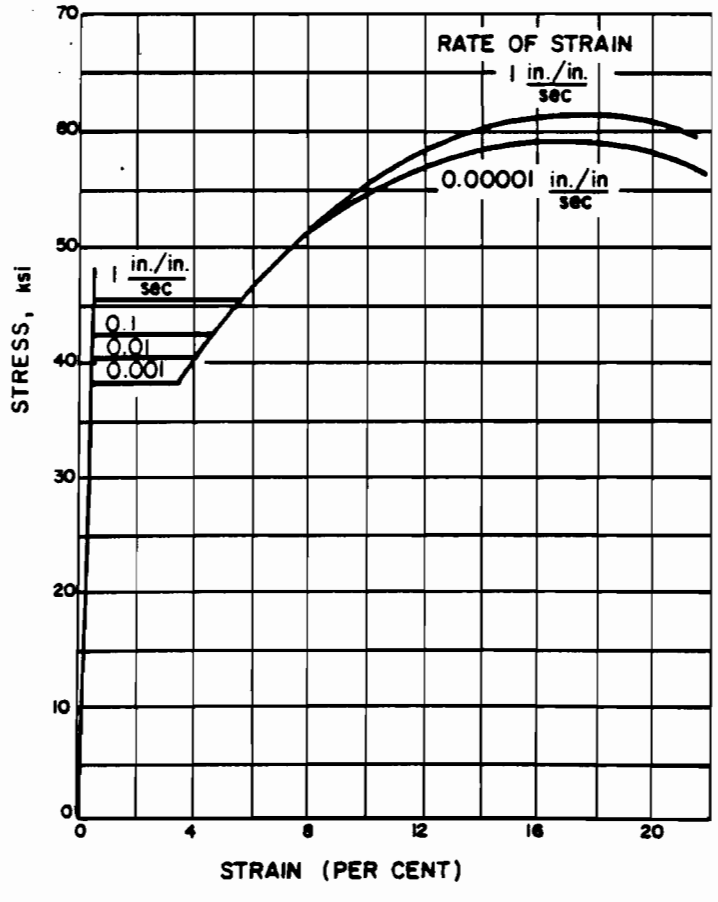

Fig. 2.7 Effect of Strain Rate on Stress-Strain Curve for Structural Steel[13]

the mechanical properties of different materials. Amoung the more noteworthy, Chatfield et al.[10] mentions a general review by Campbell[14] and the papers listed in References 15 through 18.

In 1974, Chatfield and Rote[10] completed a comprehensive report concerning the influence of strain rate on the mechanical properties of high strength, low alloy (HSLA) steels. In this report six different HSLA steels were tested with yield strengths ranging from 40 to 80 ksi. They also tested three different aluminun alloys for comparison to the HSLA steels. Approximate strain rates used were 0.008, 0.8, 8.0 and 80.0 in./in./sec. All tests were performed at room temperature and the temperature increase of the specimen during tensile tests was ignored. Figure 2.8[10] shows the relationship between yield and tensile strength, uniform elongation and strain rate for a typical HSLA steel.

As can be seen from this Figure, the yield and tensile strengths both increase substantially with increasing strain rate while the uniform elongation decreases. Total elongation, on the other hand, was relatively independent of strain rate which seems quite strange since the uniform elongation, which is the strain at the onset of necking, decreased. Since the yield and tensile strengths increased and the total elongation remained relatively stable as strain rate increased, then the absorbed energy of the HSLA steel must also increase with increasing strain rates. Such an increase in absorbed energy is obviously very desirable by the automobile industry.

The effect of strain rate on the true stress in metals may be expressed as:[5,10]

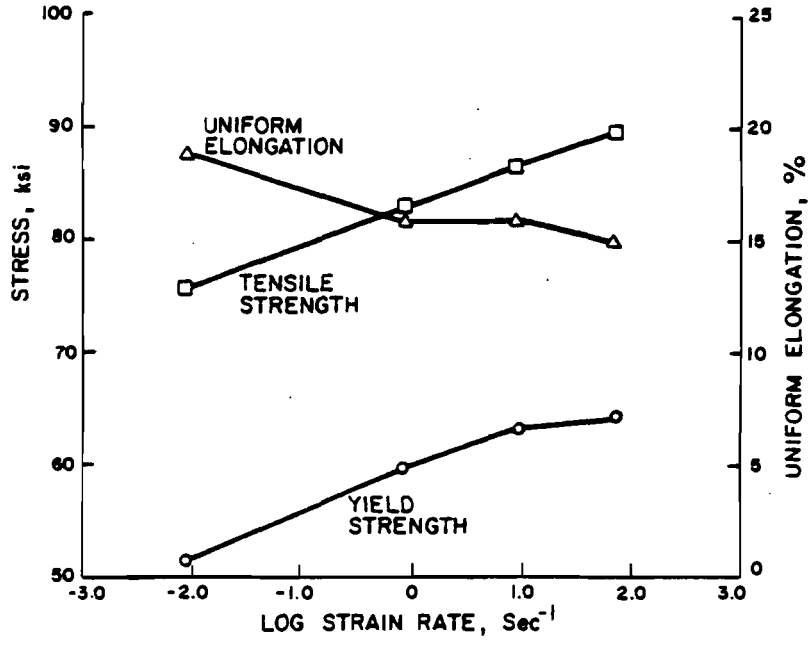

Fig. 2.8 Effect of Strain Rate on Mechanical Properties of a HSLA Steel[10]

$$\sigma = C\dot{\varepsilon}^{m} \tag{2.11}$$

where:

σ = true stress

$\dot{\varepsilon}$ = true strain rate

m = strain rate sensitivity exponent

C = constant

According to Hosford[5], the magnitude of m for most metals is usually between 0 and 0.03. However, the strain rate sensitivity increases with temperature and with strain for most metals[19]. The value of C depends on the strain, temperature and type of material[5]. For a given material, C and m are determined empirically. The resulting magnitudes of C and m for Chatfield and Rote's tests are listed in Table 2.1[10]. It

Table 2.1 Values of Strain Rate Sensitivity, m, and Equation Constant C of the Tested Materials[10]

Material	m	ln C
HRAK-AR	0.045	10.72223
HRAK-Ann+TR	0.056	10.58935
HSLA-40	0.045	10.74515
HSLA-45-1	0.035	10.94544
HSLA-45-2	0.024	10.83534
HSLA-50	0.026	10.98135
HSLA-80-1	0.020	11.36871
HSLA-80-2	0.018	11.40914

is interesting to note that their m values range from 0.018 to 0.056 which slightly exceeds the above range of m values given by Hosford. The values of ln C (and thus C) increase as the yield strength increases which is as expected. However, the m values show a steady decrease with increasing yield strength. After analyzing the results in Table 4 of

Chatfield and Rote's report[10], it seems that the increase in C is offset by the decrease in m values such that the total increase in yield strength, for a given strain rate increase, remains approximately the same regardless of the material strength.

Another useful relationship between true stress and strain rate is given by Hosford[5] as:

$$\sigma_2 = \sigma_1 * (\dot{\varepsilon}_2/\dot{\varepsilon}_1)^m \qquad (2.12)$$

where σ_1 and σ_2 are the true stresses corresponding to strain rates $\dot{\varepsilon}_1$ and $\dot{\varepsilon}_2$. Therefore, if σ_1, $\dot{\varepsilon}_1$ and m are known, then σ_2 may be found for any desired value of $\dot{\varepsilon}_2$.

If the strain rate sensitivity of a material is known as a design parameter, the engineer may use this property to his advantage and thus a more economical design may be obtained. For example, an automotive engineer that is concerned with designing a part to withstand impact loading without permanent deformation may take advantage of the increased yield point (if available) caused by the high strain rate associated with impact[10].

Another very important mechanical property that up until this time has not been mentioned is the modulus of elasticity, E. Although neither Hosford nor Chatfield mention the strain rate effects on the elastic modulus, Norris et al.[13] states that, based on a limited number of tests on ordinary structural carbon steel, the modulus of elasticity is unaffected by changing strain rates.

C. FATIGUE

1. Introduction. Since many of the applications of high strength sheet steels in automobiles involve loads that fluctuate throughout their life, it is essential that the automotive engineer have a good understanding of the effects of these loads on the performance of structural components if he is to design car bodies safely and efficiently. The study of failure under alternating or fluctuating loads is known as fatigue. The amplitude of these loads is such that any one load would not likely cause failure; however, after repeated application of this same load, failure would occur.

Fatigue failure typically consists of three stages[20]. The first stage of fatigue failure, known as crack initiation, is evidenced by the first sign of a surface crack in the material. The next stage is crack propagation which is the progressive worsening of the crack as it becomes wider and deeper. Finally, fracture of the material occurs when the cross-section is sufficiently reduced by the crack (or cracks) such that the remaining material fails under the application of one of the repeated loads. For most automotive design, fatigue failure is considered to occur at the onset of crack initiation[20].

If the amplitudes of these repeated loads (and thus the stresses) are below a certain limit, fatigue failure will not occur after an infinite number of cycles. This limit is commonly referred to as the endurance limit. For practical considerations, the endurance limit may be defined as the magnitude of stress such that failure does not occur after 10^7 cycles[8].

The following material presents a general review of the fatigue properties of steels as obtained through a relatively thorough study of

the available literature. When possible, specific mention is made of the applicability of any given information to high strength sheet steels (HSSS). However, because some of the HSSS are relatively new, it is impossible in some cases to locate specific information on all these steels. Hopefully, in those cases the material given may be used as a guide in order to establish general trends of the effects of various factors on the fatigue properties of HSSS.

For those interested in performing fatigue tests, the applicable ASTM Specifications are listed in Table 2.2.

2. Fatigue Factors. This section is dedicated to a discussion of some of the more important factors that influence the fatigue behavior of steels.

a. Load Type. Juvinall[8] uses the rotating bend test as performed using an R. R. Moore testing machine as a standard for fatigue testing. This machine subjects a round specimen to completely reversed bending stresses which are produced by uniform moment across the tested length. Therefore the maximum stresses are around the perimeter of the specimen and vary linearly to the center where the stress is always zero. If the fatigue properties of a material are obtained as described above, but the component to be designed is subjected to a different stress state (such as axial or torsion), then the correction factors, C_ℓ, given in Table 2.3[8] should be applied to the endurance limit of the metal.

Table 2.2 ASTM Requirements for Fatigue Testing

ASTM Spec. No.	Title
E466-82	Conducting Constant Amplitude Axial Fatigue Tests of Metallic Materials, Practice For
E467-76	Verification of Constant Amplitude Dynamic Loads in an Axial Load Fatigue Testing Machine, Practice For (R 1982)
E513-74	Constant Amplitude Low-Cycle Fatigue Testing, Definitions of Terms Relating to (R 1980)
E606-80	Constant-Amplitude, Low-Cycle Fatigue Testing, Recommended Practice For
E739-80	Statistical Analysis of Linear or Linearized Stress-Life (S-N) or Strain-Life (E-N) Fatigue Data, Practice For
E206-72	Fatigue Testing and the Statistical Analysis of Fatigue Data, Definition of Terms Relating to (R 1979)

Table 2.3. Endurance Limit Correction Factors for Various Loads[8]

Load Type	C_ℓ
Reversed or rotating bending	1.0
Reversed axial loading	0.9 no bending 0.6 to 0.85 with indeterminate bending
Reversed torsion	0.58 ductile metals (including all structural steels) 0.8 cast iron

b. Size. As a general rule, the endurance limit tends to decrease as the size of the specimen increases. Again a correction factor, C_D, is introduced by Juvinall[8] to modify the endurance limit determined for a standard 0.3 in. diameter specimen. For specimens smaller than 0.3 in. in diameter, C_D is conservatively taken as 1.0 whereas for larger diameters C_D may be taken as 0.9.

A similar type relationship is given in Reference 21 as

$$S_f = S_{fo}*(V/V_o)^{-0.034} \qquad (2.13)$$

where S_{fo} is a known endurance limit for a volume of specimen V_o. Therefore, the endurance limit, S_f, of a specimen with a volume, V, may be predicted using this relationship.

c. Surface Finish. The surface finish of a material may affect its fatigue life in three ways: (1) by considering the surface roughness which introduces small stress concentrations on the surface (discussed in detail in Section II.C.2.f), (2) by changing the surface properties of the material, and (3) by introducing residual stresses along the surface[19]. On page 234 of Reference 8, Juvinall presents Figure 12.6

which shows the reduction of endurance limit due to various surface finishes for steel parts. For hot-rolled steels with tensile strengths not greater than 140 ksi, the value of C_s varies from 0.45 to 0.73. The values of C_s decrease with increasing tensile strengths. It should be noted that in this case C_s is defined as the ratio of the endurance limit for a given surface condition to the endurance limit for a standard R. R. Moore mirror-polished finish[8].

d. Corrosion. Since many of the automobile components are subject to corrosive environments, the effect of corrosion on their fatigue life is an important consideration. According to Dieter[19], when corrosive attack is combined simultaneously with fatigue load there is a "pronounced" decrease in the fatigue life which is greater than that caused by previous corrosion of the surface. Also crack propogation advances at an accelerated pace when subjected to a corrosive atmosphere.

Speed of testing is not normally important for fatigue tests conducted in air over a range of from about 1,000 to 12,000 cycles/min; however, when tests are made in a corrosive environment, there is a definite dependence on the test speed. Since corrosion is a time dependent function, the faster the speed of testing, the less damage will be done by corrosion[19].

A state-of-the-art report on corrosion in the automobile has been prepared for AISI by R. J. Neville[22]. Other reports on the combined influence of fatigue and corrosion in automobiles are listed in References 23 and 24. These reports concluded that "pits formed from corrosive attack produce a 'minor' degradation of the fatigue properties"[25].

e. Cold Work Forming. Many of the automobile structural components are constructed of steels that have been subjected to cold working either by being cold reduced in thickness and/or by being cold-formed into the desired structural shape from a sheet of steel. Several recent investigations have been made to study the effects of cold working on the fatigue behavior of various types of steels. A few of these investigations are given in References 26 thru 31. For practically all the steels studied, the increase in monotonic stress-strain properties (properties obtained from engineering stress-strain curves for tensile tests) caused by cold working was largely lost in fatigue strength since these steels typically strain soften (discussed in Section II.C.2.h) upon cyclic loading. Libertini et al.[26] showed that cold working can improve the long-life fatigue properties since the corresponding stresses are relatively low. However, the short-life properties will almost certainly decrease because of the decrease in ductility caused by cold working[20].

f. Stress Concentration. Fatigue cracks almost always begin at locations of high stress concentration in a component. The stress concentration may be caused from notches or other "stress raisers" such as grooves, fillets, threads or keyways. Although it is usually impossible to completely avoid stress concentrations, it is important that the engineer understand their nature; thus, he can minimize the stress concentrations in his designs and also include their effect on the fatigue life of structures. An example of the basic principles of modifying a design such that the stress concentration is minimized is shown in Figure 2.9[8]. The notch shown in Fig. 2.9(a) represents a poor

design because the stress concentration is extremely high at the notch root. If for some reason the notch depth cannot be lessened, then removing the cross hatched material, as shown in Fig. 2.9(b), would reduce the stress concentration considerably. If the original width must stay virtually unchanged then the addition of smaller notches shown in Fig. 2.9(c) would help. If the original outer surface must remain unchanged, then small holes drilled as shown in Fig. 2.9(d) would reduce the stress concentration[8].

In order to estimate the magnitude of the local stress caused by stress raisers, a theoretical stress concentration factor, K_t, is defined. The factor, K_t, is equal to the local stress at the stress raiser divided by the nominal stress in the specimen. According to Neuber[32], the value of K_t may be determined analytically by the expression,

$$K_t = (K_\varepsilon K_\sigma)^{0.5}, \tag{2.14}$$

where:

K_ε = local elastic strain concentration factor
= local strain divided by the nominal strain

K_σ = local elastic stress concentration factor
= local stress divided by the nominal stress

In Reference 33, Peterson presents values of K_t for many different configurations which have been determined analytically or empirically.

In many cases the effect of stress raisers on fatigue life is less than would be predicted by using K_t. Therefore, a fatigue reduction factor, K_f, may be defined as the endurance limit of an unnotched material divided by the endurance limit of a notched material[8]. This is

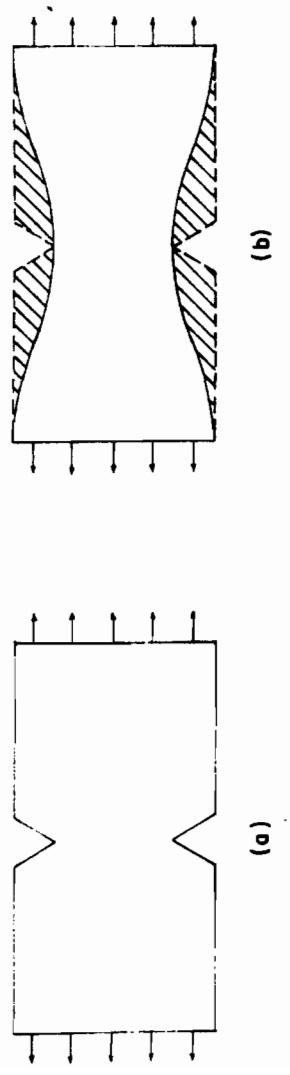

Fig. 2.9 Means of Reducing Stress Concentration[8]

by far the most accurate method of determining K_f. The range of K_f varies from 1.0 (no notch effect) to K_t. Thus it is impossible for K_f to exceed K_t. Several equations that relate K_f to K_t are given in the literature. One of the first such relations was given by Peterson[34] as

$$K_f = 1+(K_t-1)/(1+a/r), \tag{2.15}$$

where:

r = notch root radius

a = materials constant depending upon strength and ductility,

for heat treated steel a may be approximated as

$a = 10^{-3}*(300/F_u)^{1.8}$

F_u = ultimate tensile strength, ksi

In 1969, Topper et al.[35] published an alternate expression for K_f which relates the nominal or average stress (ΔS) and strain (Δe) in the specimen to the local stress and strain ($\Delta\sigma$ and $\Delta\varepsilon$) at the notch root. This equation is

$$K_f = ((\Delta\sigma\Delta\varepsilon)/(\Delta S\Delta e))^{0.5} \tag{2.16}$$

In 1983, Bhat[36] proposed still another method for estimating K_f which includes a dependence of K_f on the life level of a particular material. He found that K_f increases with increasing life up to about $5X10^6$ reversals beyond which K_f showed no additional increase.

The maximum stress used to determine the number of cycles to failure for notched specimens is the average stress multiplied by K_f, regardless of the method used to determine K_f[21].

In order to describe the susceptibility of a material to notches, a notch sensitivity factor, q, is defined as

$$q = \frac{K_f - 1}{K_t - 1} . \qquad (2.17)$$

Therefore, q = 1 indicates full notch sensitivity ($K_f = K_t$) while q = 0 ($K_f = 1$) indicates that the material is totally insensitive to notches.

g. Relationship Between Tensile Strength, Hardness and Endurance Limit. Several attempts have been made over the years to estimate the fatigue properties from the static material properties. The advantages of establishing such relationships are obvious since it is much cheaper and less time consuming to perform static tests than those tests necessary to establish fatigue properties. Hardness tests are even more desirable since they are usually non-destructive and may even be performed on actual parts[8]. According to Juvinall[8], the S-N curve (max. stress vs. no. of cycles to failure) for wrought steel may be approximated by a straight line from $S/F_u = 0.9$ at 10^3 cycles to $S/F_u = 0.5$ at 10^6 cycles. Also, for heat treated steels below about 350 Brinell hardness number (Bhn), the ultimate strength is approximately equal to 500 times the Bhn. It should be noted that these general rules are only good for low to medium strength steels and do not apply to the high strength steels[21].

h. Cyclic Stress-Strain Behavior. When steels are subjected to fully reversed stresses, they typically exhibit initial transient behavior varying from either higher or lower stress-strain curves than exist for the monotonic stress-strain curve. Usually within less than 50 percent of the fatigue life the steel will become cyclically stable (i.e. each cycle traces over the same stress-strain curve). The

stabilized stress-strain curve may be established by loading and unloading at various increments up until the maximum reversed stress as shown in Figure 2.10(a)[20]. Once the stabilized cyclic stress-strain curve has been determined it may be superimposed on the monotonic stress-strain curve for comparison. When the two types of curves are compared, the steel is said to exhibit one of the following types of cyclic behavior:

1. cyclically stable
2. cyclically harden
3. cyclically soften, or
4. complex cyclic behavior.

An example of each type of behavior is illustrated in Figure 2.10(b)[20]. If the stress required to apply the fully reversed loadings remains constant, (i.e. there is no change from the monotonic stress-strain curves), the material is said to be cyclically stable. If the stress required increases, the material cyclically hardens. If the stress required decreases, it cyclically softens. A metal exhibits complex cyclic behavior if it varies from cyclically harder or softer or remains stable for different stress ranges on the same cyclic stress-strain diagram.

It is obviously very important that a material is chosen that will either be stable or harden upon cyclic loading in order that it can adequately resist the design loads during its fatigue life.

i. Cummulative Damage-Miner's Rule. Since many loads normally applied to automobile components vary in their maximum value throughout their life, it is necessary to estimate the cummulative damage caused by each of the various stress levels. One method that is often used by the automobile industry is called Miner's Rule[39]. This rule assumes

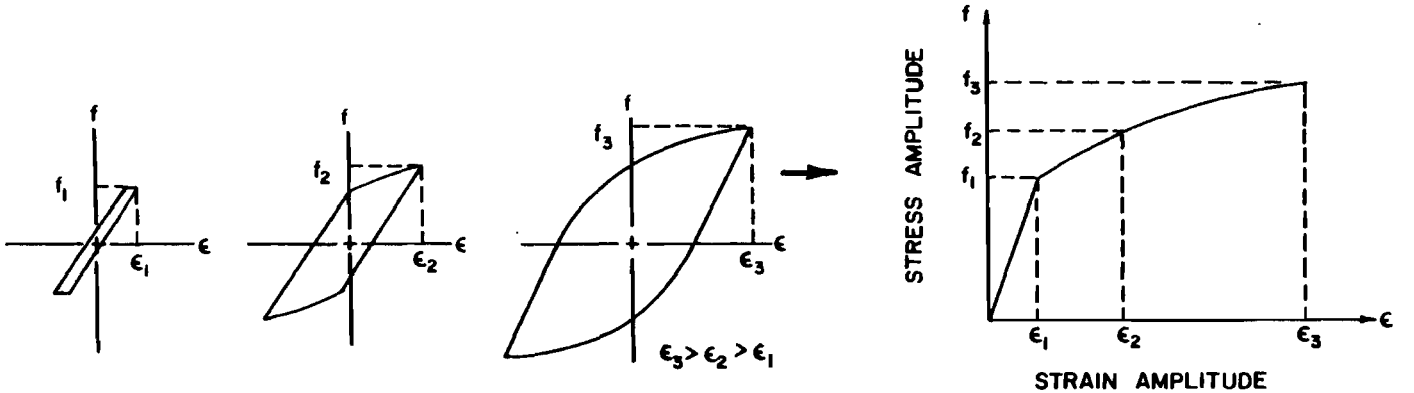

Fig. 2.10 Cyclic Stress-Strain Curves for Various Behaviors[20]

that each cycle causes a small amount of damage and that this damage may be expressed as a fraction of the fatigue life. When the sum of these fractions equals one then the structure is assumed to have failed in fatigue. Miner's Rule may be expressed in an equation form as

$$\frac{n_1}{N_1} + \frac{n_2}{N_2} + \ldots + \frac{n_k}{N_k} = 1 \qquad (2.18)$$

in which n_1, n_2, ... n_k represent the number of cycles of each respective stress cycle S_1, S_2 ... S_k and N_1, N_2, ... N_k represent the allowable number of cycles to failure for the corresponding stress cycles as determined by either the stress-life or strain-life methods. These methods will be discussed in detail in Section II.C.3.

j. Statistical Nature of Fatigue. The fatigue life of identical stress levels tend to vary much more than the strength properties obtained from static tests of the same materials. Therefore it is important to consider this variation when performing a fatigue analysis. Two outstanding studies of the relationship between the percentage of fatigue failures and the number of cycles to failure at a given stress level are given in References 40 and 41. A typical plot of this relationship is shown in Figure 2.11[21]. The objective of this plot is to determine the percentage increase of the expected component failures as the number of cycles is increased. The percentage of failures allowed by the designer obviously depends on the consequences of component failure.

Chapter 17 of Reference 8 offers an excellent description of statistics and their application to fatigue.

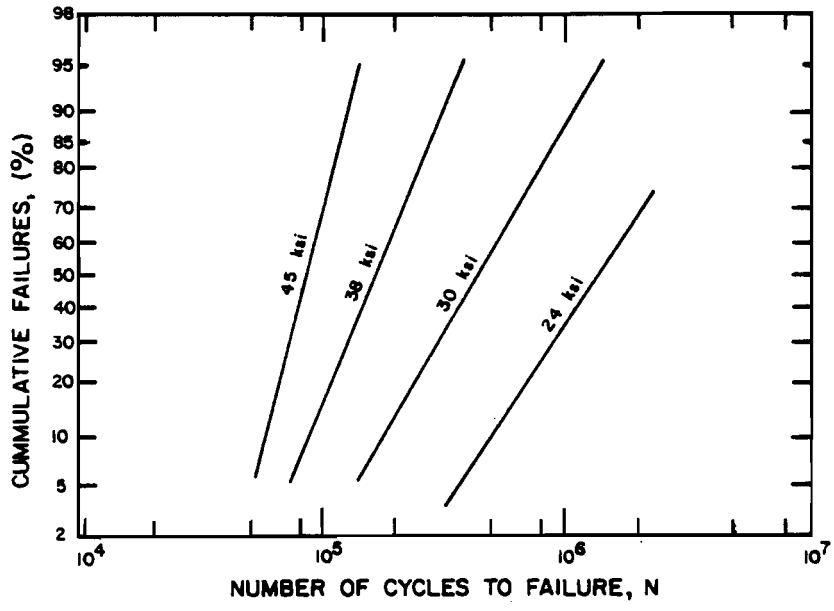

Fig. 2.11 Log-Normal Plot of Steel Plate[21]

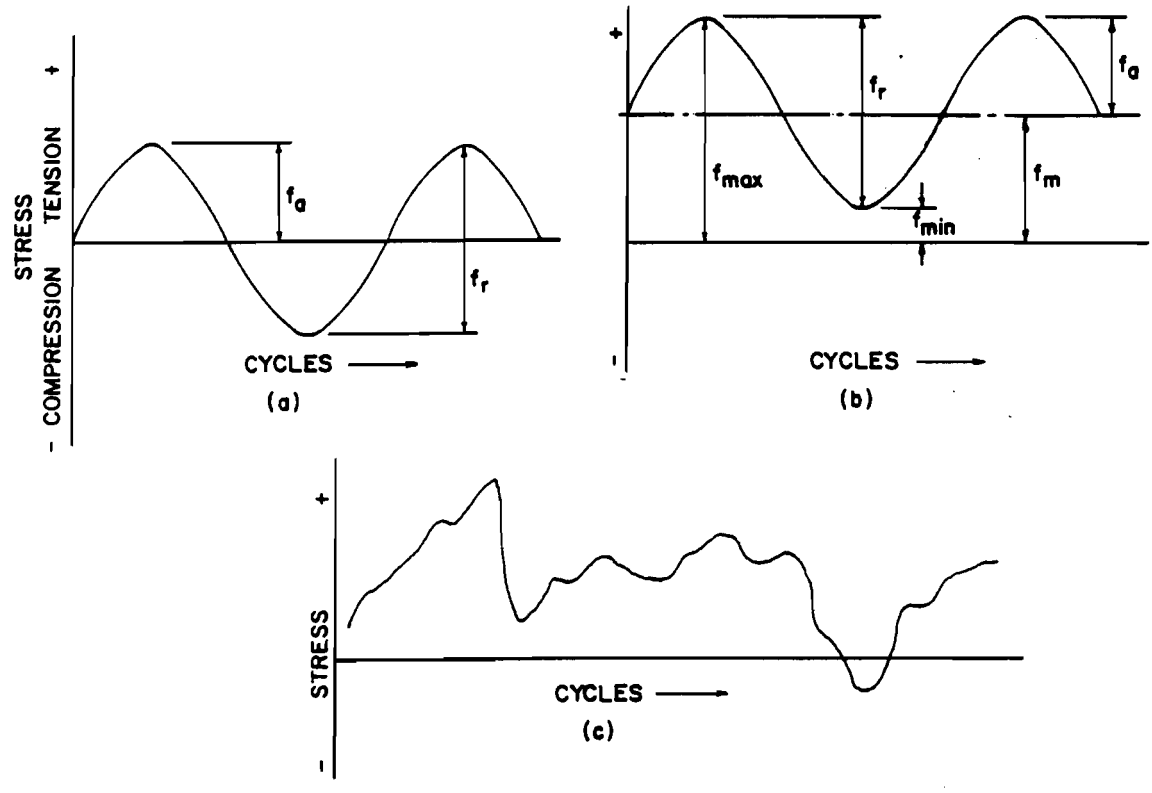

Fig. 2.12 Typical Fatigue Stress Cycles. (a) Reversed Stress; (b) Repeated Stress; (c) Irregular or Random Stress Cycle[19]

3. Fatigue Analysis Methods. According to Barsom et al.[25], the automobile industry currently uses two types of analysis procedures to predict the fatigue life of automotive structures. They are the stress-life approach and the strain-life approach. Each method has its own distinct advantages and disadvantages as will be pointed out in the following discussion.

a. Stress-Life Approach. The stress-life approach has been used to predict fatigue life in one form or another for over a hundred years. The first comprehensive study using this method was performed by Wohler in 1870[42]. Many of the original concepts proposed by Wohler are still in use today.

Some useful terms often used in the stress-life method are shown in Figure 2.12[19]. Fig. 2.12(a) shows the stress cycle for a completely reversed loading. In this type of loading the maximum stress, f_{max}, and minimum stress, f_{min}, are equal in absolute value. Fig. 2.12(b) shows a stress cycle where the maximum stress varies about some value of mean stress, f_m. For this type of loading the maximum stress is equal to the mean stress plus the alternating stress, f_a, or

$$f_{max} = f_m + f_a \tag{2.19}$$

and similarly the minimum stress may be expressed as

$$f_{min} = f_m - f_a \ . \tag{2.20}$$

The stress range, f_r, is defined as the algebraic difference between the maximum and minimum stresses, i.e.

$$f_r = f_{max} - f_{min} \ . \tag{2.21}$$

The alternating stress, f_a, then is half of the stress range or

$$f_a = f_r/2 \ . \qquad (2.22)$$

Another useful term is the stress ratio, R, which is equal to the minimum stress divided by the maximum stress or

$$R = f_{min}/f_{max} \ . \qquad (2.23)$$

Many automotive components are subjected to loads that vary irregularly in maximum amplitude as shown in Fig. 2.12(c). However, the fatigue life of such loadings may be predicted using the same basic procedures as used for the smooth loadings. The only difference being that the cummulative damage caused by each of the stress cycles must be summed using Miner's Rule as discussed in Section II.C.2.i.

The most common way of presenting stress-life fatigue data is by so-called S-N curves. In these curves the maximum stress amplitude, f_{max} or S, is plotted on the ordinate and the number of cycles to failure, N, is plotted on the abscissa. Usually semilog or log-log coordinates are chosen for S-N curves. Unless noted otherwise, S-N curves are applicable to fully reversed loadings only (i.e. $f_m = 0$). An example of a log-log S-N curve is shown in Figure 2.13[20]. As shown by Figure 2.13, for long lives the total fatigue life consists primarily of the crack initiation life, whereas for short lives the crack initiation life is negligible. However, a typical S-N curve for a particular material is usually determined as a composite of the points obtained by applying different stress fluctuations, S, and recording the number of cycles to failure, N, for each value of S. Therefore the resulting S-N curve corresponds with the total life curve shown in Figure 2.13 and thus the crack initiation data desired by the automotive engineer cannot be obtained from a typical S-N curve[20].

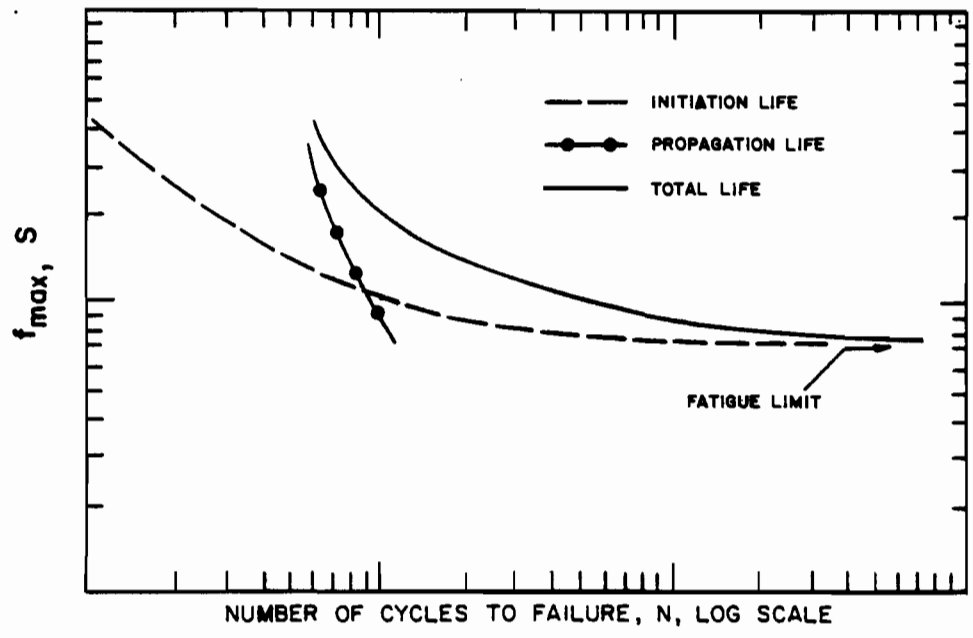

Fig. 2.13 Initiation and Propagation Life for a Schematic S-N Curve[20]

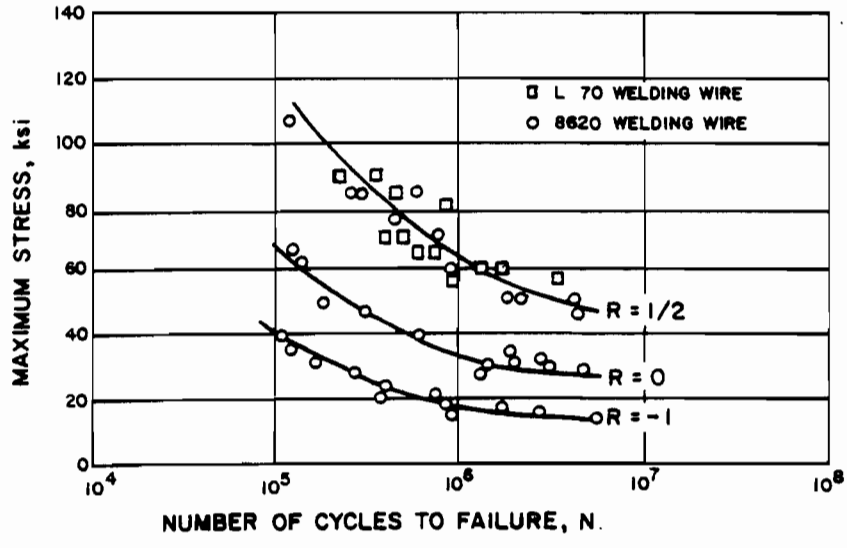

Fig. 2.14 Semi-Log S-N Curve[20]

For stress cycles that vary about some mean stress, f_m, there are several different methods of presenting the fatigue life data. One of the most straightforward methods is to use the traditional S-N diagram with the curves representing different values of mean stress being designated by their respective stress ratios, R. An example of this type of curve is shown in Figure 2.14[20], in which R = -1 represents fully reversed loadings.

An alternate method of presenting the same basic information that is often used by design engineers is the modified Goodman diagram as shown in Figure 2.15[20].

b. Strain-Life Approach. The strain-life approach for predicting fatigue life is a relatively new technique that is often used in the automobile industry[25]. This method is based on the assumption that the critical area, such as a notch, for fatigue of any structure is normally subjected to plastic stresses whereas the average stress in the structure remains in the elastic range. Therefore the plastic local stresses at points of stress concentration are surrounded by an elastic field such that even when the structure is stress-controlled, the localized plastic zones are approximately strain-controlled. In order to approximate the fatigue behavior of the localized plastic zones, smooth specimens with minimum cross-sections that makeup some fraction of the plastic zones, as shown in Figure 2.16[20], are tested under strain-controlled conditions[43]. "However, suitable correction factors must be used to account for differences in stress state, size and strain gradient between the smooth specimen and the plastic zone of the structural detail of interest"[25]. Reference 44 provides more information on these correction factors.

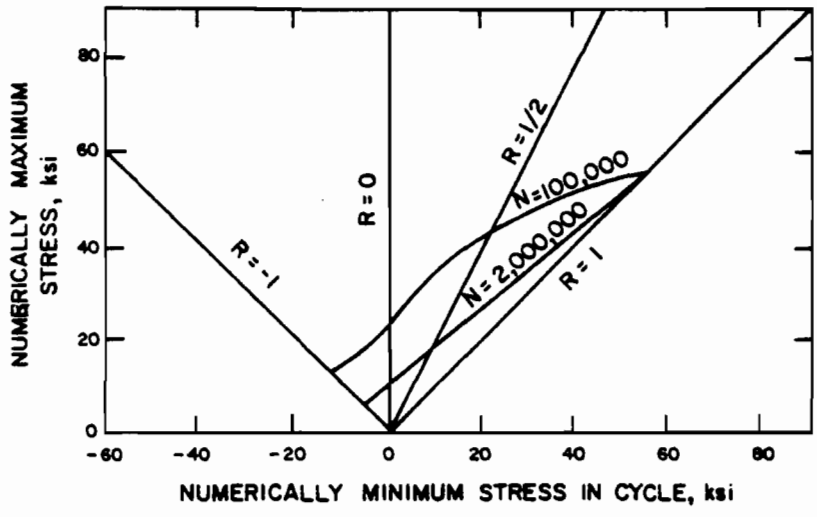

Fig. 2.15 Modified Goodman Diagram[20]

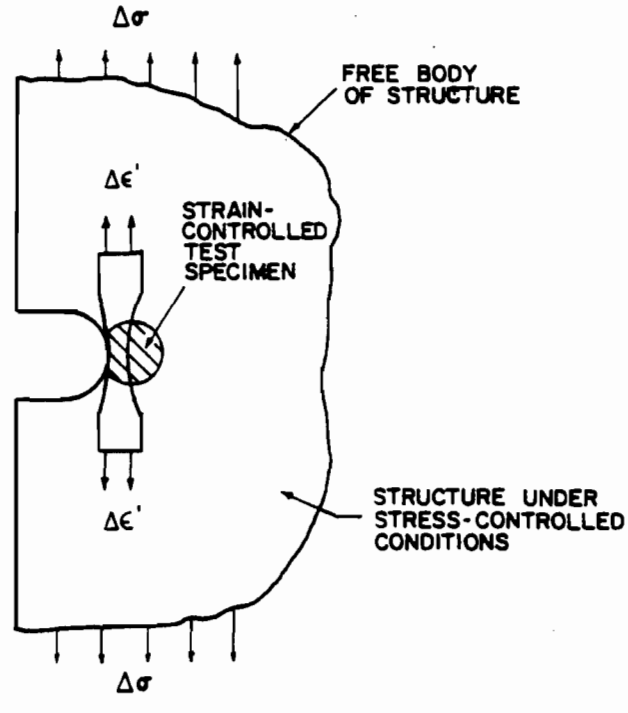

Fig. 2.16 Strain Controlled Test Specimen Simulation for Stress Concentrations in Structures[20]

The total true strain, $\Delta\varepsilon'$, used in the strain-life approach is shown for a stable stress-strain hysteresis loop in Figure 2.17[20] and may be expressed as

$$\Delta\varepsilon' = \Delta\varepsilon'_e + \Delta\varepsilon'_p, \tag{2.24}$$

where $\Delta\varepsilon'_e$ is the total elastic strain and $\Delta\varepsilon'_p$ is the total plastic strain. It is important to note that the stresses (σ) and strains (ε') used in the strain-life approach are true stresses and strains as opposed to engineering stresses and strains. Formulas are given in Section II.A.2 for converting from engineering to true stresses and strains.

A more convenient method of expressing the total strain is by the strain amplitude, ε'_a, where

$$\varepsilon'_a = \Delta\varepsilon'/2 = \Delta\varepsilon'_e/2 + \Delta\varepsilon'_p/2 \ . \tag{2.25}$$

Also, the elastic strain may be expressed as $\Delta\sigma/E$ where E is the modulus of elasticity such that

$$\varepsilon'_a = \Delta\sigma/2E + \Delta\varepsilon'_p/2 \ . \tag{2.26}$$

The relationship between the applied loads and the resulting stresses and strains may be obtained by either attaching a strain gage directly to the critical fatigue area (such as a notch) or by using finite element techniques as described on page 18 of Reference 25.

For short lives the strain amplitude primarily consists of plastic strains since the corresponding stresses are very high. If the plastic strain amplitude, $\Delta\varepsilon'_p/2$, is plotted against the number of reversals to failure, $2N_f$, on a log-log scale the data points will lie roughly along a straight line as shown on Figure 2.18[21]. It should be noted here that a stress or strain reversal is defined by any points along the stress-

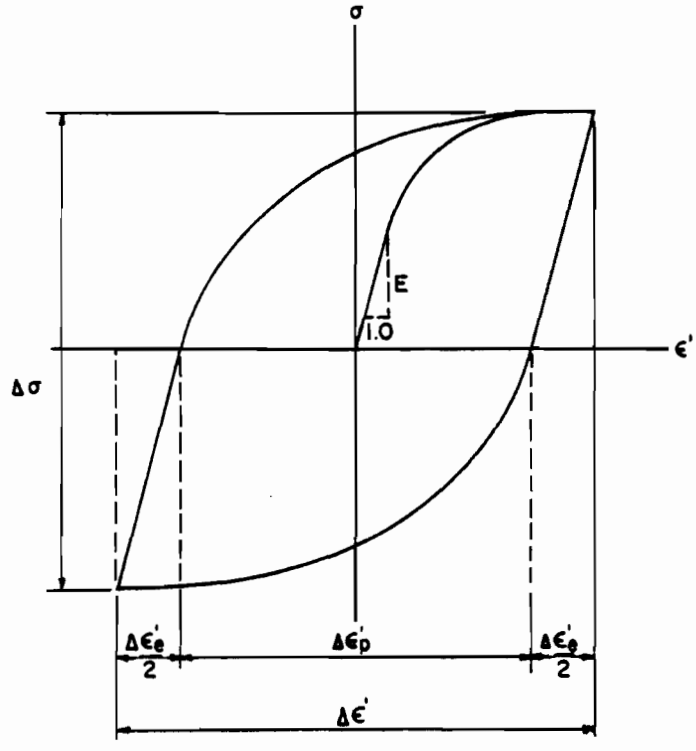

Fig. 2.17 Schematic of a Stress-Strain Hystersis Loop[20]

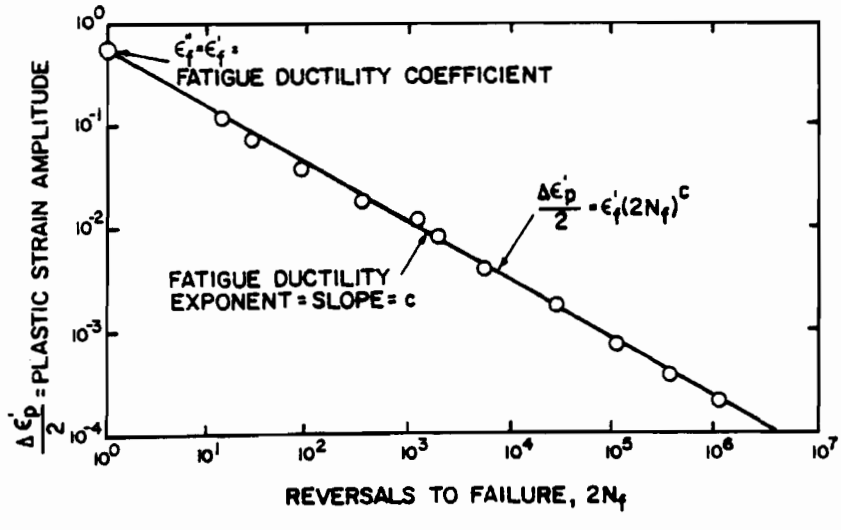

Fig. 2.18 Fatigue Ductility-Life Plot for Annealed SAE 4340 Steel[21]

strain curve where the first derivative changes sign (i.e. where the slope changes from positive to negative or vice-versa).

The equation of the line relating $\Delta\varepsilon'_p/2$ to $2N_f$ may be expressed as

$$\Delta\varepsilon'_p/2 = \varepsilon''_f*(2N_f)^c, \tag{2.27}$$

where c is the fatigue ductility exponent with a value of approximately -0.60 and ε''_f is the fatigue ductility coefficient. The value of ε''_f may be approximated by the true fracture ductility, ε'_f, obtained from a monotonic tension test, or

$$\varepsilon''_f \approx \varepsilon'_f = \ln(100/(100-\%RA)) \tag{2.28}$$

where %RA is the percentage reduction in area at fracture.

For long lives the strain amplitude consist primarily of elastic strain since the corresponding stresses are relatively small. If the stable elastic stress amplitude, $\Delta\sigma/2$, is plotted against $2N_f$ on a log-log scale the following relationship is obtained:

$$\Delta\sigma/2 = \sigma_a = \sigma'_f*(2N_f)^b \tag{2.29}$$

where:

σ_a = True fatigue strength

σ'_f = Fatigue strength coefficient

b = Fatigue strength exponent

As shown in Figure 2.19[21], σ'_f is defined as the allowable stress amplitude for one reversal. Therefore, σ'_f may be approximated by the true fracture strength, σ_f; however, σ_f must be corrected for necking[21]. For steels with a hardness of less than 500 Bhn, σ'_f may be estimated by

$$\sigma'_f \approx F_u + 50 \text{ ksi} \tag{2.30}$$

where F_u is the engineering ultimate strength in ksi.

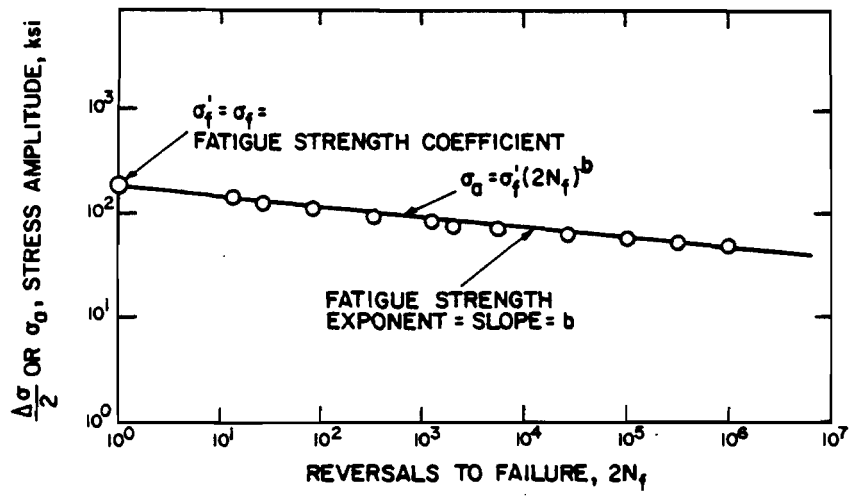

Fig. 2.19 Fatigue Strength-Life Plot for Annealed SAE 4340 Steel[21]

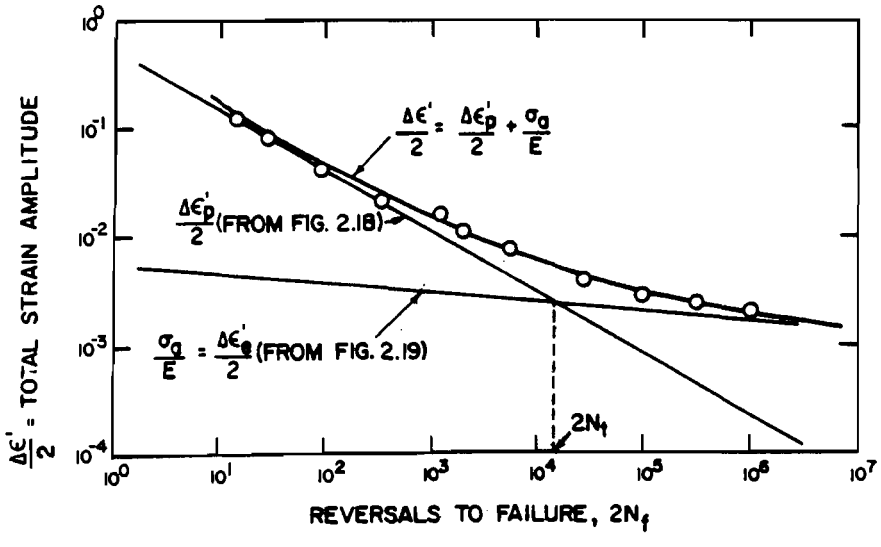

Fig. 2.20 Total Strain-Life Plot for Annealed SAE 4340 Steel[21]

The value of the fatigue strength exponent, b, may be approximated for most metals as

$$b \simeq -(1/6)\log(2\sigma_f'/F_u) \quad . \tag{2.31}$$

The elastic strain amplitude, $\Delta\varepsilon_e'/2$, may be expressed in terms of the fatigue strength coefficient and the fatigue strength exponent by dividing the stress amplitude, σ_a, by the modulus of elasticity, E, or

$$\Delta\varepsilon_e'/2 = \sigma_a/E = \sigma_f'(2N_f)^b/E \quad . \tag{2.32}$$

For intermediate fatigue lives, the total life is obviously dependent on both the elastic and plastic strains; therefore, the total strain amplitude, $\Delta\varepsilon'/2$, as a function of reversals to failure, $2N_f$, may be obtained by adding equations 2.27 and 2.32 or

$$\varepsilon_a' = \Delta\varepsilon'/2 = \sigma_f'(2N_f)^b/E + \varepsilon_f''(2N_f)^c \quad . \tag{2.33}$$

A graphical representation of equation 2.33 as well as 2.27 and 2.32 is shown in Figure 2.20[21].

Inspecting equation 2.33 it should be obvious that for long lives (where the strain is predominately elastic) the first term is all that is needed. For short lives the strain is mainly plastic and thus the second term is the most significant. It is often helpful to determine the transition fatigue life, $2N_t$, where the elastic and plastic strain amplitude contributions are identical. This is done by setting $\Delta\varepsilon_e'/2 = \Delta\varepsilon_p'/2$. The resulting fatigue life (shown in Figure 2.20 by the vertical dashed line) is

$$2N_t = (E\varepsilon_f''/\sigma_f')^{1/(b-c)} \quad . \tag{2.34}$$

Since Equation 2.33 was derived for the fully reversed cyclic loading as shown in Figure 2.17[20], special provisions must be made to account for any mean stress that might be present. One method of

predicting the effect of mean stress, σ_m, is given by[37]

$$\sigma_{cr} = \sigma_a/(1 - \sigma_m/\sigma'_f), \tag{2.35}$$

where σ_{cr} is an effective reversed stress amplitude which gives the same fatigue life as the combined effects of the mean stress and stress stress amplitude, σ_m and σ_a. For long lives, σ_a in Equation 2.29 may be replaced by σ_{cr} in order to predict the effect of mean stress on the fatigue life, or

$$2N_f = (\sigma_{cr}/\sigma'_f)^{1/b} = (\sigma_a/(\sigma'_f - \sigma_m))^{1/b}. \tag{2.36}$$

For short lives the relationship between plastic strain and $2N_f$ is[37]

$$2N_f = (\Delta\varepsilon'_p/2\varepsilon''_f)^{1/c}. \tag{2.37}$$

Looking at Equation 2.36 it can be seen that compressive mean stresses ($-\sigma_m$) increase fatigue life whereas tensile ($+\sigma_m$) mean stresses decrease fatigue life.

The effect of residual stresses on fatigue life is similar to that of mean stresses[21]. Reference 45 contains a summary of several programs conducted to study residual stress effects on fatigue life.

c. Comparison of Stress-Life and Strain-Life Methods. Although both the stress-life and strain-life fatigue analysis methods are commonly used in the automobile industry, it is generally accepted that the strain-life approach will be the preferred concept in the future for the following reason[25]. The strain-life approach "usually describes the basic-material (polished and or with as-rolled surfaces) fatigue behavior ... more broadly and accurately than that determined by the conventional stress-life approach"[25]. An important reason for this

increased accuracy is believed to be caused from the fact that the strain-life approach treats the plastic and elastic stress and strain states separately whereas the stress-life approach only considers the total stress on the structure.

Because of the complexity of the strain-life approach it is usually only applied to critical applications such as the analysis of new geometries or new grades of steel[25].

Regardless of the fatigue analysis procedure chosen there is a great variation between the predicted and actual fatigue lives. A recent study tested twelve different local strain and stress approaches. Their results were recorded as the predicted fatigue life divided by the actual fatigue life or vice-versa, depending of which one had a value greater than unity. The results varied from a ratio of 17 on the conservative side to 160 on the unconservative side[25]. Obviously much work remains to be done in this area before fatigue failure can ever be predicted precisely.

4. Fatigue Design of Sheet Steel Connections. Up until this point all the discussion has been of the fatigue analysis of monolithic structures with no specific mention being made of the fatigue design of connections. The following information is based on a research project conducted by Klippstein[46] involving the design of connections in sheet steels.

Since no uniform fatigue design provisions, such as codes or specifications, have been developed for fabricated sheet steel details, a research program to study the possibility of using the stress-range fatigue design concept for sheet steel details was sponsored by the

American Iron and Steel Institute at the U. S. Steel Research Laboratory. The stress-range concept has been successfully used for steel-plate fabrication details for some time; therefore, it seemed logical to explore the possibility of extending its use to sheet steel details.

The existing steel plate fatigue design provisions, which are based on the stress-range concept, classify different types of details in categories A through E depending on the level of notch severity and residual stress intensity with the severity increasing from A to E. Mean stress, stress ratio, and steel grades are not considered to have any effect on the total fatigue life. Any effects that stress concentrations or residual stresses might have on the fatigue life is taken care of in the categorization process.

The results of this research indicated that it may be possible to apply the stress-range concept to sheet steel connections. If so, this method "could be used as an effective and lower-cost alternative to the strain-life and bogey tests currently being used"[46] by the automobile industry. However, before the stress-range method can be adopted wholeheartedly, Klippstein states that additional tests must be performed.

5. Component Testing. Since there is such a great variation in the predicted and actual fatigue lives as discussed in Section II.C.3.c, it is necessary to verify the adequacy of a design by subjecting the component to fatigue tests that will simulate the actual service conditions of the component. Tests of this type are often referred to as "bogey" tests in the automobile industry.[25]. A bogey test subjects the

component to a set number of cycles of constant or varying stress, strain or load amplitudes. The number of cycles of a given loading that the part must endure is calculated either by Miner's Rule or is known from experience[25].

Another type of testing that is very useful to the automotive engineer is service testing. As the name implies, for this type of testing the component is subjected to actual service conditions. The actual loadings and number of cycles to failures are recorded by mobile computers; thus giving the engineer an excellent description of the fatigue behavior of the component in question.

6. Conclusions and Future Research Needs. From the wide spread between actual and predicted fatigue lives it is obvious that much research needs to be done in the fatigue analysis area. Also, since the strain-life concept is based on the stress-strain behavior of virgin materials it is difficult to use this information to predict the fatigue life of formed or fabricated sections and especially welded sections. Therefore, more research should be performed in this area to come up with modifications of the strain-life approach to account for cold-forming[25]. Also, further research needs to be done to continue the work begun by Klippstein[46] to study the applicability of the stress-range design method for steel plate connections to the design of sheet steel connections.

III. EXPERIMENTAL PROGRAM

A. MATERIALS

1. Description of the Sheet Steels Selected for Testing. An AISI publication entitled "High Strength Sheet Steel Source Guide"[47] lists 61 different high strength sheet steels that are commercially available from North American producers. Of these sheet steels, six different types were selected by members of the AISI Task Force on Structural Research of the Transportation Department[48] for determination of their representative mechanical properties and stress-strain curves. These materials are listed in Table 3.1a along with their trade designations and nominal sheet size. From this table it can be seen that these materials include both hot-rolled and cold-rolled steels with yield points ranging from 80 to 140 ksi. Table 3.1b lists the chemical composition of each steel[48].

The AISI material designation for high strength sheet steels consists of three parts: (1) the minimum specified yield point, (2) the chemical composition, and (3) the classification of the deoxidation practices.

The chemical composition is designated by S, X, W, or D where:

S = structural quality

X = low alloy

W = weathering

D = dual phase

Table 3.1a
Sheet Steels Used in Phase I of the Study[48]

AISI Designation*	Trade Designation	Nominal Sheet Size
80SK	Cold-Rolled, stress relieved, annealed, killed sheet steel	0.061" x 45" x 96"
80DF	Hot-rolled dual phase sheet steel	0.114" x 33" x 83"
80DK	Cold-rolled sheet steel	0.048" x 48" x 120"
80XF	Hot-rolled sheet steel	0.082" x 48" x 120"
100XF	Cold-rolled sheet steel	0.062" x 52" x 120"
140XF	Cold-rolled sheet steel	0.043" x 45" x 25"

* The AISI designation is illustrated as follows:

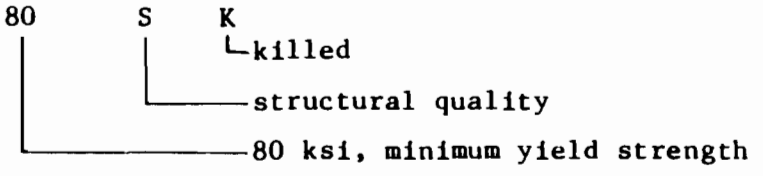

Table 3.1b

Chemical Composition of the Sheet Steels Used in Phase I of the Study (Percent)[48]

AISI Designation	C	Mn	P	S	Si	Cu	Ni	Cr	Mo	Al	N	Ce	Cb	Zr
80SK	0.073	0.30	0.003	0.022	---	---	---	---	---	0.065	--	---	---	---
80DF	0.06	0.94	0.009	0.011	1.61	0.02	0.02	0.50	0.39	0.01	--	0.02	---	---
80DK	0.09	0.52	0.06	0.003	---	---	---	---	---	---	--	---	---	---
80XF	0.08	0.33	0.009	0.021	---	---	---	---	---	---	--	---	---	---
100XF	0.07	0.43	0.006	0.023	---	0.11	---	---	---	0.056	--	---	0.064	0.08
140XF	0.08	0.92	0.006	0.014	0.04	---	---	---	---	0.069	--	---	0.110	0.08

The deoxidaton practice is designated by F, K, or O where:

F = killed plus sulfide control

K = killed

O = non-killed

An example of a typical AISI material designation is given at the bottom of Table 3.1a.

The combinations of chemical composition and deoxidation practice represented by the six sheet steels chosen for testing are: SK, DF, and XF. The following description of each combination is taken directly from Reference 47.

> "Structural Quality (SK)
> Typically, this family of high strength steels is produced with higher carbon and manganese levels than are present in low carbon steel. Strengthening elements, such as nitrogen or phosphorus, can be added at the producer's discretion. Not generally considered to be microalloying elements, these can be specifically prohibited by the user. Strengthening can also be achieved in cold rolled structural quality steels by special cooling and annealing practices, i.e., stress relief annealing.
>
> One major advantage of structural quality sheet steels is their generally lower cost compared to other high strength grades. Although the formability of structural quality high strength grades is reasonably good, they generally do not form as easily as most low carbon steels. Similarly, these high strength grades usually do not form as easily as most microalloyed sheet steels of the same strength level.
>
> When formed, all sheet steels increase in strength. Structural quality grades containing nitrogen additionally gave a particularly pronounced strain-aging effect and frequently are specified by users for this characteristic. For instance, steels containing this element typically gain about 15-20 ksi in yield strength after being strained 10 percent and aged at room temperature (20°C) for a week. Heat, as in a paint-bake cycle, accelerates this mechanism. It is important to note, however, that this hardening effect occurs only where sufficient strain is induced during the forming operation.
>
> Structural quality high strength sheet steel grades are readily weldable with conventional equipment used in joining low carbon sheet steel. Some welding practice modifications,

however, are required for certain grades and individual steel producers should be consulted regarding the need for such modifications.

Low Alloy (XF,XK)
Sheet steels in this category generally are more expensive and generally permit better formability than structural quality grades at comparable strength levels. Their strength is attained through the addition of small quantities of alloying elements and the steels usually provide higher production and service performance.

The inclusion control low alloy (XF) grades are frequently referred to as 'better forming' steels. This is because the sulfides present are reduced in volume or their shape is modified to allow more severe forming. The X grades exhibit good weldability using conventional equipment, but some welding practice adjustments may be required. Producers should be consulted for specific suggestions regarding these grades.

Dual Phase (DF,DK)
These steels predominately exhibit martensite in a ferrite matrix microstructure, although retained austenite and bainite may also be present.

In many applications, dual phase steels are more formable and provide greater work hardening characteristics than low alloy steels of comparable strength. In this respect, the 80DF grade may exhibit better formability than the 80XF grade. In certain applications, dual phase steels may permit production of more intricately shaped parts than can be made satisfactorily with other high strength grades. The work hardening effect in dual phase steels occurs only where sufficient strain is induced during manufacture of the part.

The weldability of these products is generally similar to low alloy grades".

2. Material Requirements of Existing AISI Specifications. There are three specifications currently published by the American Iron and Steel Institue (AISI) that could possibly provide background information for the needed material requirements of the automobile industry. A brief outline of the scope of each document along with a summary of the material requirements is presented for each Specification in one of the following sections.

a. Specification for the Design of Cold-Formed Steel Structural Members[49]. Research began on the study of cold-formed steels at Cornell University in 1939 under the sponsorship of AISI[50]. Based on this research, the first specification entitled, "Specification for the Design of Light Gage Steel Structural Members[51]," was published in 1946. Since that time several other Editions of the Specification have been published with the latest Edition being the "Specification for the Design of Cold-Formed Steel Structural Members[49]," which was published in 1980. Consequently, this Specification is the subject of this review.

The materials accepted by the 1980 AISI Specification include a variety of carbon and low-alloy steels in the form of steel sheets, strip, plate, or bar one inch or less in thickness. Table 3.2[48] lists these materials along with their mechanical properties. Of these steels the yield point ranges from 25 to 70 ksi while the tensile strength varies from 42 to 85 ksi. Ductility is important for these sheet steels in order to ensure that the structural shapes may be cold-formed without fracture. For the accepted steels described above the ultimate-to-yield strength ratios range from 1.17 to 2.22 and the elongation values vary from 12 to 27 percent for 2-in. gage lengths and from 15 to 20 percent for 8-in. gage lengths[48].

The Specification's provisions are intended only for materials with tensile-to-yield point ratios of 1.08 or greater and elongations of at least 10 percent in a 2-in. gage length or 7 percent in a 8-in. gage length. An exception to the ductility requirement is made for Grade E of the A446 and A611 steels. Since these steels have an F_u/F_y ratio of

Table 3.2

Mechanical Properties of Steels Referred to in Section 1.2.1 of the AISI Specification[48]

Trade designation	ASTM designation	Thickness, in.	Minimum yield point or yield strength, F_y ksi	Minimum ultimate strength, F_u ksi	F_u/F_y ratio	Minimum elongation, percent	
						in 2-in. gage length	in 8-in. gage length
Zinc-coated Steel Sheets of Structural Quality	A446 A		33	45	1.36	20	-
	B		37	52	1.41	18	-
	C		40	55	1.38	16	-
	D		50	65	1.30	12	-
	E		80	82	1.03	--	-
	F		50	70	1.40	12	-
Hot-Rolled Carbon Steel Sheets and Strip of Structural Quality	A570 A	0.0255 to 0.2299	25	45	1.80	23-27	-
	B		30	49	1.63	21-25	-
	C		33	52	1.58	18-23	-
	D		40	55	1.38	15-21	-
	E		42	58	1.38	13-19	-
Hot-Rolled and Cold-Rolled High-Strength, Low-Alloy Steel Sheet and Strip with Improved Corrosion Resistance	A606 Hot-Rolled as Rolled Coils		45	65	1.44	22	-
	Hot-Rolled as Rolled Cut Lengths		50	70	1.40	22	-

Table 3.2 (continued)

Mechanical Properties of Steels Referred to in Section 1.2.1 of the AISI Specification[48]

Trade designation	ASTM designation	Thickness, in.	Minimum yield point or yield strength, F_y ksi	Minimum ultimate strength, F_u ksi	F_u/F_y ratio	Minimum elongation, percent	
						in 2-in. gage length	in 8-in. gage length
Hot-Rolled and Cold-Rolled High-Strength, Low-Alloy Columbium and/or Vanadium Steel Sheet and Strip	A607Gr 45		45	60	1.33	Hot-Rolled 25	-
						Cold-Rolled 22	-
		50	50	65	1.30	Hot-Rolled 22	-
						Cold-Rolled 20	-
		55	55	70	1.27	Hot-Rolled 20	-
						Cold-Rolled 18	-
		60	60	75	1.25	Hot-Rolled 18	-
						Cold-Rolled 16	-
		65	65	80	1.23	Hot-Rolled 16	-
						Cold-Rolled 15	-
		70	70	85	1.21	14	-
Cold-Rolled Carbon Structural Steel Sheet	A611	A	25	42	1.68	26	-
		B	30	45	1.50	24	-
		C	33	48	1.45	22	-
		D	40	52	1.30	20	-
		E	80	82	1.03	--	-

Table 3.2 (continued)

Mechanical Properties of Steels Referred to in Section 1.2.1 of the AISI Specification[48]

Trade designation	ASTM designation	Thickness, in.	Minimum yield point or yield strength, F_y ksi	Minimum ultimate strength, F_u ksi	F_u/F_y ratio	Minimum elongation, percent	
						in 2-in. gage length	in 8-in. gage length
Hot-Rolled, High Strength, Low Allow Steel Sheet and Strip with Improved Formability	A715 Gr 50	up to 0.097"	50	60	1.20	22	-
	60		60	70	1.17	20	-
	A715 Gr 50	over 0.097"	50	60	1.20	24	-
	60		60	70	1.17	22	-
Structural Steel	A36		36	58-80	1.61-2.22	23	-
High-Strength Low-Alloy Structural Steel	A242	3/4 & under	50	70	1.40	--	18*
		3/4 to 1-1/2	46	67	1.46	21	18

Table 3.2 (continued)

Mechanical Properties of Steels Referred to in Section 1.2.1 of the AISI Specification[48]

Trade designation	ASTM designation	Thickness, in.	Minimum yield point or yield strength, F_y ksi	Minimum ultimate strength, F_u ksi	F_u/F_y ratio	Minimum elongation, percent	
						in 2-in. gage length	in 8-in. gage length
High-Strength Low-Alloy Structural Manganese Vanadium Steel	A441	3/4 & under	50	70	1.40	--	18*
		3/4 to 1-1/2	46	67	1.46	21	18
High-Strength Low-Alloy Columbium-Vanadium Steels of Structural Quality	A572 Gr 42		42	60	1.43	24	20
	45		45	60	1.33	22	19
	50		50	65	1.30	21	18
	55		55	70	1.27	20	17
	60		60	75	1.25	18	16
	65		65	80	1.23	17	15

1.02 their use is limited to applications where only a small amount of cold-forming is required. Typical uses of this steel are for roofing, siding, and floor decking[50].

b. Guide for Preliminary Design of Sheet Steel Automotive Structural Components[3]. In 1981, AISI published the "Guide for Preliminary Design of Sheet Steel Automotive Structural Components[3]" for use by the automobile industry. The primary purpose of the Guide is to provide simplified design expressions to be used for the preliminary design of automotive strutural components. The provisions of the Guide are based on the 1968 Edition of the "Specification for the Design of Cold-Formed Steel Structural Members[52]."

The design provisions of the Guide differ from the AISI Specification[52] in the following ways:

(1) The design equations are based on an ultimate strength basis. Thus, the magnitude of the factor of safety is left up to the designer.

(2) Many of the design expressions have been simplified since they are presented primarily for preliminary design and since the automobile industry customarily subjects their new products to performance tests.

(3) The design equations have been modified such that their range of applicability is extended to cover steels with yield strengths up to 80 ksi.

The material provisions of the Guide are much more general than those given by the 1980 Specification[49]. The design expressions of the Guide may be applied to any structural steel that has a yield strength

not greater than 80 ksi and a proportional limit equal to or greater than 70 percent of the yield strength. The only ductility requirement is that the material possesses "adequate ductility to form the part and serve the intended function"[3].

c. Specification for the Design of Cold-Formed Stainless Steel Structural Members[53]. In 1968, the publication of the "Specification for the Design of Light Gage Cold-Formed Stainless Steel Structural Members[54]," marked the first set of published guidelines for the design of cold-formed stainless steel members. The range of applicable stainless steel materials was increased in 1974 with the publication of the "Specification for the Design of Cold-Formed Stainless Steel Structural Members[53]." The 1974 Specification[53] was expanded to include not only sheet and strip material but also flat plates and bars. In summary, the 1974 Specification[53] applies to any sheet, strip, plate, and flat bar stainless steel that meets the requirements of ASTM Designation A666-72, "Austenitic Stainless Steel, Sheet, Strip, Plate, and Flat Bar for Structural Applications."

Since stainless steels, particularly the 1/4 and 1/2-hard tempers, typically exhibit considerable anisotropy, in much the same manner as the high strength sheet steels, the design expressions that were originally developed for the stainless steels may very well apply to high strength sheet steels. Of course, considerable research and testing would be required to prove the applicability of the stainless steel equations.

A comparison of the stress-strain curves for stainless steel and the traditional carbon or low alloy steels is shown in Figure 3.1[48].

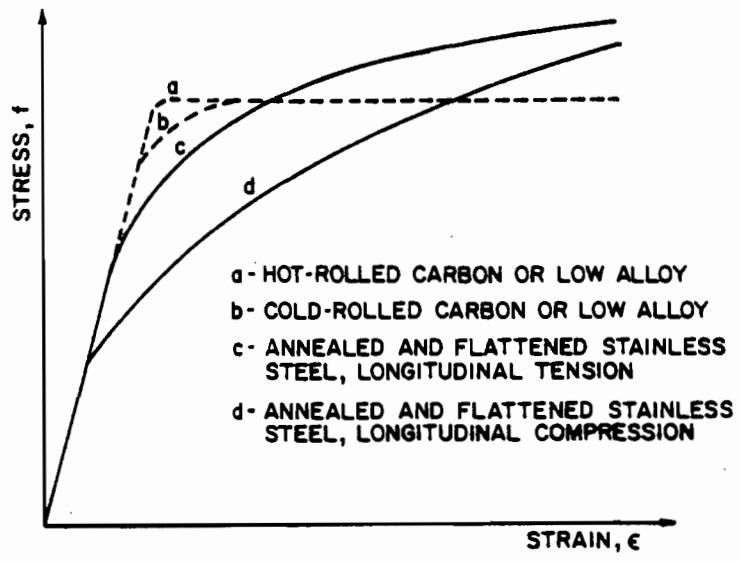

Fig. 3.1 Difference Between Stress-Strain Curves of Carbon and Stainless Steels[48]

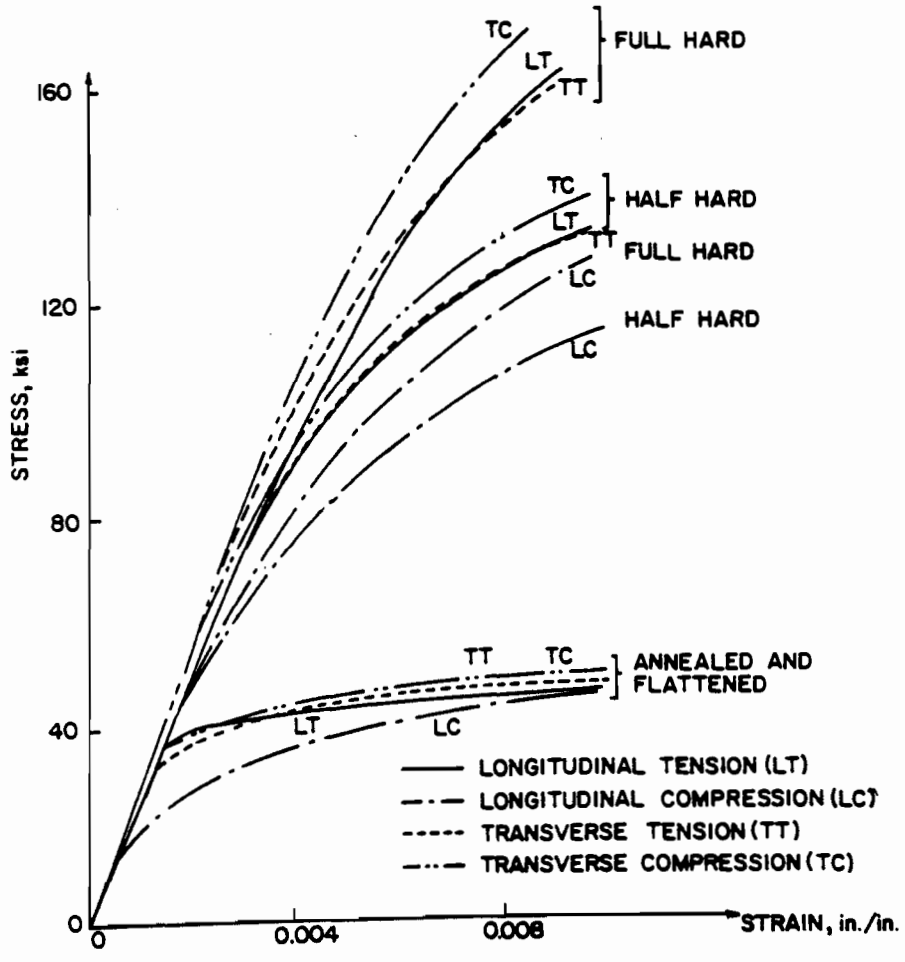

Fig. 3.2 Comparison of Stress-Strain Curves of Annealed Half-Hard and Full-Hard Stainless Steels[48]

Figure 3.2[48] illustrates the anisotropic nature of the stainless steels.

B. UNIAXIAL TESTS

The six materials were uniaxially tested in the longitudinal (parallel to the direction of rolling) and transverse (perpendicular to the direction of rolling) directions in both tension and compression. The test specimens (or coupons) were cut from the quarter points of the steel sheets as shown in Figure 3.3[48]. For each type of steel, four tests were performed in longitudinal tension (LT), transverse tension (TT), longitudinal compression (LC), and transverse compression (TC). A detailed description of the testing procedures is given in the following sections for tension testing (Section III.B.1) and compression testing (Section III.B.2). Section III.C describes the instrumentation employed in obtaining the stress-strain data as well as the method used to manipulate this stress-strain data to get the desired mechanical properties.

1. Tension Tests.

a. ASTM Specifications. The tension tests followed the procedures outlined in the ASTM Specifications listed below:

E8-69 Tension Testing of Metallic Materials

E83-67 Standard Method of Verification and Classification of Extensometers

E111-82 Standard Test Method for Young's Modulus, Tangent Modulus and Chord Modulus

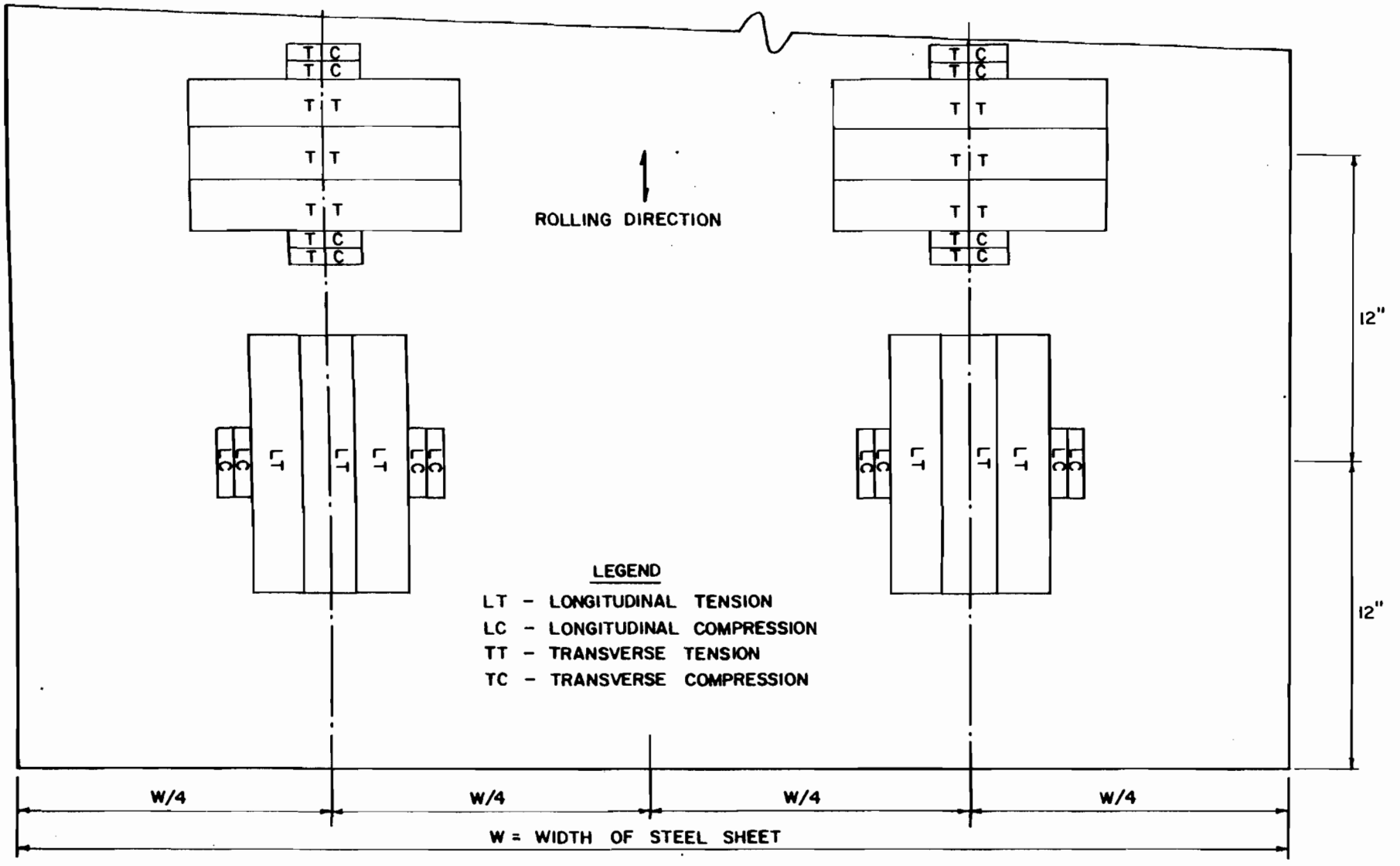

Fig. 3.3 Location of Tension and Compression Coupons

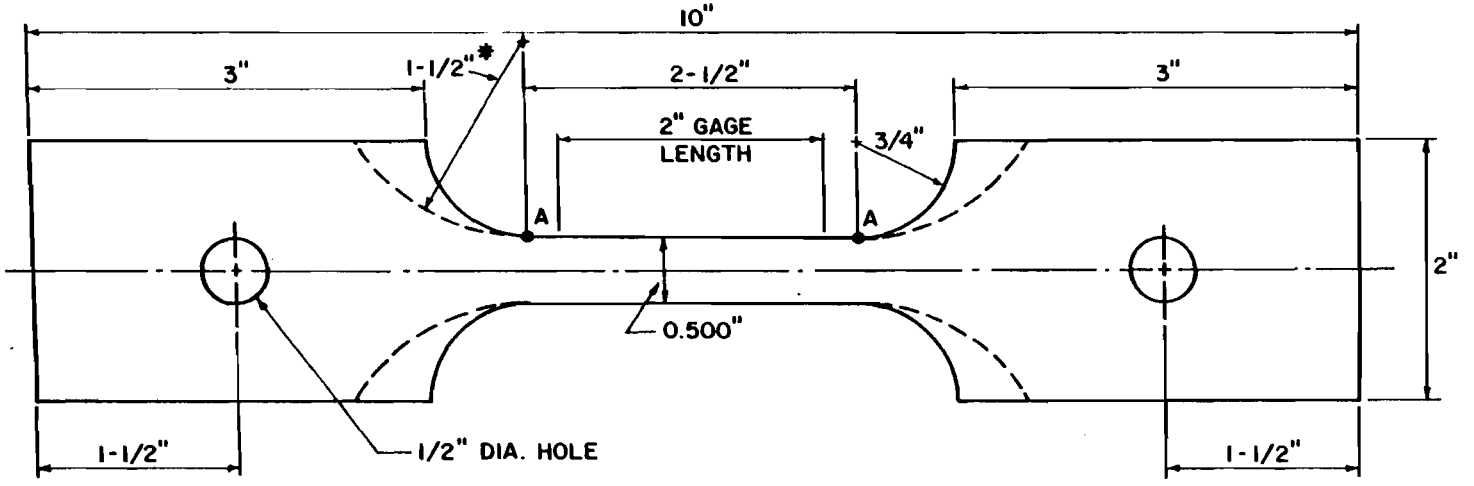

Fig. 3.4 Nominal Dimensions of Tension Coupons Used for 80SK, 80DF, 80DK, 80XF, and 100XF[48]

b. Specimens. Tensile specimens in the longitudinal and transverse directions were prepared by the Machine Shop at the University of Missouri-Rolla. The sketch in Figure 3.4[48] shows the tensile specimen dimensions for all materials except the 140XF steel. For the 140XF steel, the fillet radius was increased from 3/4 to 1-1/2 in. and the reduced section was tapered gradually from the ends to the center. However, the width at the ends was no more than 0.005 in. larger than at the center.

The 140XF specimens were modified because of consistent failure at the fillet radius-to-reduced section junction (point A, Fig. 3.4) when the standard type specimens were used. Since this failure was outside the gage length of the extensometer, the resulting stress-strain data were deemed unreliable. The reason for failure at the radius-reduced section junction is believed to be caused from the stress concentration at this transition point; thus, the fillet radius was increased in an effort to reduce the stress concentration.

The stress concentration problem for the 140XF material has been studied in detail. Upon inspection of the results in Table 3.10 it can be seen that, for the 140XF steel, the F_u/F_y ratio is only 1.00 and the elongation is only 4.3 percent in longitudinal tension and 1.5 percent in transverse tension. These ductility properties are all much lower than that of the 80 ksi steels and the elongation is much less than the corresponding values of the 100XF steel while the F_u/F_y ratio is the same at 1.00. Since the yield stress is first reached at the stress concentration point, a significant amount of ductility is required to enable the stress to flow plastically until the yield stress can spread

over the entire cross section. However, since the 140XF steel has very little ductility, the material fractures before a uniform yield stress can be obtained.

c. Equipment. All the specimens were tested in a 120,000 pound Tinius Olsen testing machine located in the Engineering Research Laboratory at UMR. Figure 3.5[48] shows this testing machine along with the remaining equipment used in the tension test. Other equipment used is the data acquisition system (Fig.3.6), graphic display (Fig. 3.7), X-Y plotter (Fig. 3.8), strain rate monitor (SRM) (Fig. 3.9), and a Tinius Olsen model no. 90828 extensometer (Fig. 3.10a, Fig. 3.10b, and Fig. 3.11). These figures were originally presented in Reference 48.

A Tinius Olsen extensometer with a 2-in. gage length was used in order to measure the strain from zero load to failure. The accuracy of this extensometer was found to be between the Class B-1 and B-2 classifications according to the regulations given in ASTM Specification E83-67. A description of the calibration procedures and the classification calculations are included in the Appendix for this extensometer.

d. Procedure. Prior to testing, the dimensions of the tensile specimens were measured to the nearest 0.001 in., cleaned with acetone, and the gage length (2-in.) was marked in ink. The specimen was then placed in the jaws of the Tinius Olsen testing machine such that the longitudinal axis of the specimen coincided with the centerline of the testing machine heads. Next the extensometer was attached to the specimen such that the extensometer grips approximately lined up with the gage marks as illustrated in Figure 3.10a[48]. A preload of about 30

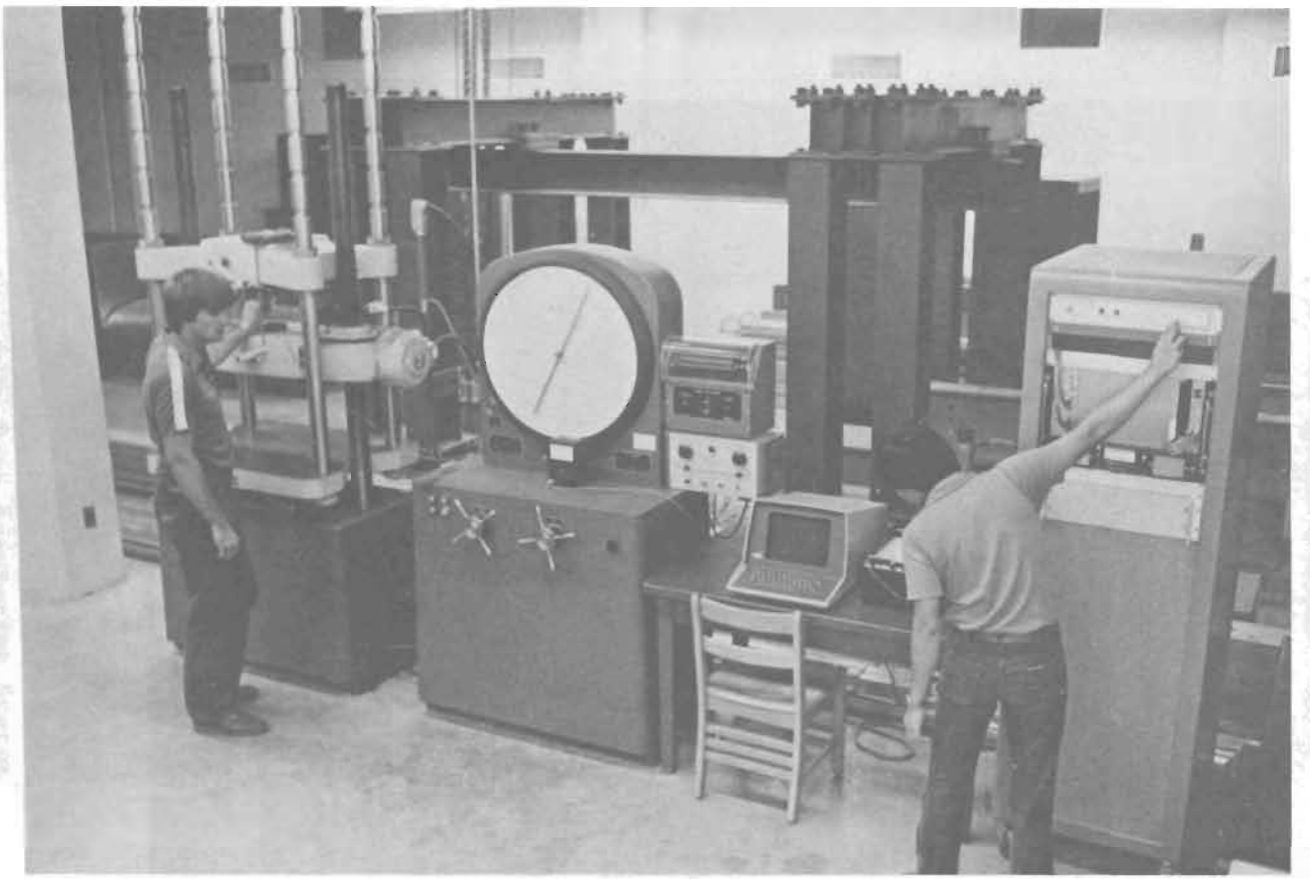

Fig. 3.5 Tinius Olsen Universal Testing Machine Used for Tension Tests[48]

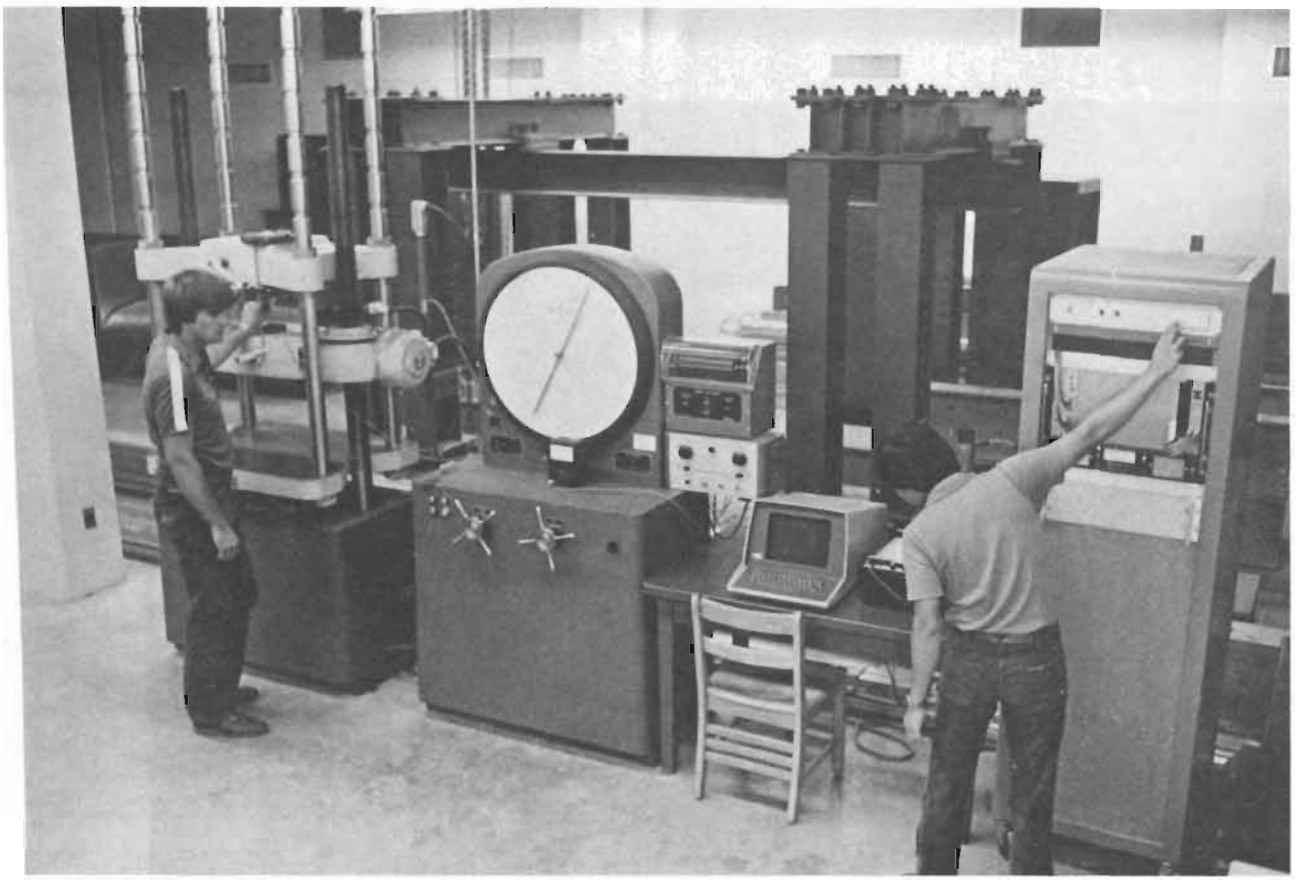

Fig. 3.5 Tinius Olsen Universal Testing Machine Used for Tension Tests[48]

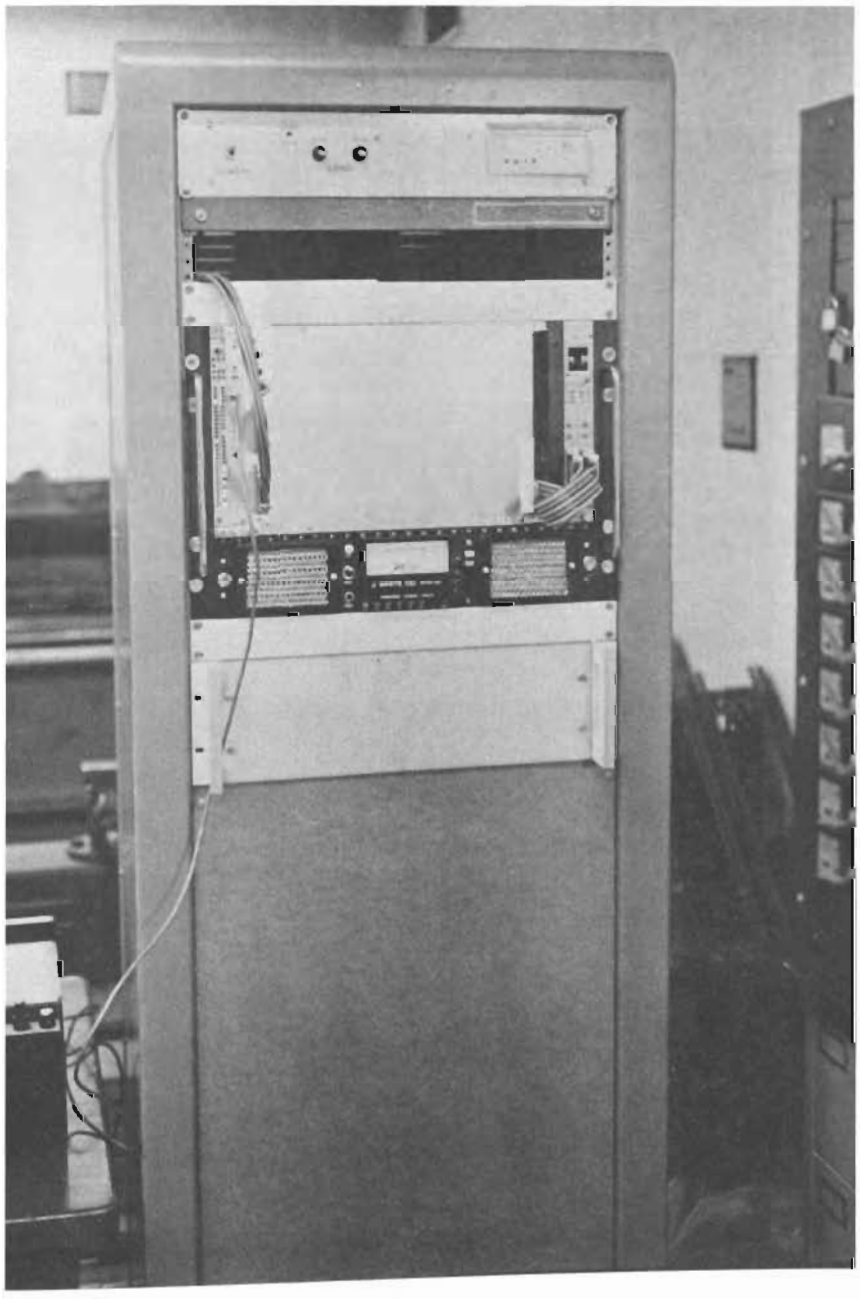

Fig. 3.6 Data Acquistion System[48]

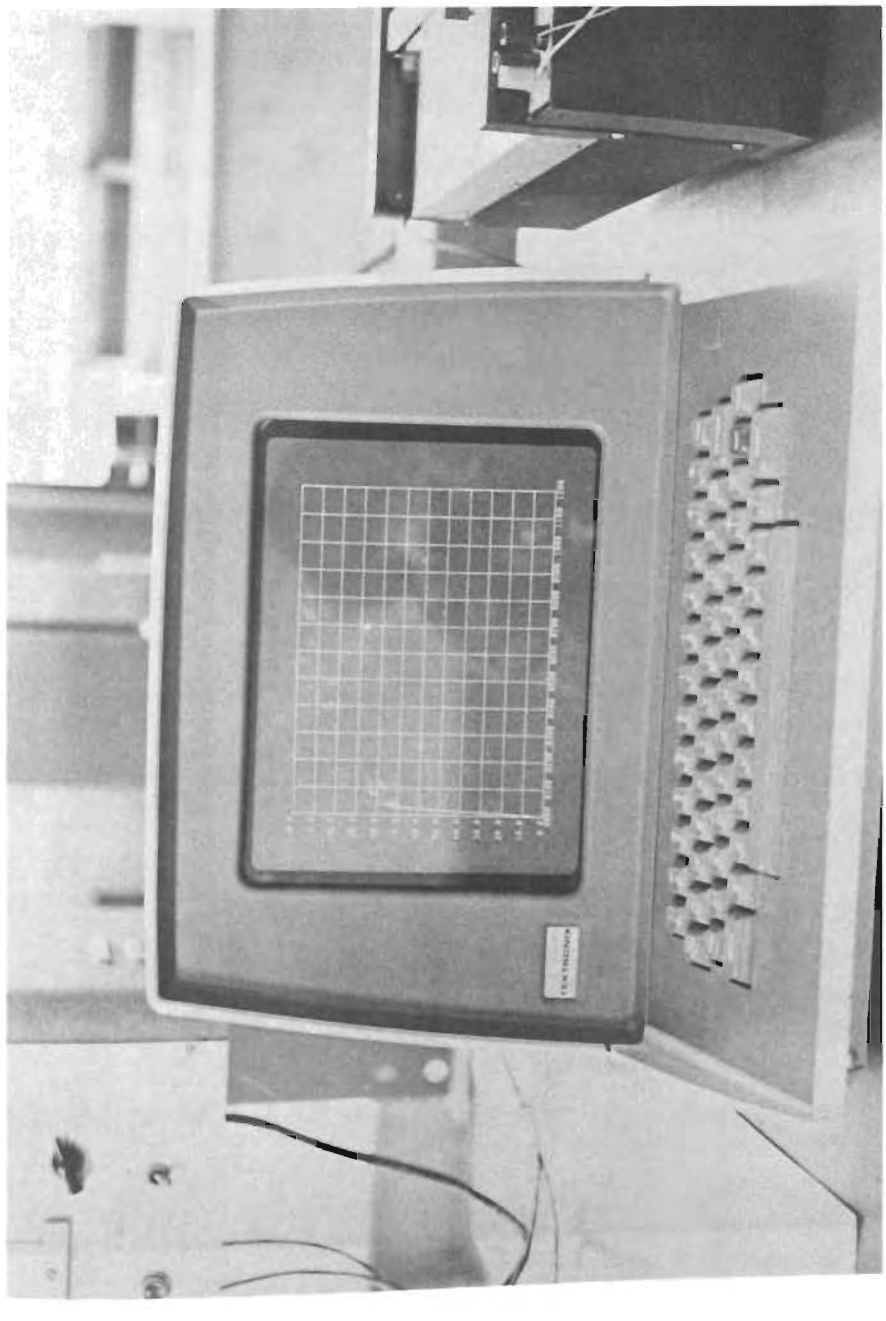

Fig. 3.7 Graphic Display Terminal[48]

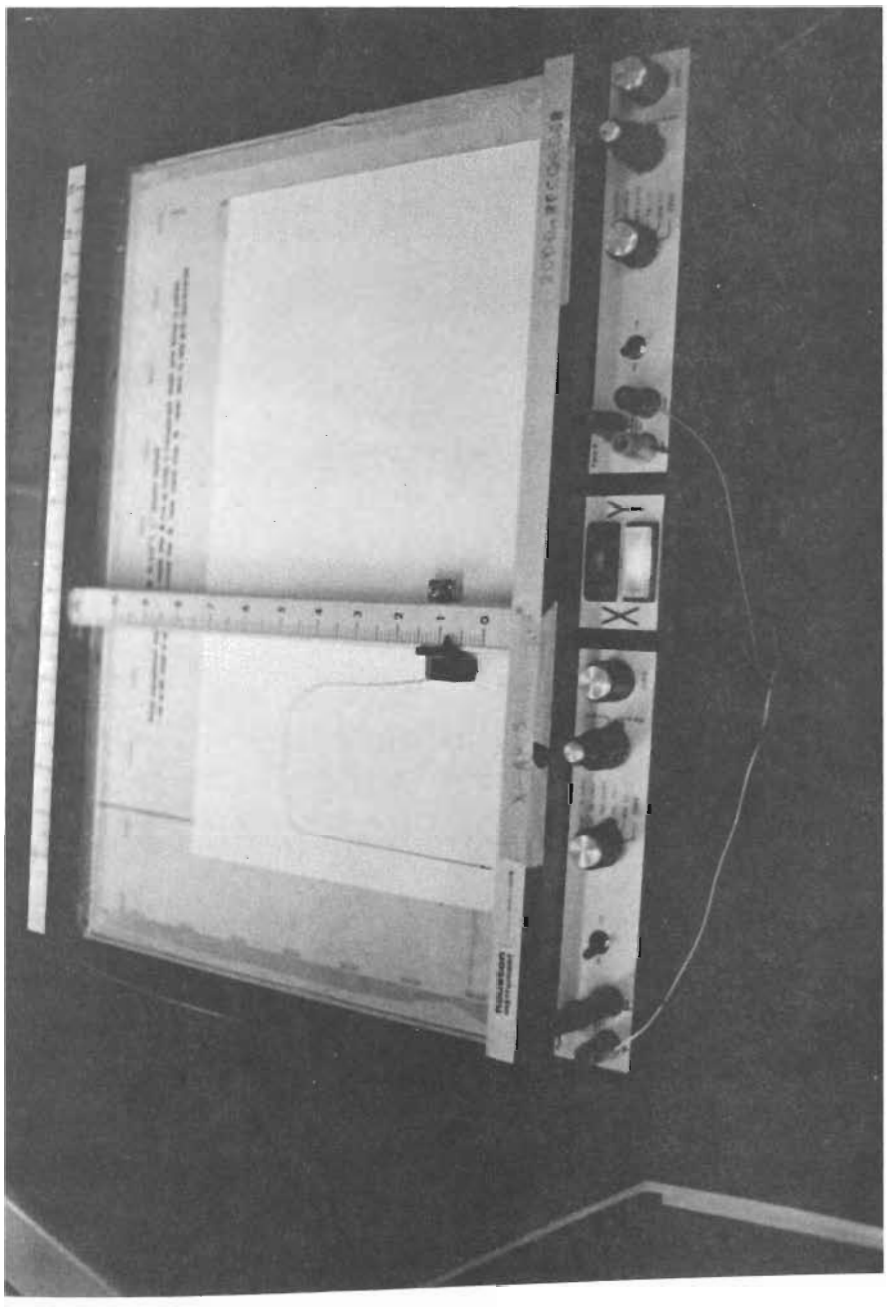

Fig. 3.8 X-Y Plotter[48]

Fig. 3.9 Strain Rate Monitor (Marked as SRM)[48]

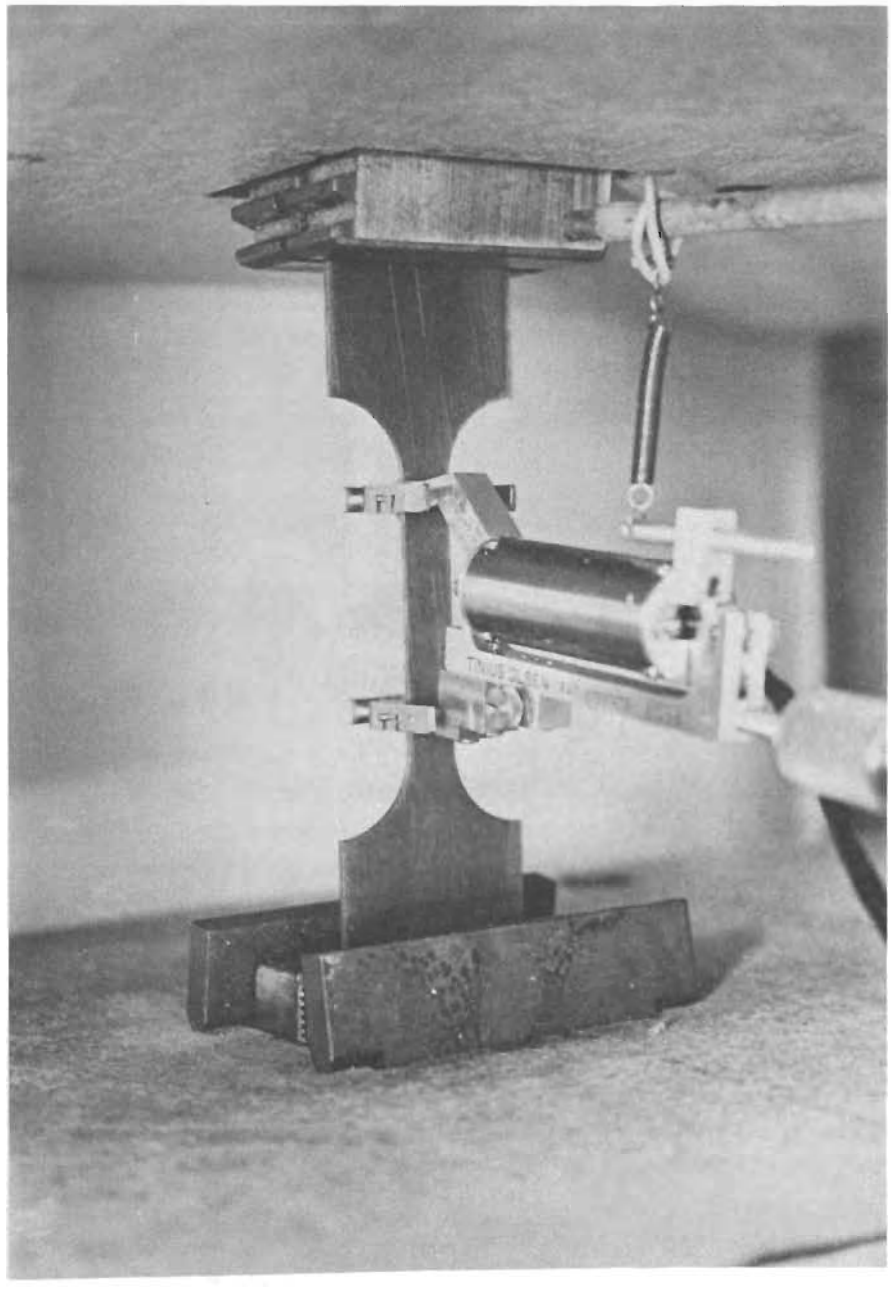

Fig. 3.10a Test Setup Showing the Attachment of Extensometer[48]

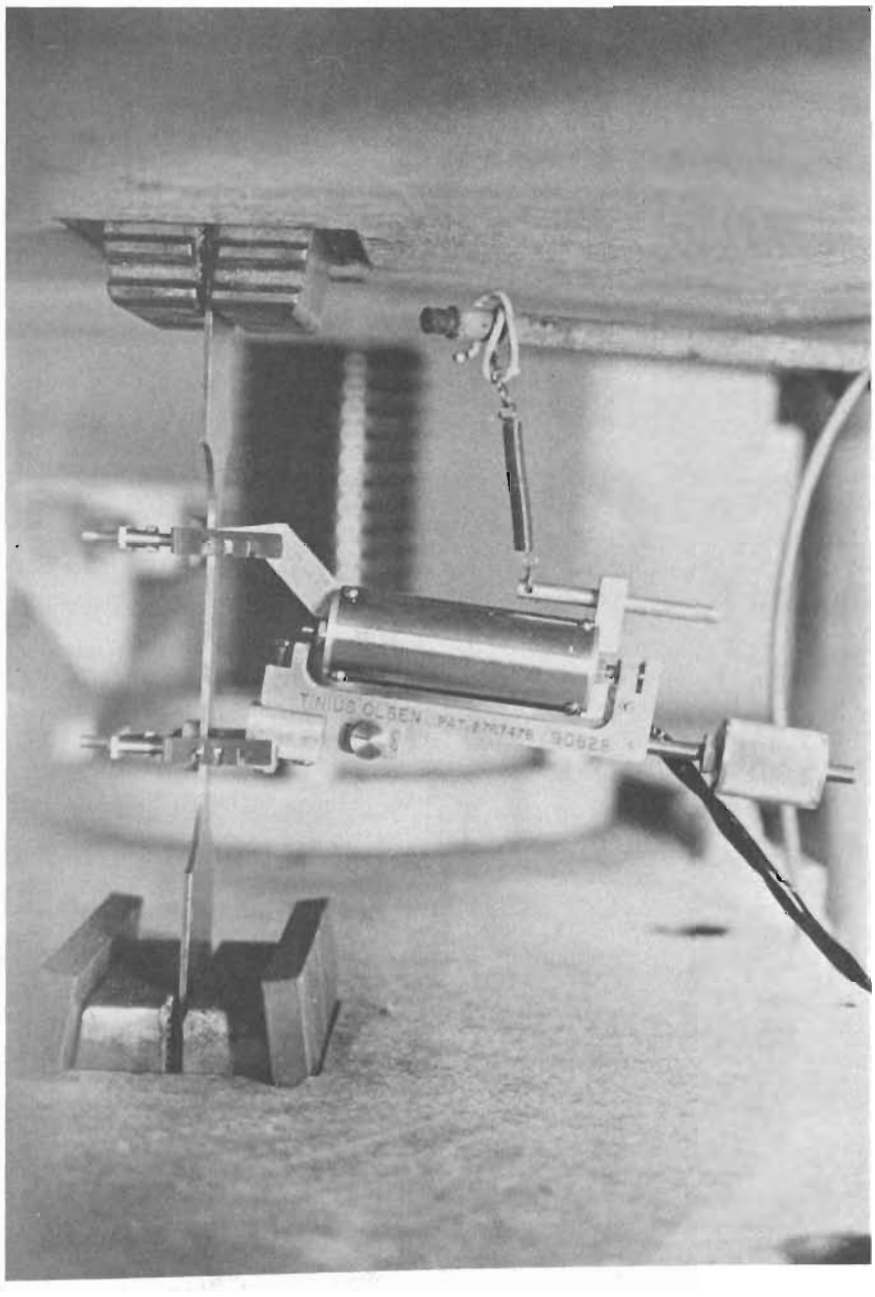

Fig. 3.10b Test Setup Showing the Attachment of Extensometer[48]

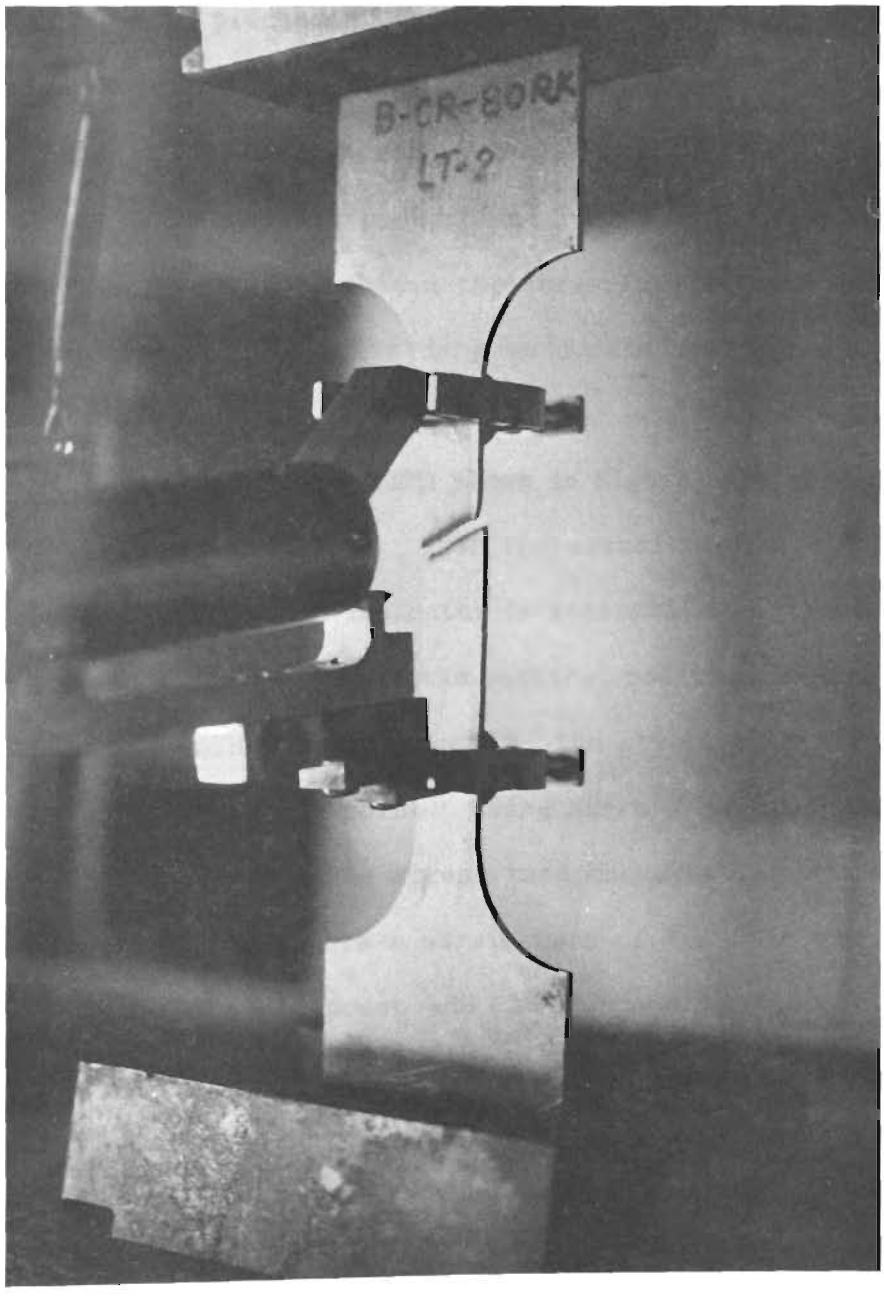

Fig. 3.11 Failure of the Tesnion Test Specimen[48]

percent of the yield stress was applied and then released prior to testing in order to minimize any slipping that might occur in the early test stages.

As the test proceeded the stress-strain graph was plotted simultaneously on the graphic display terminal and the X-Y plotter. Stress and strain data were stored by a computer for later plotting and determination of mechanical properties. Section III.C describes the instrumentation employed to obtain the stress-strain data and also the procedure for manipulating this data to obtain the desired mechanical properties.

The strain rate monitor (SRM) shown in Figure 3.9[48] electronically measured the rate of straining. When the actual strain rate equals the desired strain rate, the SRM indicator is vertical; thus the load may be adjusted to keep the indicator in the vertical position.

According to ASTM Specification E8, the stress rate should be 100 ksi/min. up until the yield point. Using Hooke's Law and a modulus of elasticity of 29,500 ksi, this stress rate converts to a strain rate of 0.0034 in./in./min. Therefore a strain rate of 0.003 in./in./min. was attempted up to the yield point and then changed to 0.03 in./in./min. from the yield point to fracture of the material. A spot checking of the actual strain rates showed that the strain rate used in the tests varied from about 0.004 to 0.006 in./in./min. in the elastic range while the strain rate was very close to desired rate of 0.03 in./in./min. in the plastic range. Equation 2.12 of the literature review shows that if the rate of strain is doubled the resulting stress would increase approximately 3 percent assuming an m value of 0.04. Therefore, the

slightly higher strain rates actually used in the tests should not significantly affect the resulting yield stresses and tensile strengths. A typical plot of strain versus time for the four 80DF longitudinal tension tests is shown in Figure 3.12.

2. Compression Tests.

a. ASTM Specifications. The compression tests followed the procedures outlined in the ASTM Specifications listed below:

E9-70 Standard Methods of Compression Testing of Metallic Materials at Room Temperature

E83-67 Standard Method of Verification and Classification of Extensometers

E111-82 Standard Test Method for Young's Modulus, Tangent Modulus, and Chord Modulus

b. Specimens. Compression specimens, cut in the longitudinal and transverse direction, were also prepared by the Machine Shop at UMR. Figure 3.13[48] shows the configuration of the compression coupons. The specimen dimensions were made to fit a Montgomery-Templin compression test fixture. The notches along one edge were for the installation of the knife edges of the compressometer. Special care had to be taken to ensure that the ends of the specimen were parallel and thus the same length for both longitudinal sides of the specimen. If the ends were not parallel, two types of inaccurate stress-strain diagrams occured depending on whether or not the longer side of specimen contained the compressometer notches.

The first case, shown in Figure 3.14(a), occurs when the notches are on the specimen's longest side. When the load, P, is applied

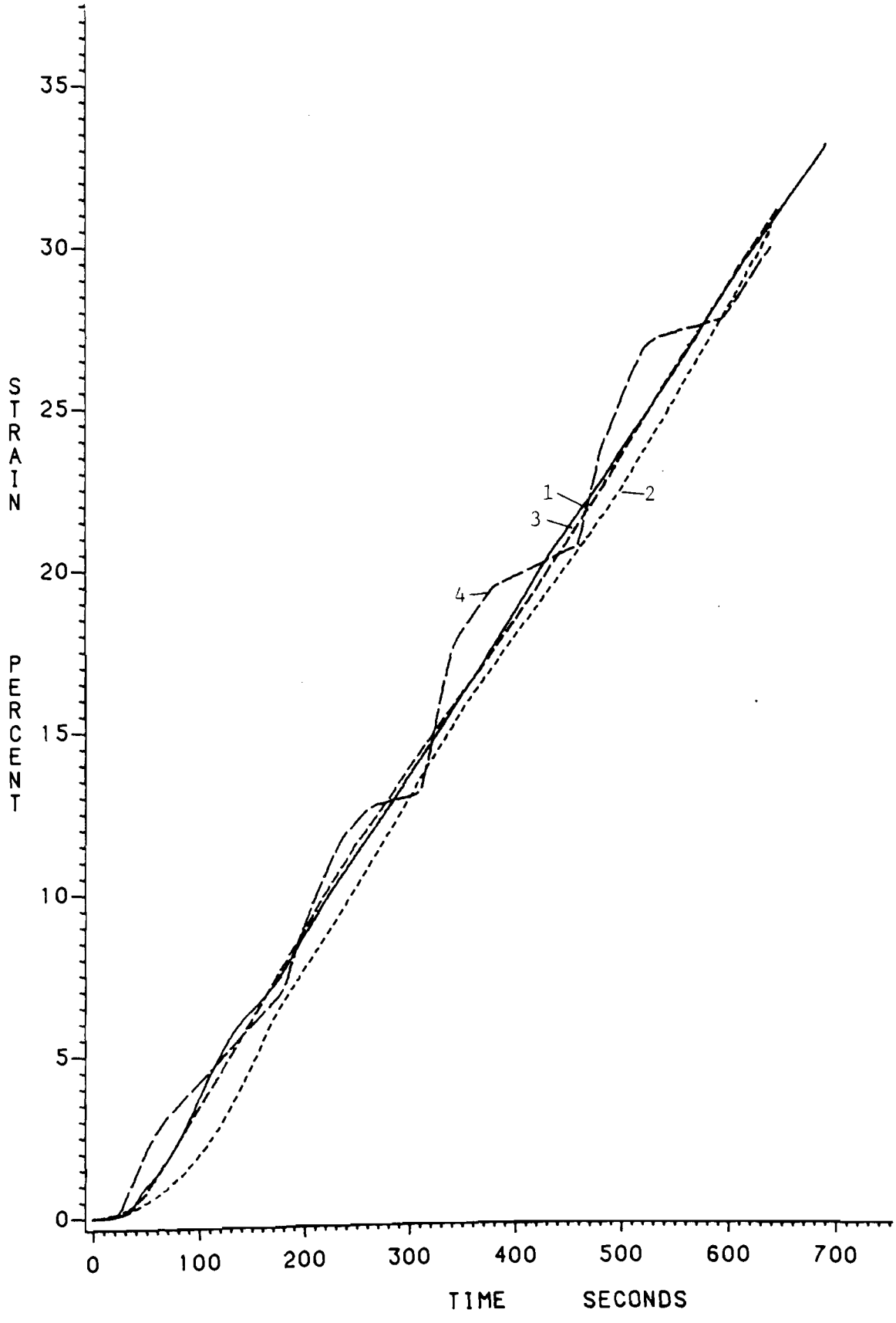

Fig. 3.12 Strain-Time Curves for 80DF-LT (Four Samples)

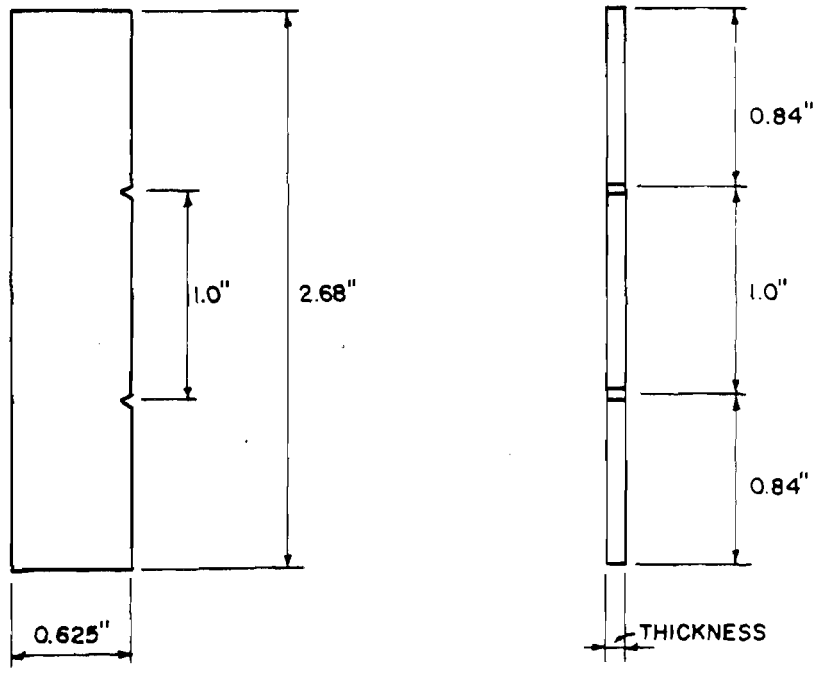

Fig. 3.13 Nominal Dimensions of Compression Coupons Used for All Sheet Steels[48]

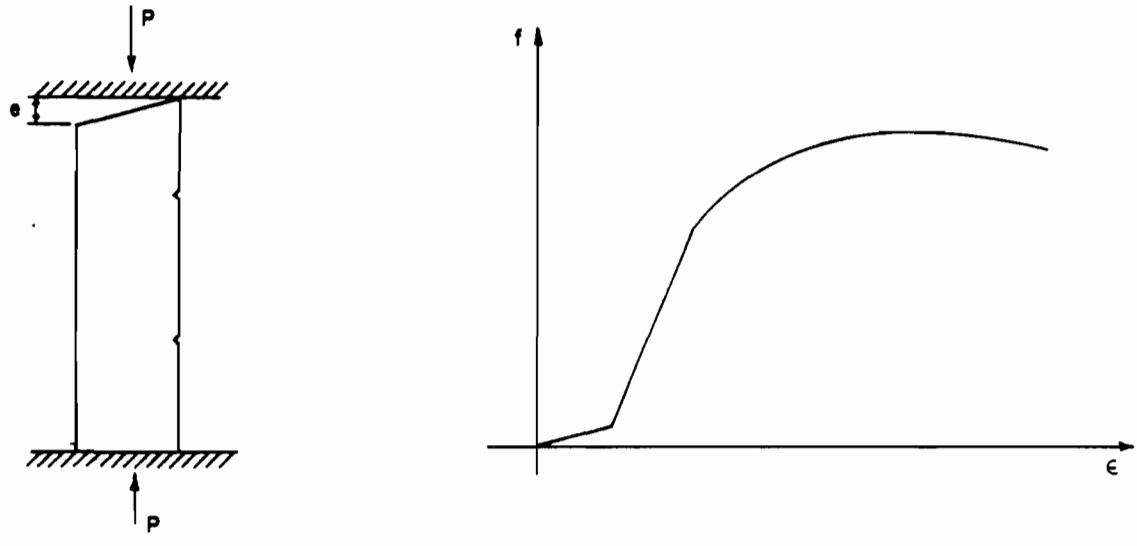

(a) e on Opposite Side of Specimen from Compressometer

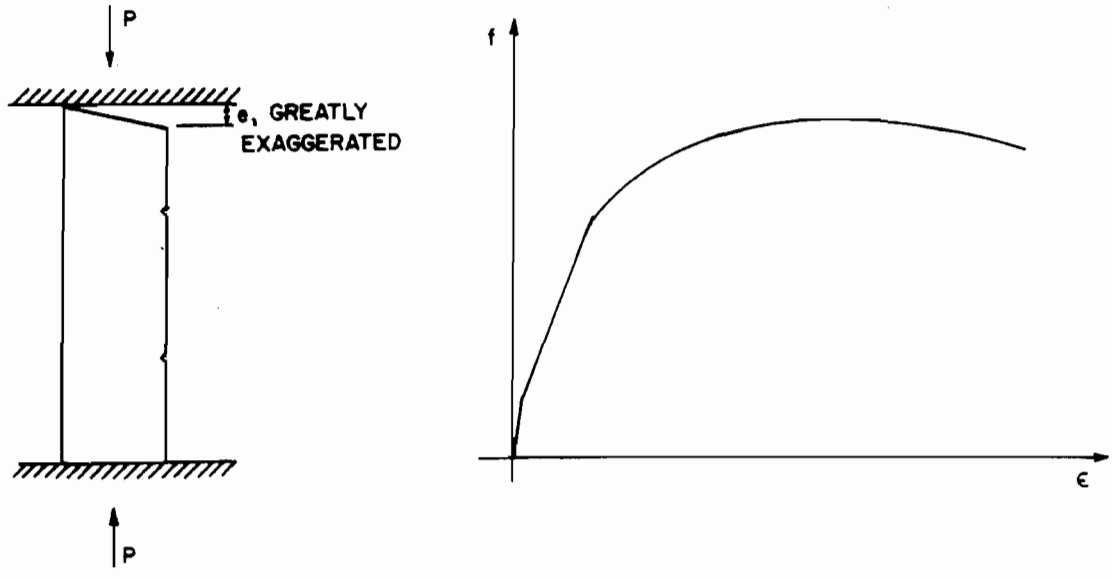

(b) e on Same Side of Specimen as Compressometer

Fig. 3.14 Effect of Non-Parallel Ends of Compression Specimens

initially only an extremely small area is available to resist the load. Therefore, the stress, which is calculated by the load divided by the full, original cross-sectional area increases very little for a given increase in strain.

The other case, shown in Figure 3.14(b), occurs when the notches are on the shorter side of the specimen. For this case, virtually no strain is recorded on the specimen's notched side, since the majority of the initial load was transferred along the longer side. Thus, there was an initial, almost vertical segment of the stress-strain curve that typlified this case.

For either case, the initial side length difference, e, disappeared after the load increased sufficiently to cause yielding of the longer side. From that point the stress-strain curve closely resembled the correct stress-strain diagram. However, when either of the above cases occurred in the actual tests, the results were discarded and the test repeated with a new specimen. In mosts cases, this problem could be avoided by placing the specimen in the testing apparatus (Figure 3.18) and observing any light between the specimen and ram of the subpress (the function of the subpress is discussed in Section III.B.2.c).

c. Equipment. The compression tests were performed in the same 120,000 pound Tinius Olsen testing machine, shown in Figure 3.15[48], as used for the tension tests. An assembly of all the equipment used in the compression tests is shown in Figure 3.16[48]. The load was applied to the compression specimen by means of a specially made subpress (Figure 3.17(a)). The subpress base and ram are constructed of hardened

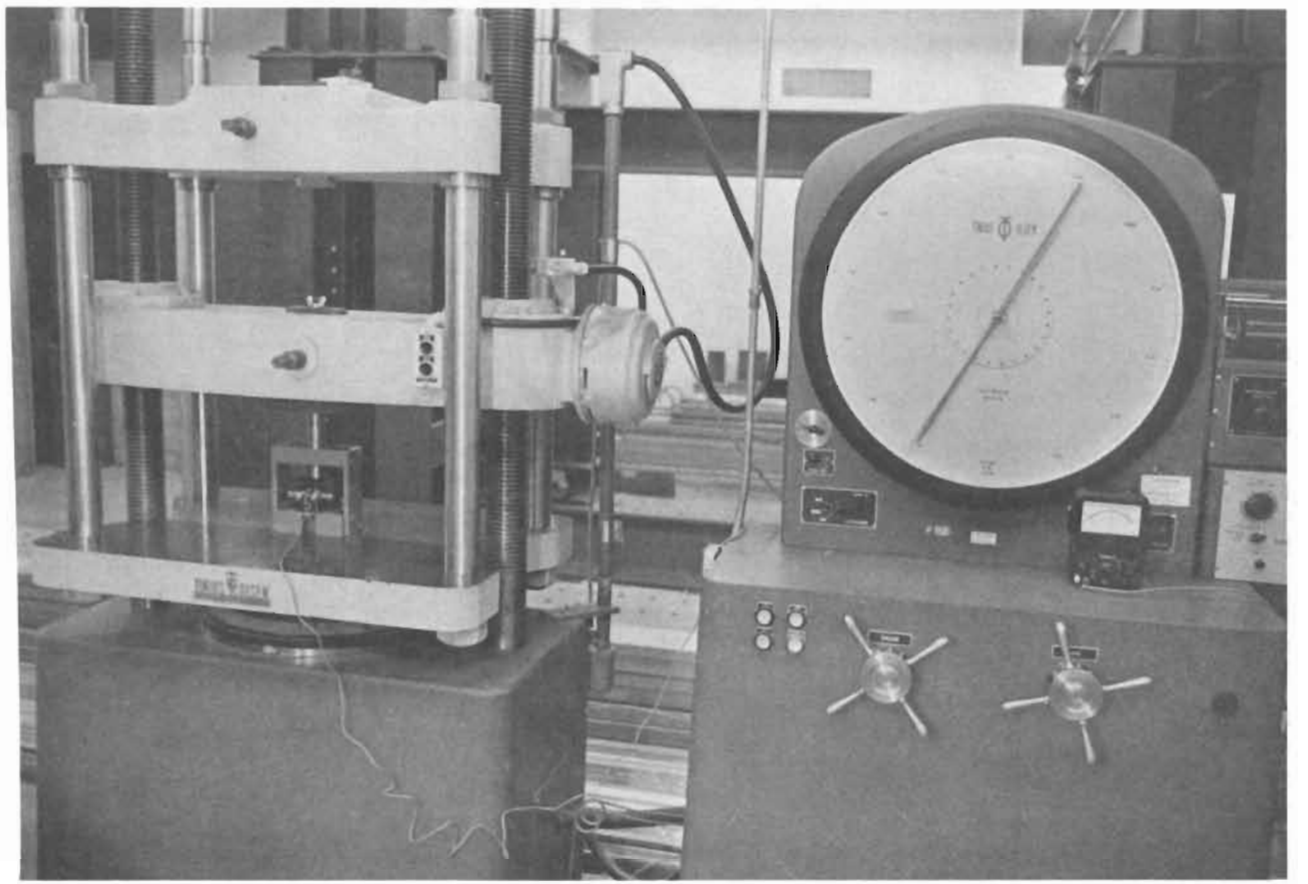

Fig. 3.15 Tinius Olsen Universal Testing Machine Used for Compression Test[48]

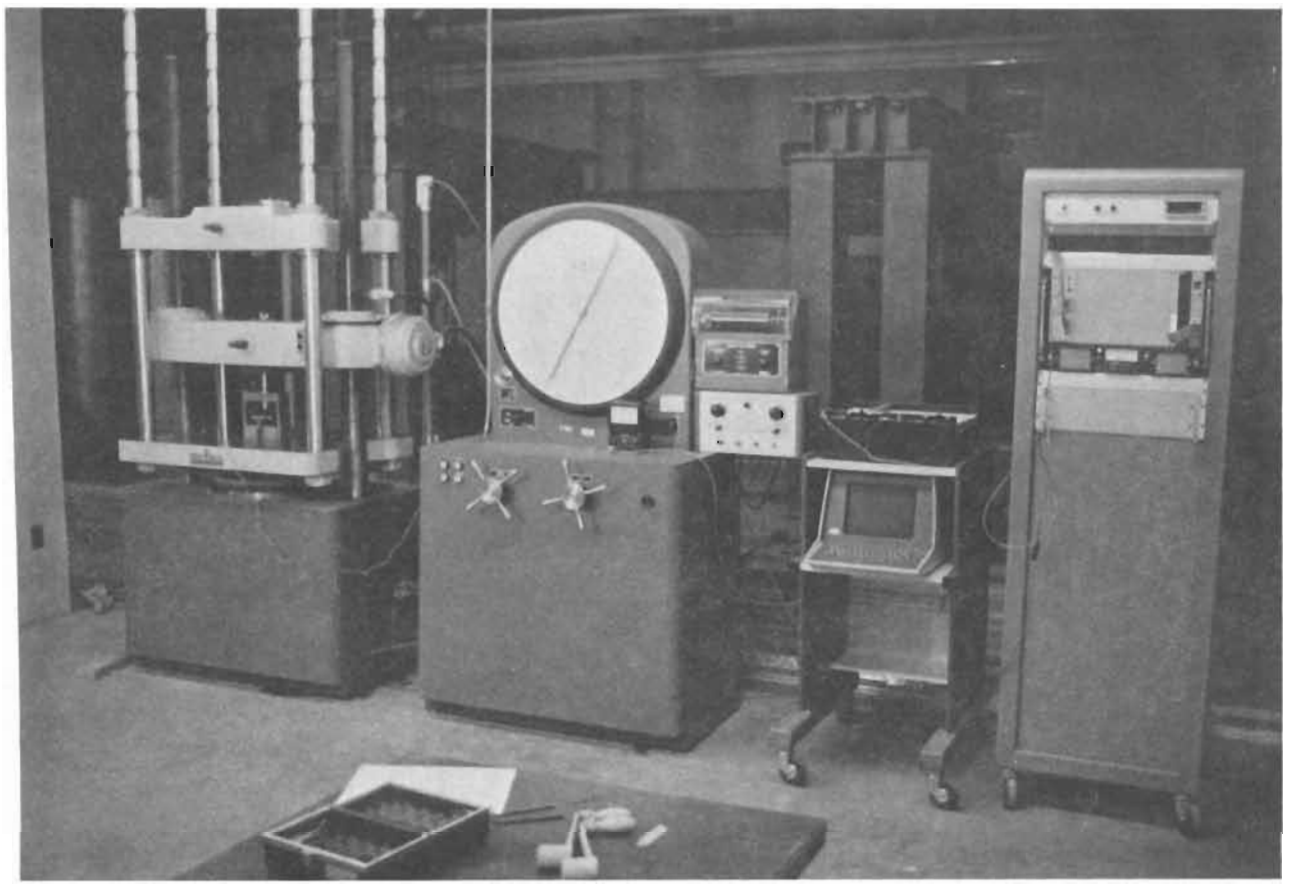

Fig. 3.16 Testing Machine, Data Acquisition System, Graphic Display Terminal, S-Y Plotter, and Strain Rate Monitor Used for Compression Tests[48]

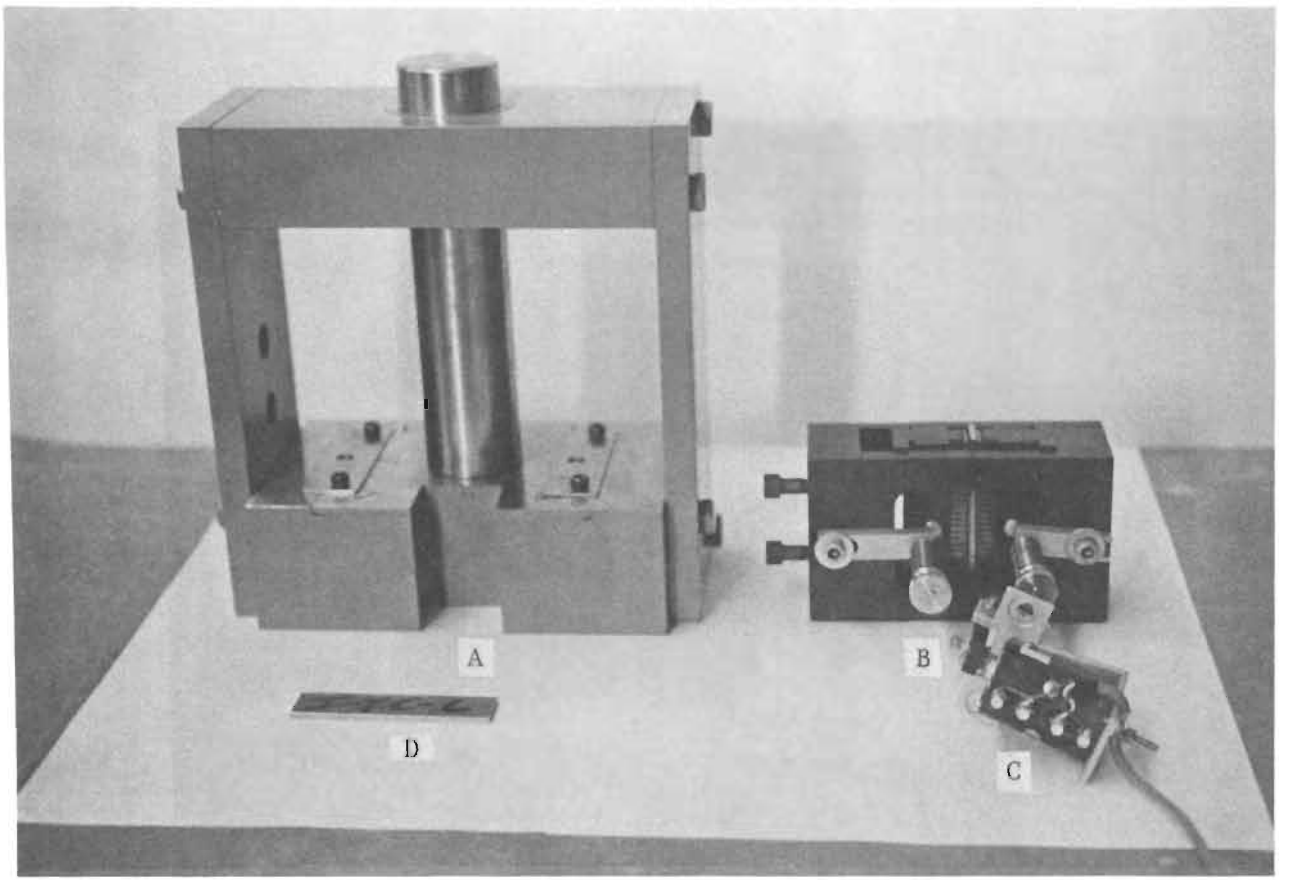

A- Compression Subpress
B- Compression Jig
C- Compressometer
D- Test Specimen

Fig. 3.17 Compression Subpress, Jig, Compressometer and Test Specimen Used for Compression Tests[48]

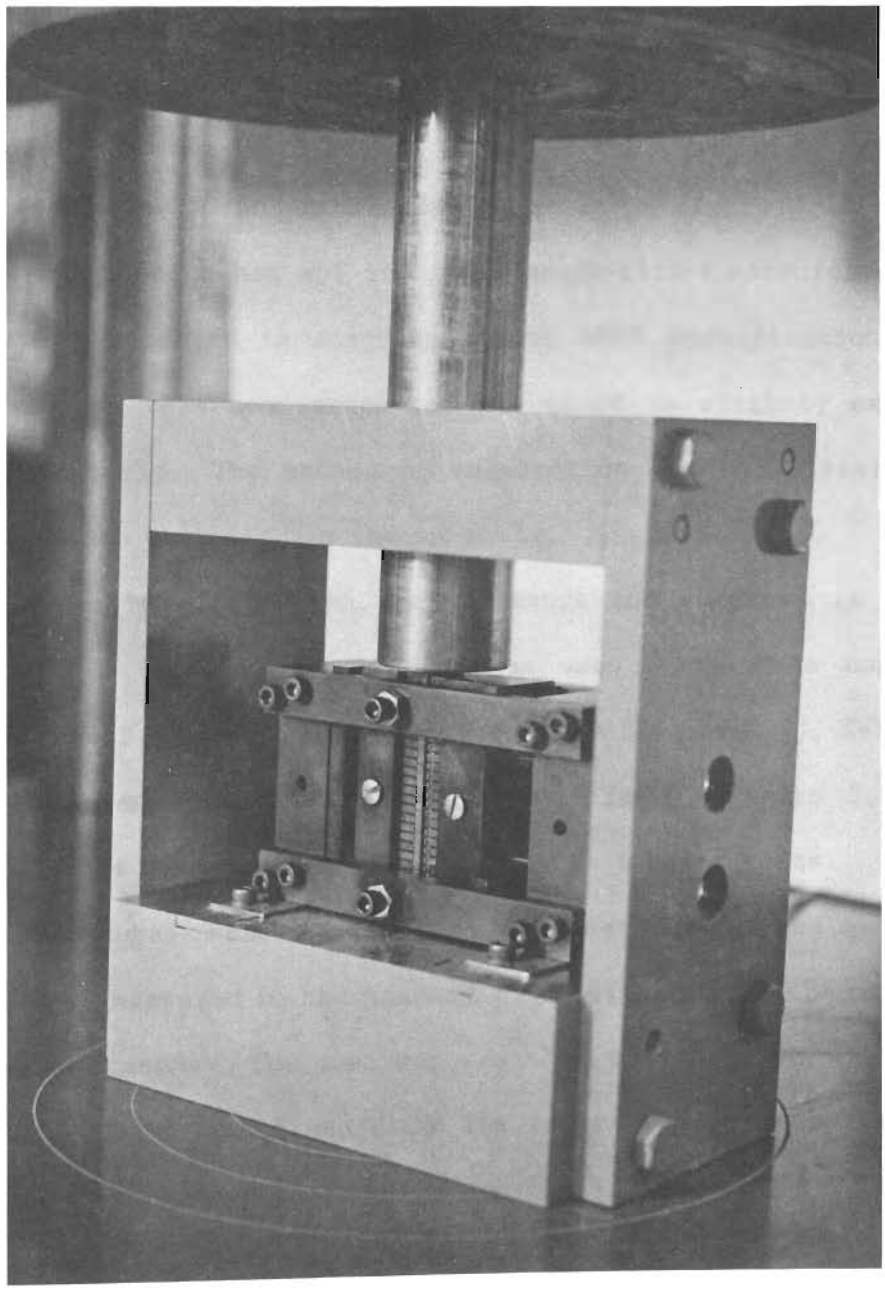

Fig. 3.18 Assembly of Compression Subpress, Jig, and Compressometer[48]

steel in order to minimize their deformation when applying the load. The compression specimen was held in a Montgomery-Templin compression test fixture (Figure 3.17(b)) which contains a series of rollers that may be tightened against the specimen to prevent buckling. The strain was measured by the PC-5M compressometer shown in Figure 3.17(c). This compressometer, which has a 1 in. gage length with a microformer at the bottom, was calibrated in accordance with ASTM Specification E83-67. The accuracy of this compressometer was found to slightly exceed the class B-1 criteria. The method of calibration and the classification calculations are presented in the Appendix.

The assembly of specimen, test fixture and subpress is shown in Figure 3.18[48]. Other equipment that was used is the data acquisition system (Figure 3.6), graphic display terminal (Figure 3.7), X-Y plotter (Figure 3.8), and the strain rate monitor (SRM) (Figure 3.9). The function of this equipment is identical to the tension tests.

d. Procedure. Prior to testing, the dimensions of the compression specimens were measured to the nearest 0.001 in. and the specimens were cleaned with acetone. The specimen was then placed in the Montgomery-Templin compression test fixture and the lateral roller supports of the fixture were tightened firmly against the sides of the specimen. Special care was taken to ensure that the specimen was aligned vertically in the test fixture. Next, the PC-5M compressometer was attached to the side of the test fixture such that the knife edges of the compressometer smoothly inserted into the notches of the compression specimen. Then, with the specimen, test fixture, and compressometer attached together as a unit, the entire unit was placed

in the compression subpress. A small stub is provided on each side of the bottom surface of the test fixture. These stubs fit into indentions on the base of the subpress in order to ensure proper alignment of the subpress ram with the specimen's longitudinal axis. The final step before loading was to place the subpress, with the test fixture, compressometer, and specimen attached, between the heads of the testing machine such that the longitudinal axis of the subpress lined up with the centerline of the testing machine heads. A preload of approximately 30 percent was then applied to the specimen to minimize any slipping that might occur during the initial portion of the actual tests.

During the tests the stress-strain curves were plotted simultaneously on the graphic display terminal and the X-Y plotter. The stress-strain data were stored by a computer for plotting and determination of the mechanical properties at a later time. Buckling of the unsupported length of the specimen limited the obtainable range of the stress-strain curves to approximately 1.5 percent.

The function of the instrumentation employed in the compression tests is described in Section III.C along with the procedures used to obtain the desired mechanical properties.

The rate of straining was measured by the (SRM) in exactly the same manner used for the tension tests. The desired strain rate was taken from ASTM Specification E9 as 0.0034 in./in./min. For the compression tests, a uniform strain rate was attempted throughout the tests. A spot checking of the actual strain rate used in the tests showed a range of from 0.003 to 0.004 in./in./min. This strain rate is sufficiently close to the ASTM recommended strain rate that the resulting stress-strain

relationship will not be significantly affected. A typical plot of the strain-time relationship for the four 80SK longitudinal compression tests is shown in Figure 3.19.

C. ACQUISITION OF STRESS-STRAIN DATA

1. Equipment. The following is a simplified description of the electronics used to obtain stress-strain relationships in either tension or compression. Figure 3.20 is given to illustrate the flow of information from the specimen to the computer.

The extensometer (tension tests) or compressometer (compression tests) is attached directly to the specimen. As the test proceeds the elongation (+ or -) is measured by the extensometer or compressometer as a change in voltage. The amplifier reads this change in voltage and enlarges the voltage range from -10V to +10V. The voltage read by the amplifier is then transformed to a digit by the analog to digital (A/D) converter. The A/D converter has a range of from -2000 to +2000 which corresponds to -10V to +10V obtained from the amplifier. Thus the 10V range of the amplifier is divided into 2000 pieces such that each volt is 2000/10 or 200 digits. The computer reads the digital output from the A/D converter then divides the digital output by 200 to convert back to voltage. (The conversion back to voltage is not necessary but is done so only as a convenience to the programmer since he is more familiar with the voltage output.) Finally, the strain is recorded as the voltage multiplied by a strain calibration factor. It should be noted that the voltage now is recorded in increments of 0.005 since the digital output was divided by 200 to get voltage.

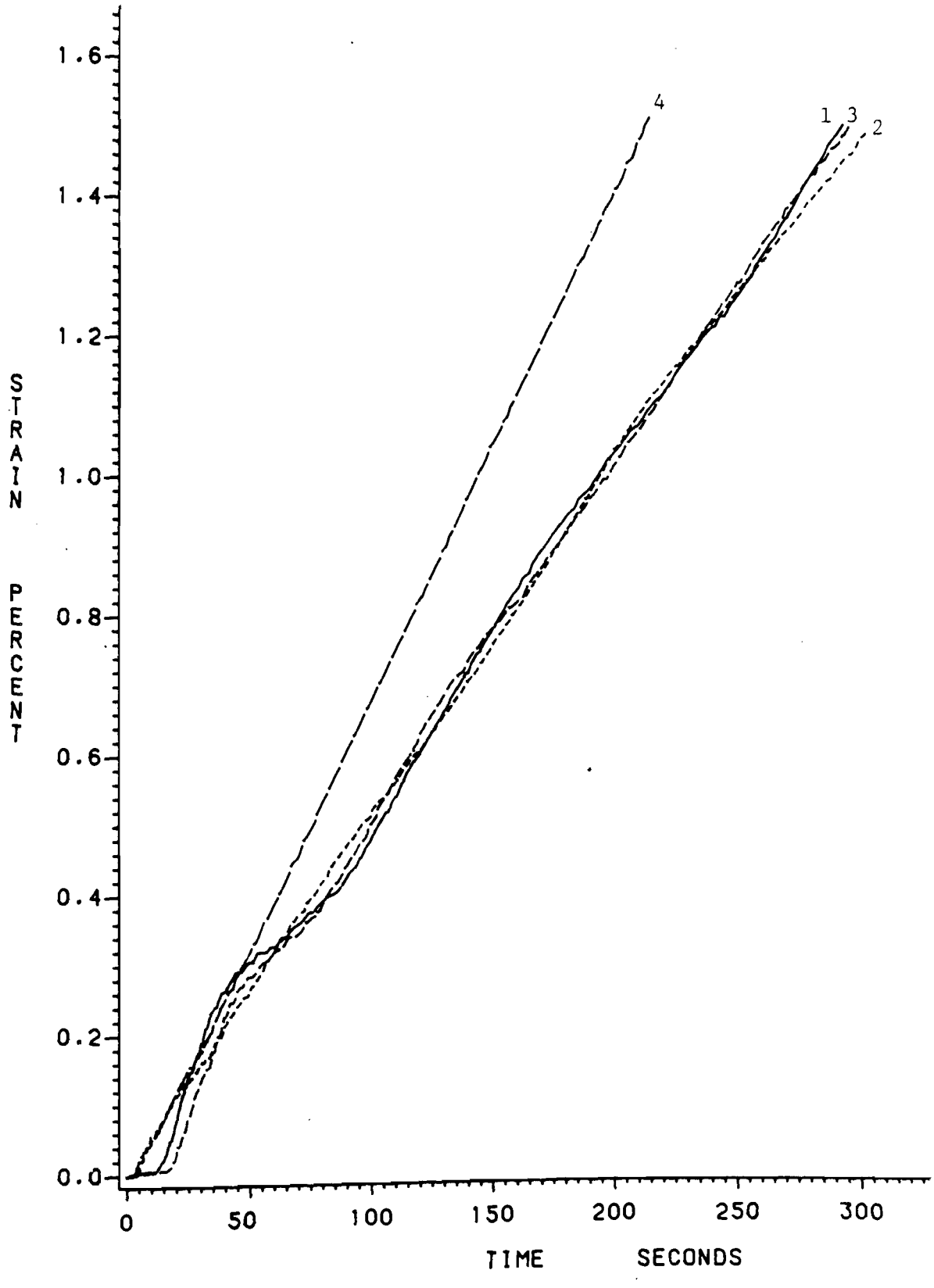

Fig. 3.19 Strain-Time Curves for 80SK-LC (Four Samples)

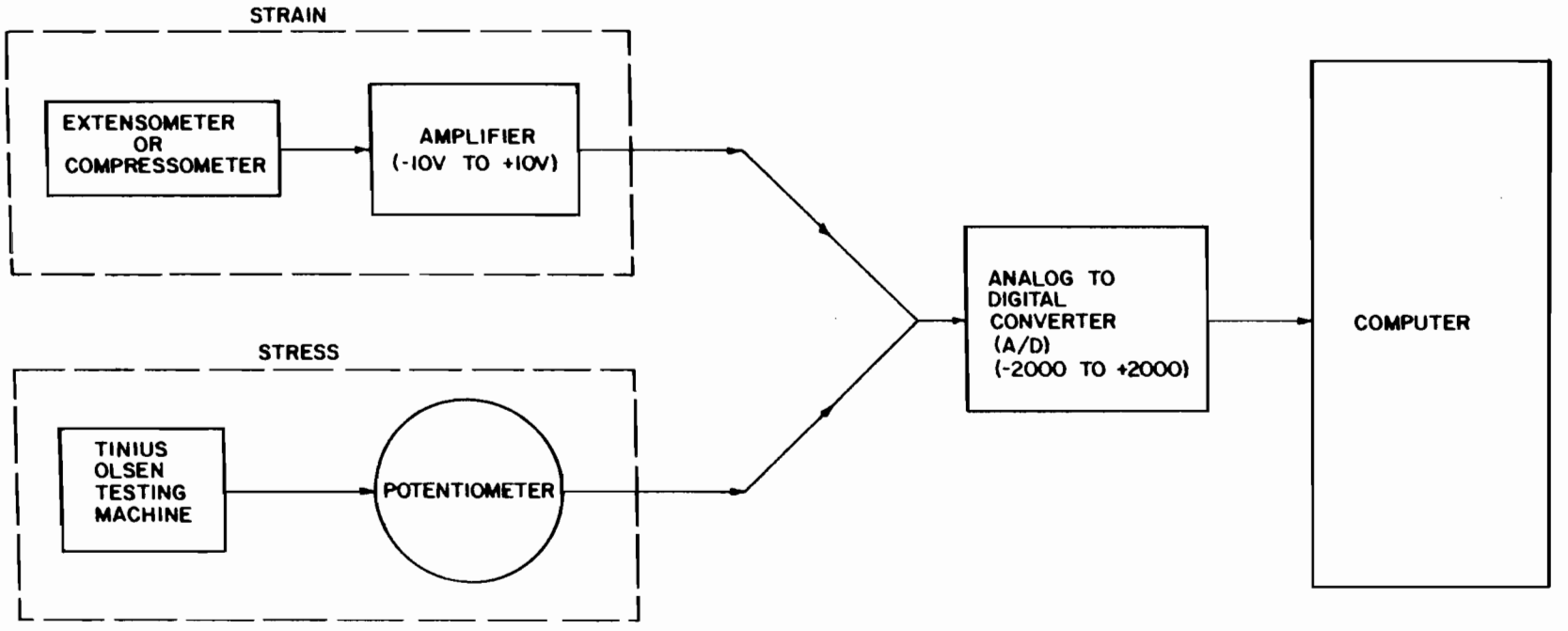

Fig. 3.20 Schematic Diagram of Testing Equipment Used in Obtaining Stress-Strain Relationships

The strain calibration factor is obtained by applying known increments of strain and recording the corresponding voltage values. The resulting relationship between strain and voltage is assumed to be linear and thus linear regression is used to obtain the slope of the resulting straight line. The slope of the strain vs. voltage line is the calibration factor, C, and has the units of strain divided by voltage.

Since the voltage input in the computer is now expressed in increments of 0.005, the resulting strain values will also have distinct increments in their values. The magnitude of the strain increment will be 0.005 times the calibration factor, C. This can easily be seen by comparing strains, ε_1 and ε_2, for two consecutive voltage values, V_1 and $V_2 = V_1 + 0.005$, or

$$\varepsilon_1 = V_1 * C$$

$$\varepsilon_2 = V_2 * C = (V_1 + 0.005) * C$$

$$\Delta\varepsilon = \varepsilon_2 - \varepsilon_1 = ((V_1 + 0.005) - V_1) * C$$

$$\Delta\varepsilon = \text{strain increment} = 0.005 * C. \qquad (3.1)$$

Therefore, the resulting stress-strain curves using this system are characterized by small steps or shifts in the strain direction at points where the strain changes from one strain level to another. These steps can be clearly seen in Figure 3.21.

The stress is calculated in a similar manner. To calculate stress the load is obtained from the Tinius Olsen testing machine by measuring the change in voltage recorded by its potentiometer. This voltage ranges from 0 to 10 volts and is read into the A/D converter as before. From this point the calculations are identical in form to the strain

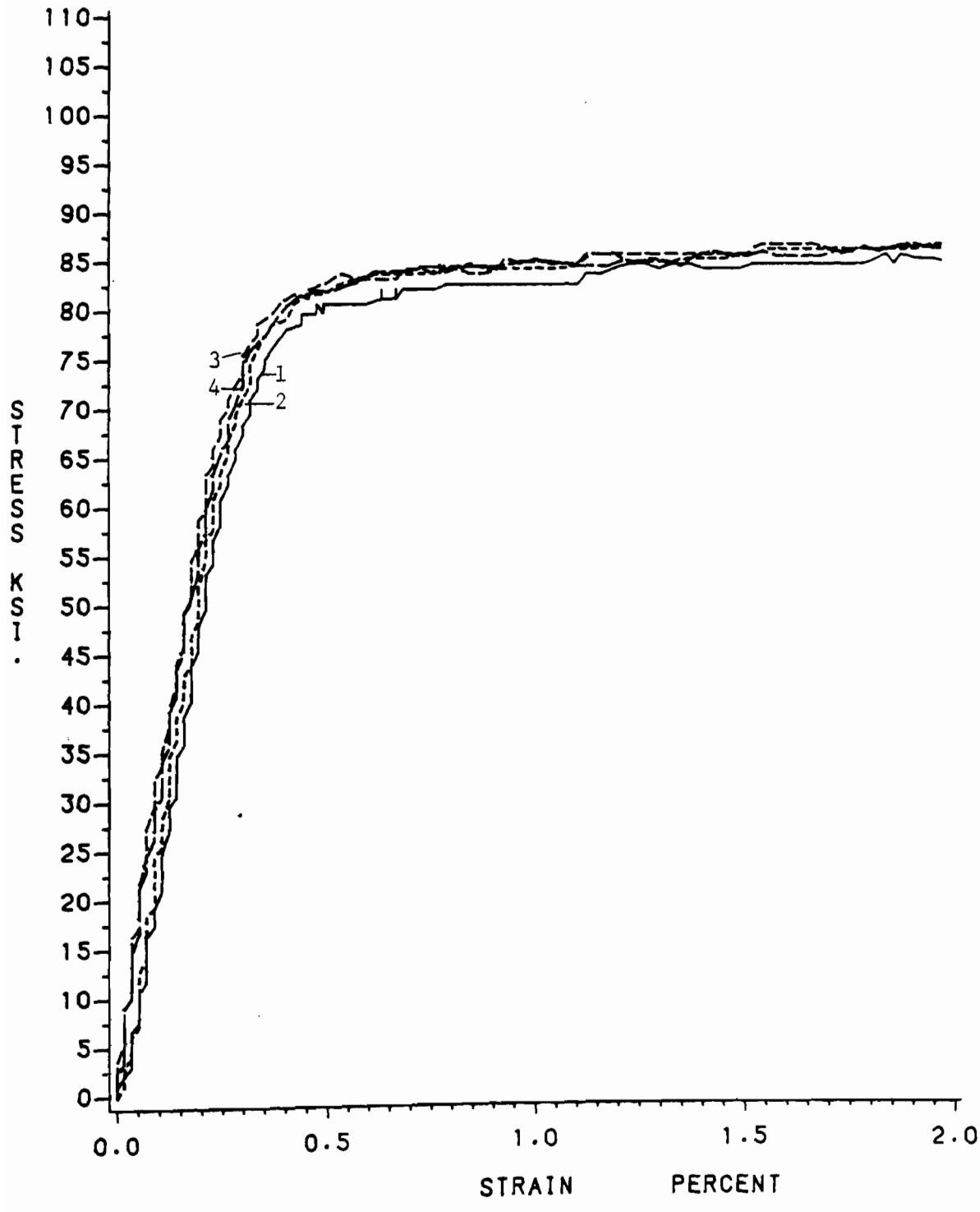

Fig. 3.21 Typical Steps in Stress-Strain Curve for 80SK-LT

calculations except that the resulting load is divided by the original cross-sectional area to compute the engineering stress. Since the stress measurement also passes through the A/D converter, the stress values will also have an incremental step equal to 0.005 times the stress calibration factor. However, this step is only evident after yielding of the material since the stress increases rapidly for a given increase in strain in the elastic range.

Figure 3.21 shows the stress steps in the plastic range as well as the strain steps in the elastic range for the 80SK-LT sheet steel.

The original stress-strain data were stored by a computer for later use such as plotting the original data (Section III.D.1), fitting the original data with polynomials in order to "smooth" the stress-strain curves (Section III.C.2), and determination of the mechanical properties (Section III.D.2).

2. Statistical Analysis System. In order to negate the effects of the stress and strain steps and thus better represent the actual stress-strain relationship, the Statistical Analysis System (SAS) available through the Computer Center at UMR was used to fit smooth curves to the stress-strain data. The SAS system uses a "least squares" regression technique to obtain a best fit for polynomials. Included in the SAS system output is an R-square value for the chosen polynomial which gives the user an idea of the closeness of the fitted polynomial to the actual stress-strain data. The value of R-square varies from 0 to 1.0. In general, the higher the value of R-square the better the curve fit[55]. For practically all the polynomials used, R-square was greater than 0.90.

For the purpose of curve fitting, each material's stress-strain curve was divided into two or three segments depending on whether the stress-strain curve was gradual or sharp yielding and whether the stress-strain data resulted from compression or tension tests (since the compression tests were only performed to 1.5 percent strain). Each segment of the stress-strain curve was then fitted with a polynomial of appropriate degree to accurately represent the actual stress-strain data.

The entire elastic range of all the stress-strain curves was represented by a straight line. The slope of this line is the modulus of elasticity which is discussed in detail in Section III.D.2.a.

Beyond the elastic range the different stress-strain curves are grouped into four separate categories according to the number and degree of polynomials necessary to represent the actual stress-strain curves. These categories along with their respective types of tests are summarized in Table 3.3. Table 3.3 also lists, for each category, the degree of the second and third (if necessary) curves. Appropriate figures that illustrate the typical range of each SAS curve are also given for each category as well as an example of the resulting polynomial equations for one of the tests.

The polynomial equations were plotted for each curve segment over the approximate ranges shown in part (b) of Figures 3.22 to 3.25. The ends of each curve were then smoothly connected by using a cubic spline that is available through the SAS system.

In an effort to determine an average or "representative" stress-strain curve for each type of test and material, a single curve was

Table 3.3

Summary of SAS Curves

Category	Type of Test	Degree of Curve 2	Degree of Curve 3	Figures Showing Range of Curves	Figures Showing Ex. Polynomial Equations
1	80SK-LT* 80SK-TT** 80DF-LT 80DF-TT 80DK-LT 80DK-TT	3	6	Fig. 3.22(a)	Fig. 3.22(b)
2	80XF-LT 80XF-TT	1	6	Fig. 3.23(a)	Fig. 3.23(b)
3	100XF-LT 100XF-TT 140XF-LT 140XF-TT	6	NONE	Fig. 3.24(a)	Fig. 3.24(b)
4	ALL COMPRESSION TESTS	3	NONE	Fig. 3.25(a)	Fig. 3.25(b)

* LT - longitudinal tension
** TT - transverse tension

fitted to the four individual polynomials over each curve segment. The representative stress-strain curves were treated in exactly the same manner as the individual test stress-strain curves for the purposes of determining representative mechanical properties. The procedure used to obtain the mechanical properties of these sheet steels is described in Section III.D.2.

D. RESULTS

1. Stress-Strain Curves. The original stress-strain data, determined as described in Section III.C, was recalled from computer storage and plotted using the plotting features of the SAS system. Typical examples of the original stress-strain curves are presented in part (a) of Figures 3.22 through 3.25. A complete coverage of all the original stress-strain curves is given in Reference 48. Since these stress-strain curves were determined by dividing the load by the original cross-sectional area of the specimen, they should be regarded as engineering stress-strain curves.

Figures 3.26 through 3.31[48] compare the representative stress-strain curves in each of the tested directions (i.e. LT, TT, LC, TC) for each material. Upon inspection of these curves it can be seen that high strength sheet steels are quite anisotropic with the transverse direction almost always stronger than the longitudinal direction.

The representative stress-strain curves for all the materials in a given test direction are presented in Figures 3.32 through 3.35[48]. Inspection of these figures shows the wide range in ductility and strength in the six different sheet steels tested.

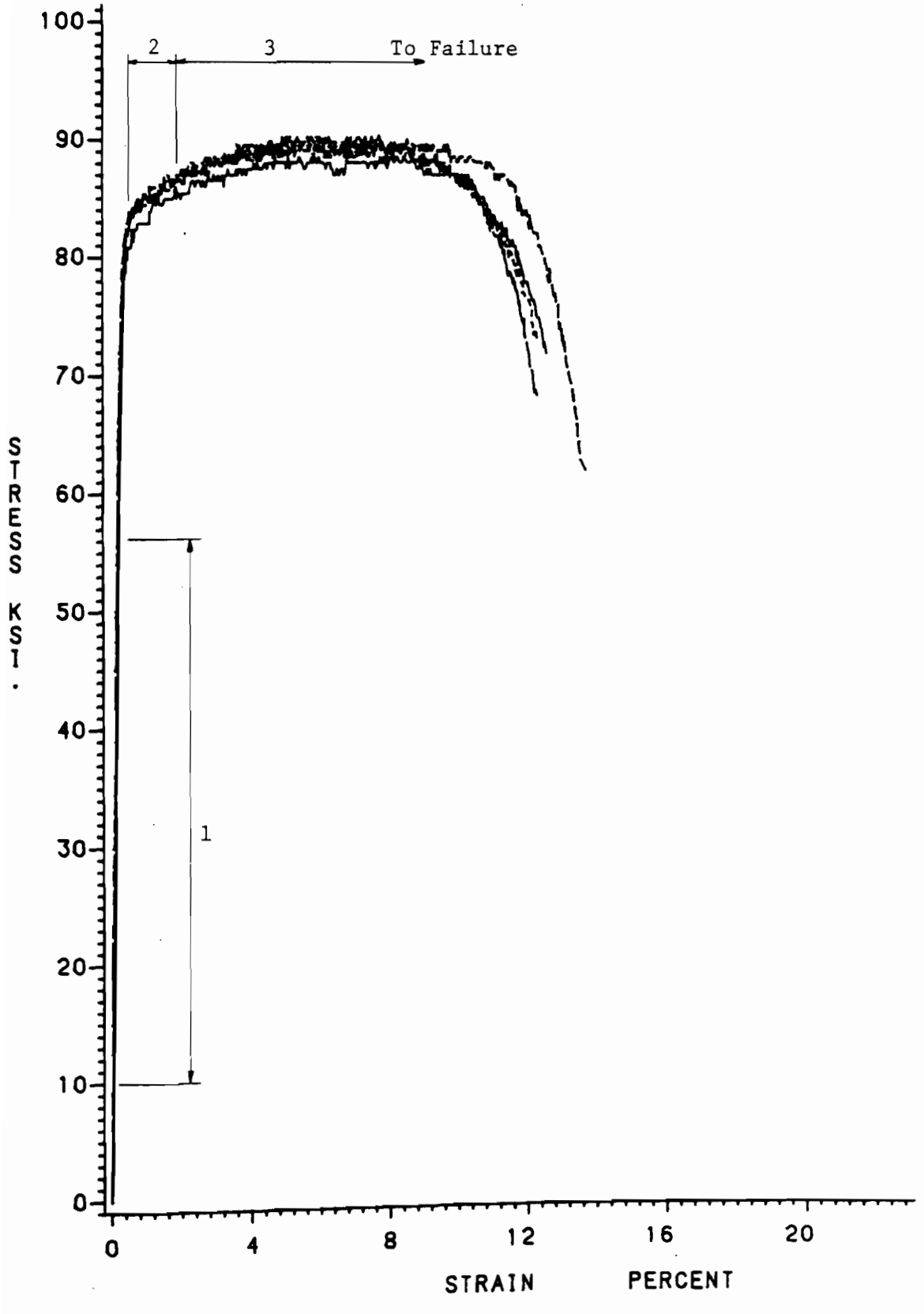

Fig. 3.22(a) Individual Stress-Strain Curve for 80SK-LT

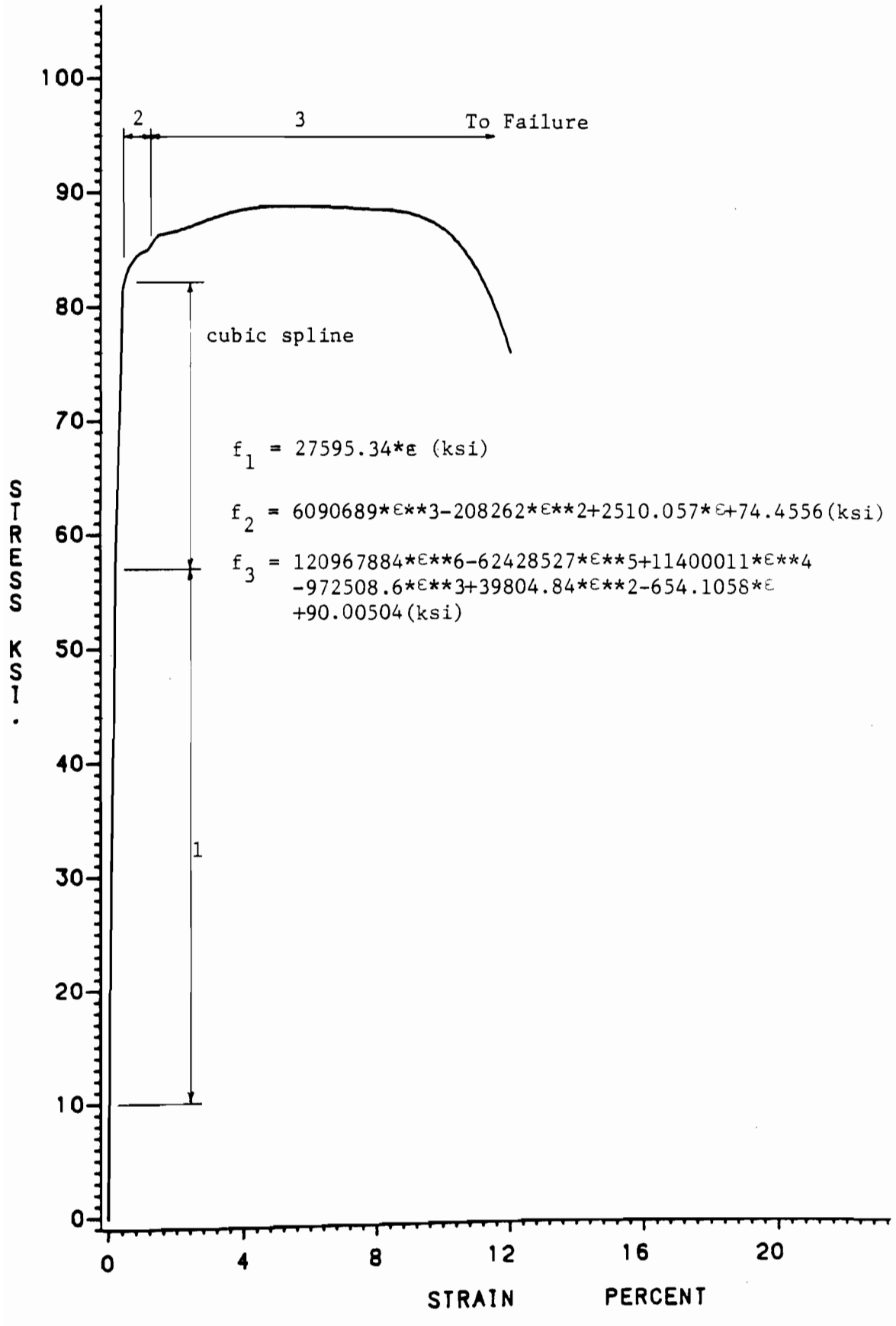

Fig. 3.22(b) Stress-Strain Curve for 80SK-LT-2

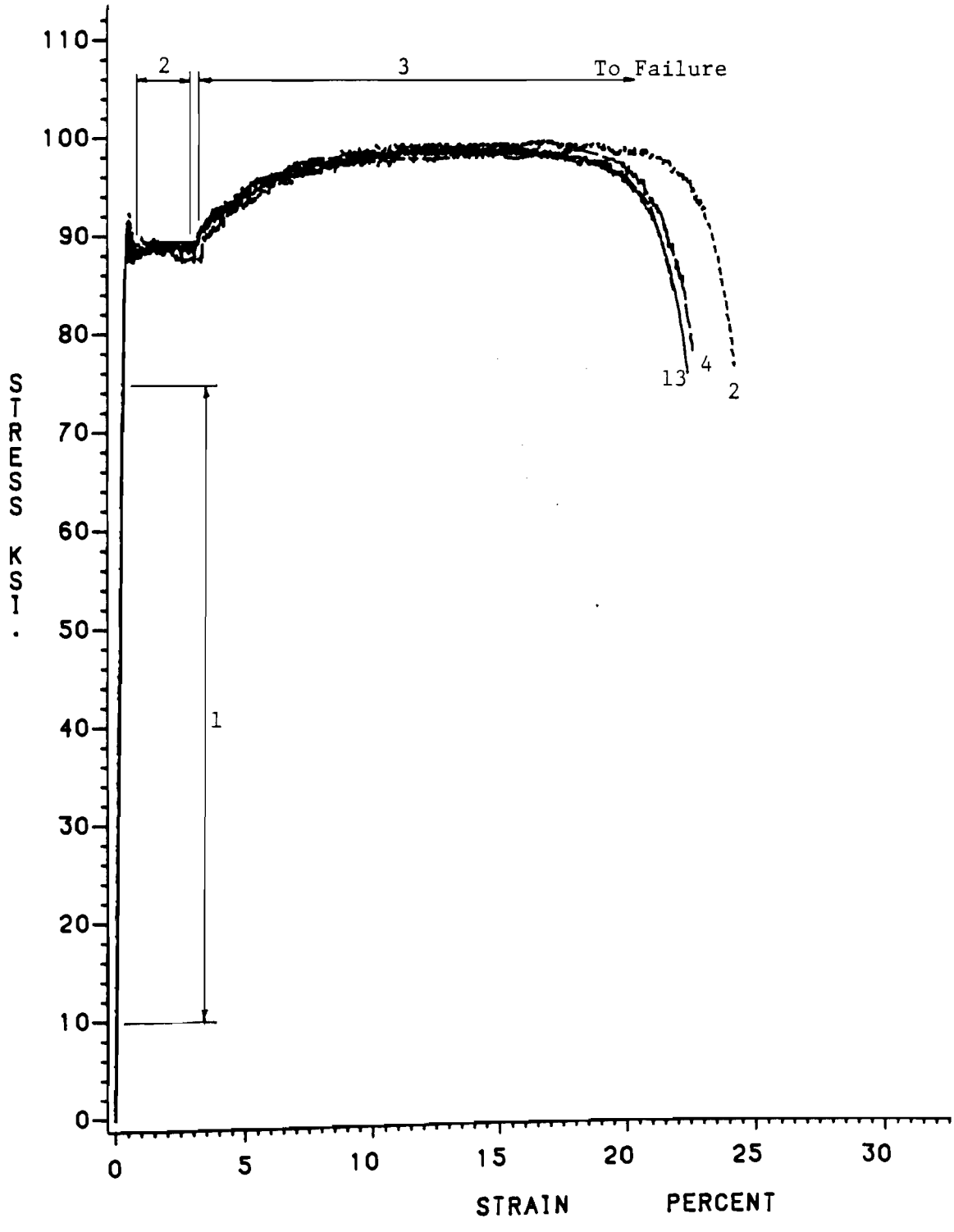

Fig. 3.23(a) Individual Stress-Strain Curve for 80XF-LT

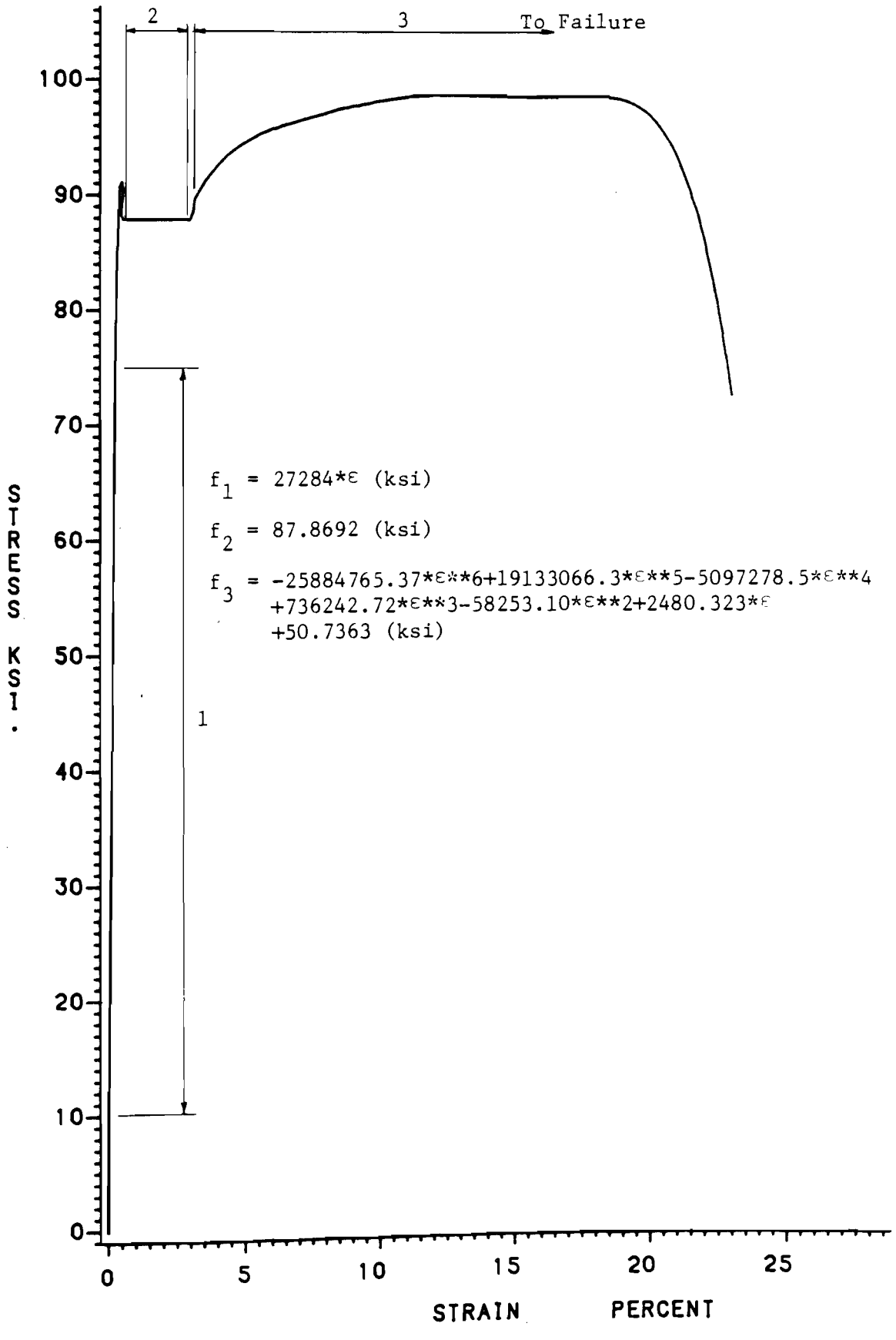

Fig. 3.23(b) Stress-Strain Curve for 80XF-LT-4

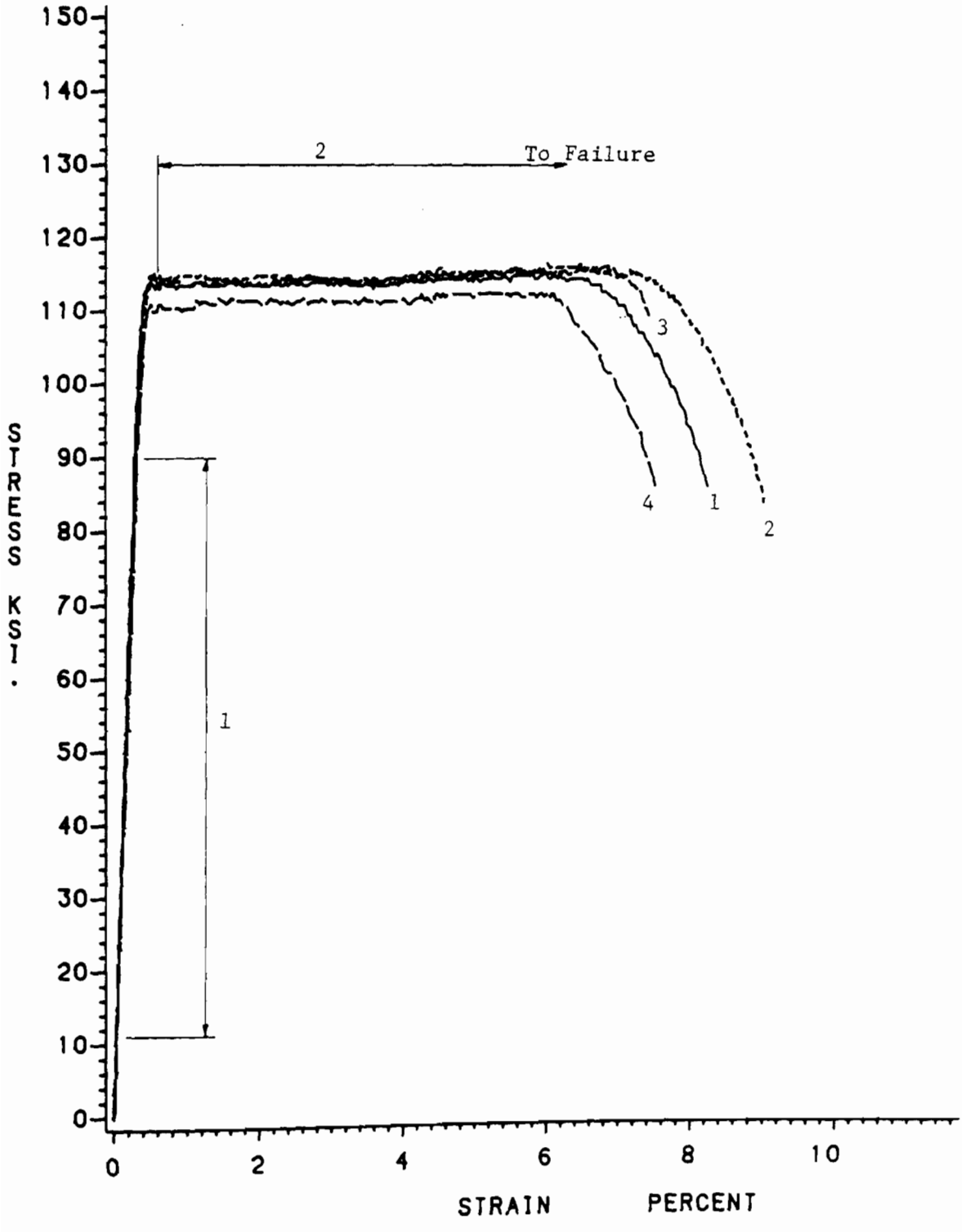

Fig. 3.24(a) Individual Stress-Strain Curve for 100XF-LT

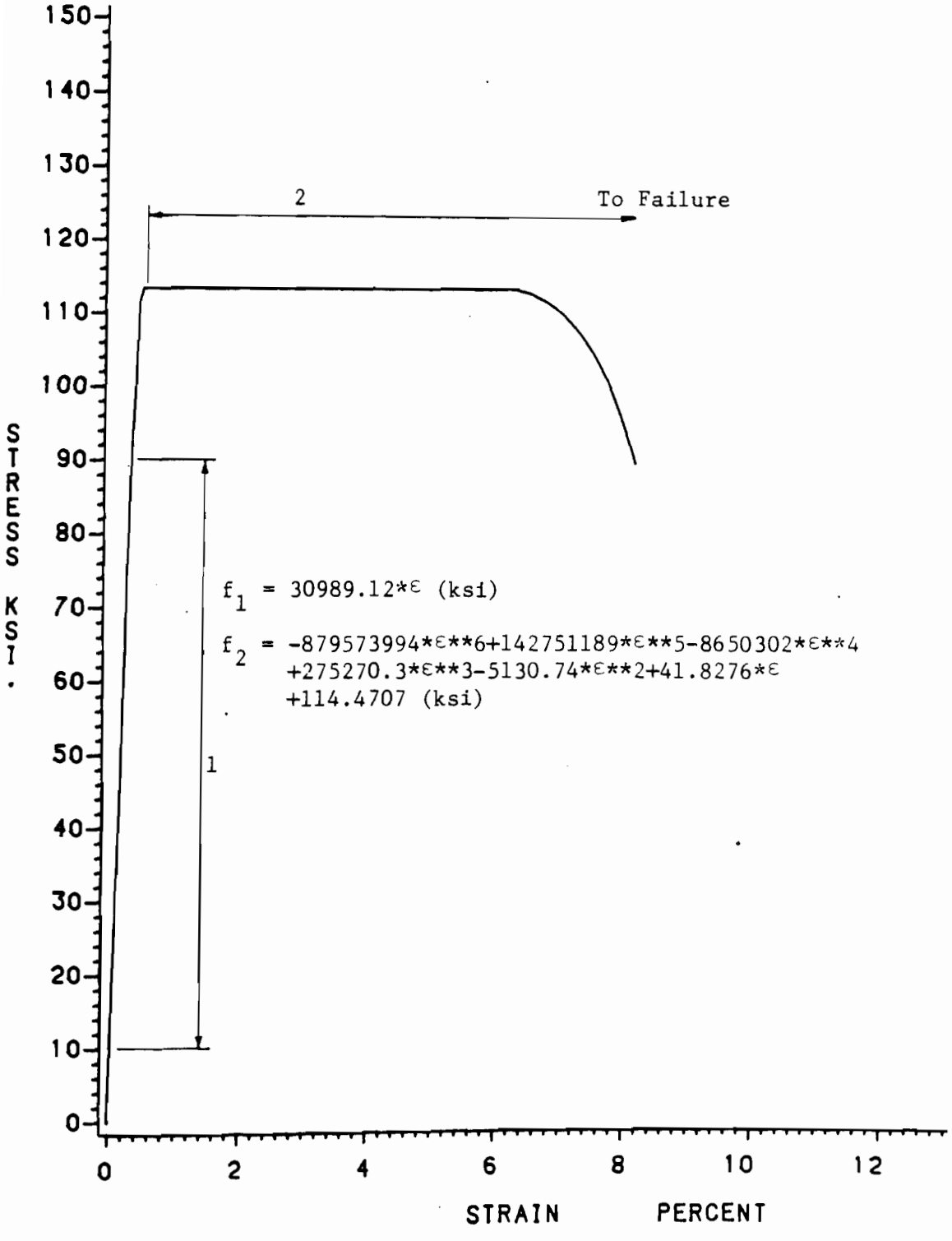

Fig. 3.24(b) Stress-Strain Curve for 100XF-LT-1

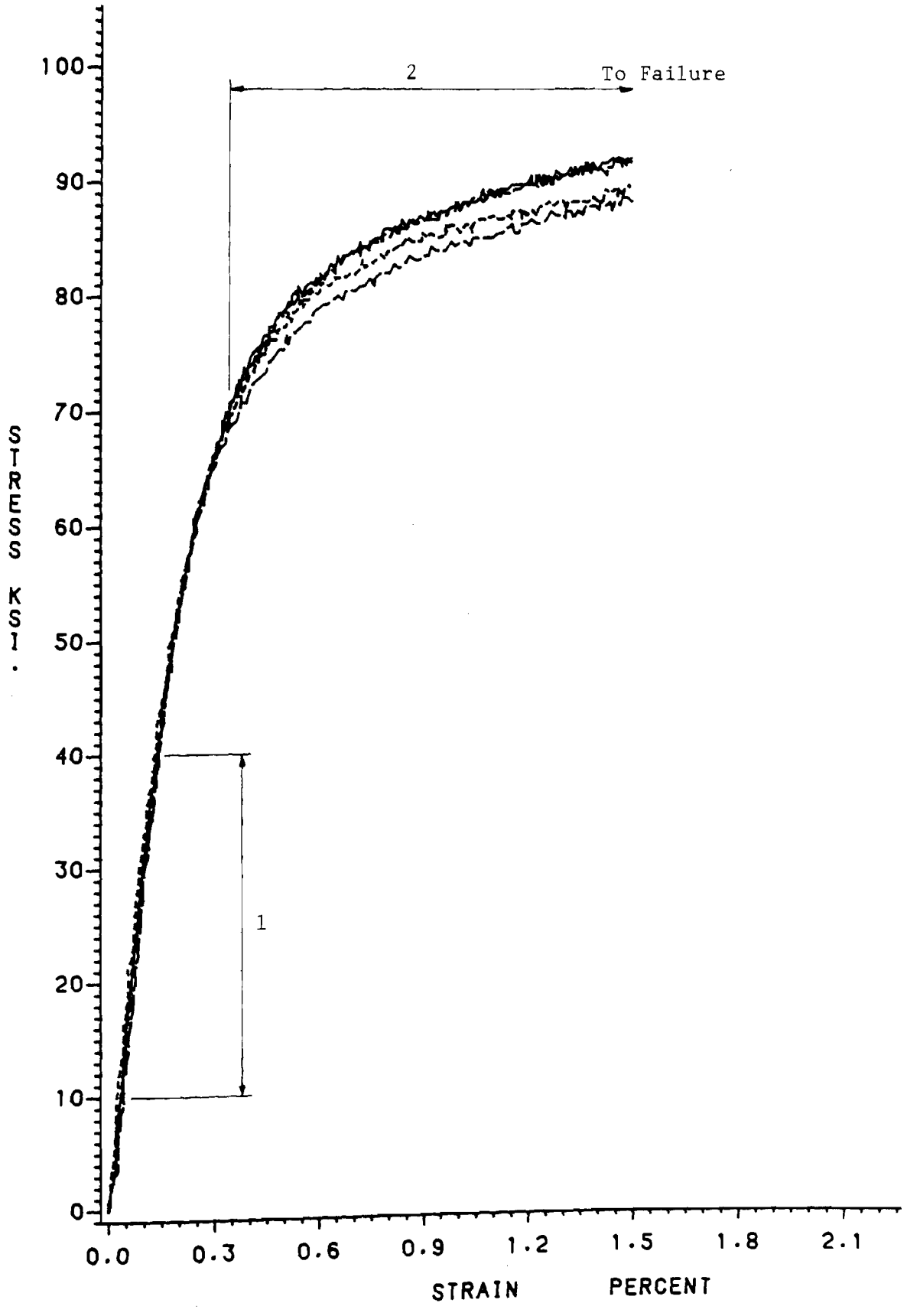

Fig. 3.25(a) Individual Stress-Strain Curve for 80SK-LC

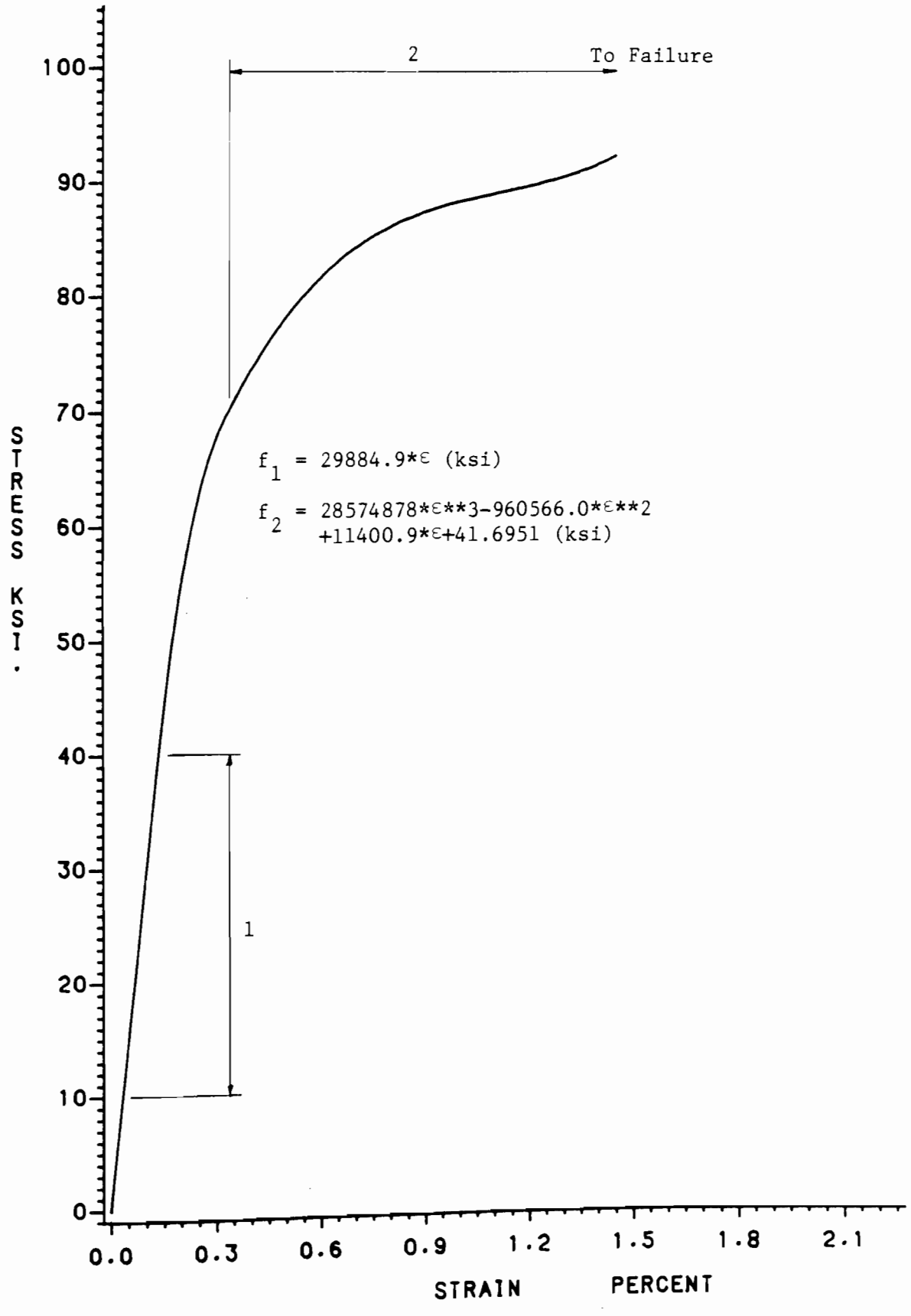

Fig. 3.25(b) Stress-Strain Curve for 80SK-LC-1

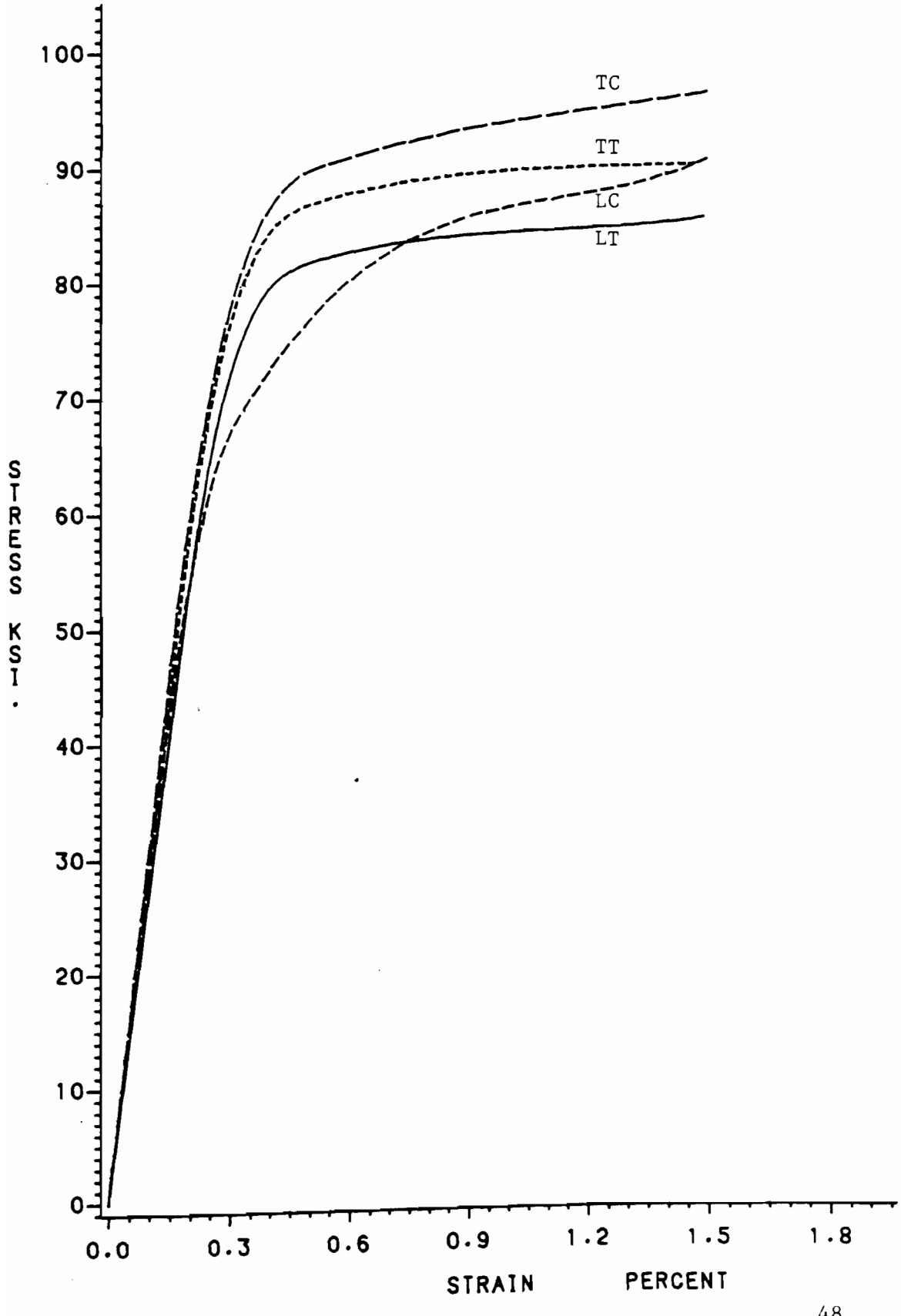

Fig. 3.26 Comparison of Various Tests for 80SK[48]

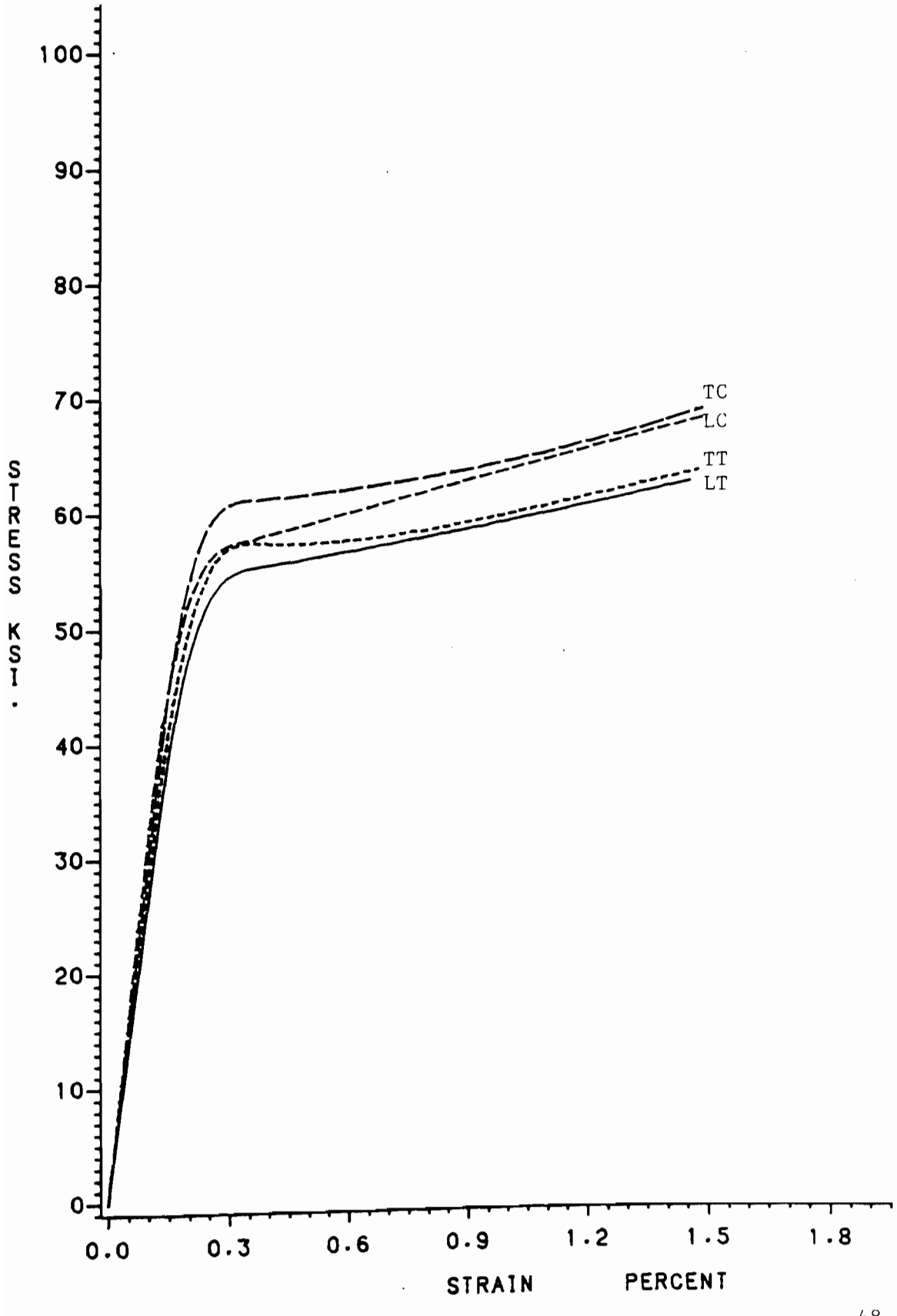

Fig. 3.27 Comparison of Various Tests for 80DF[48]

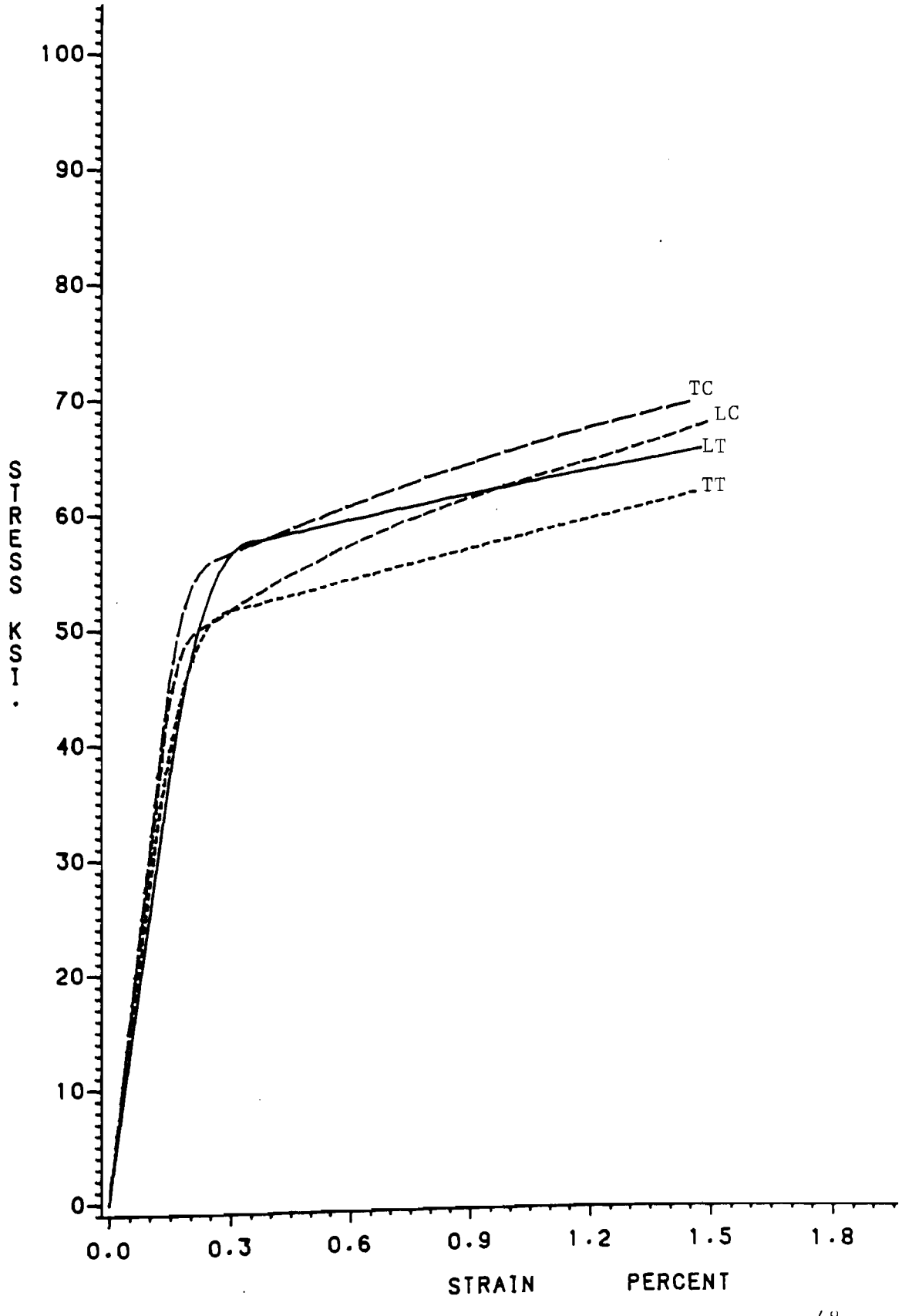

Fig. 3.28 Comparison of Various Tests for 80DK[48]

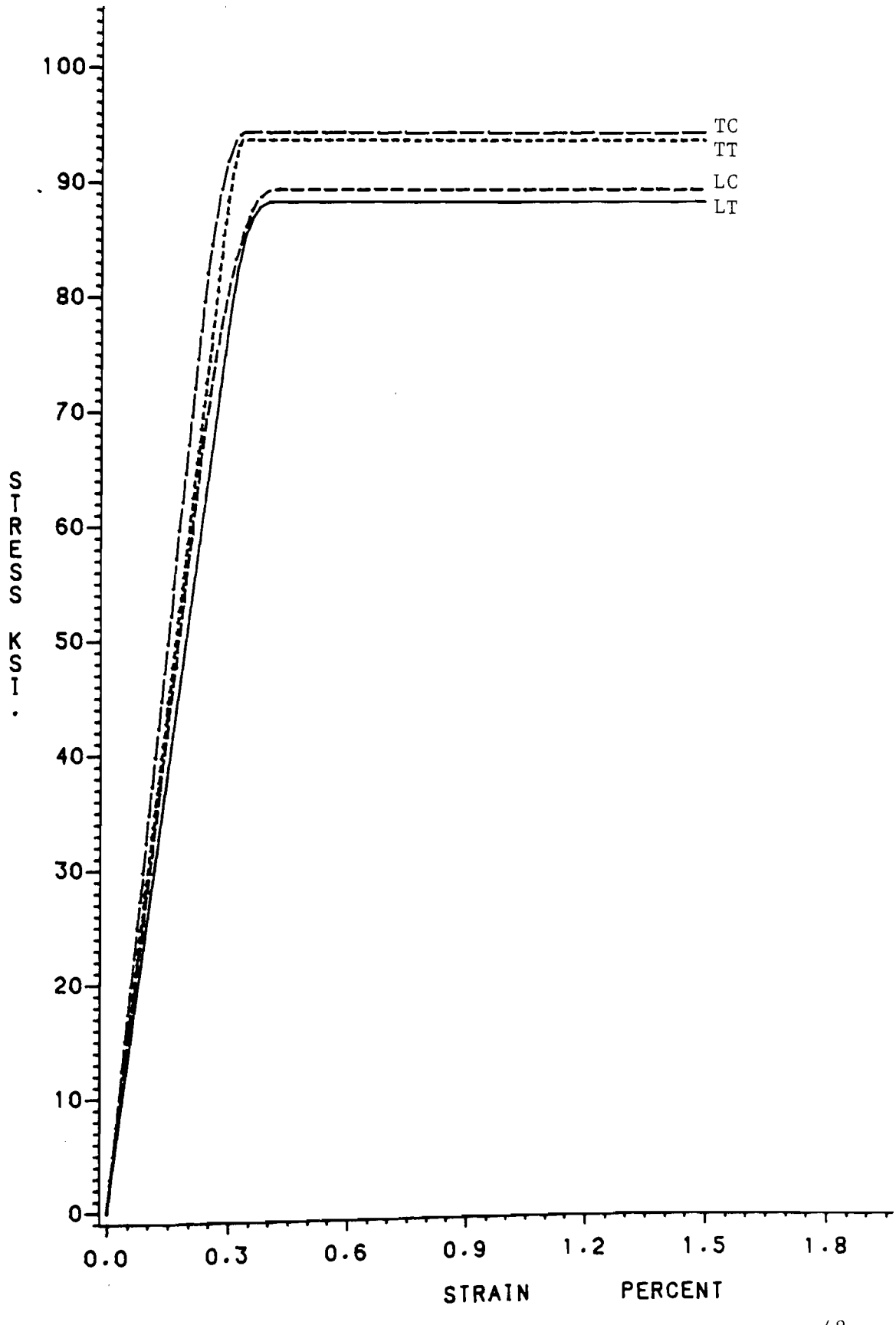

Fig. 3.29 Comparison of Various Tests for 80XF[48]

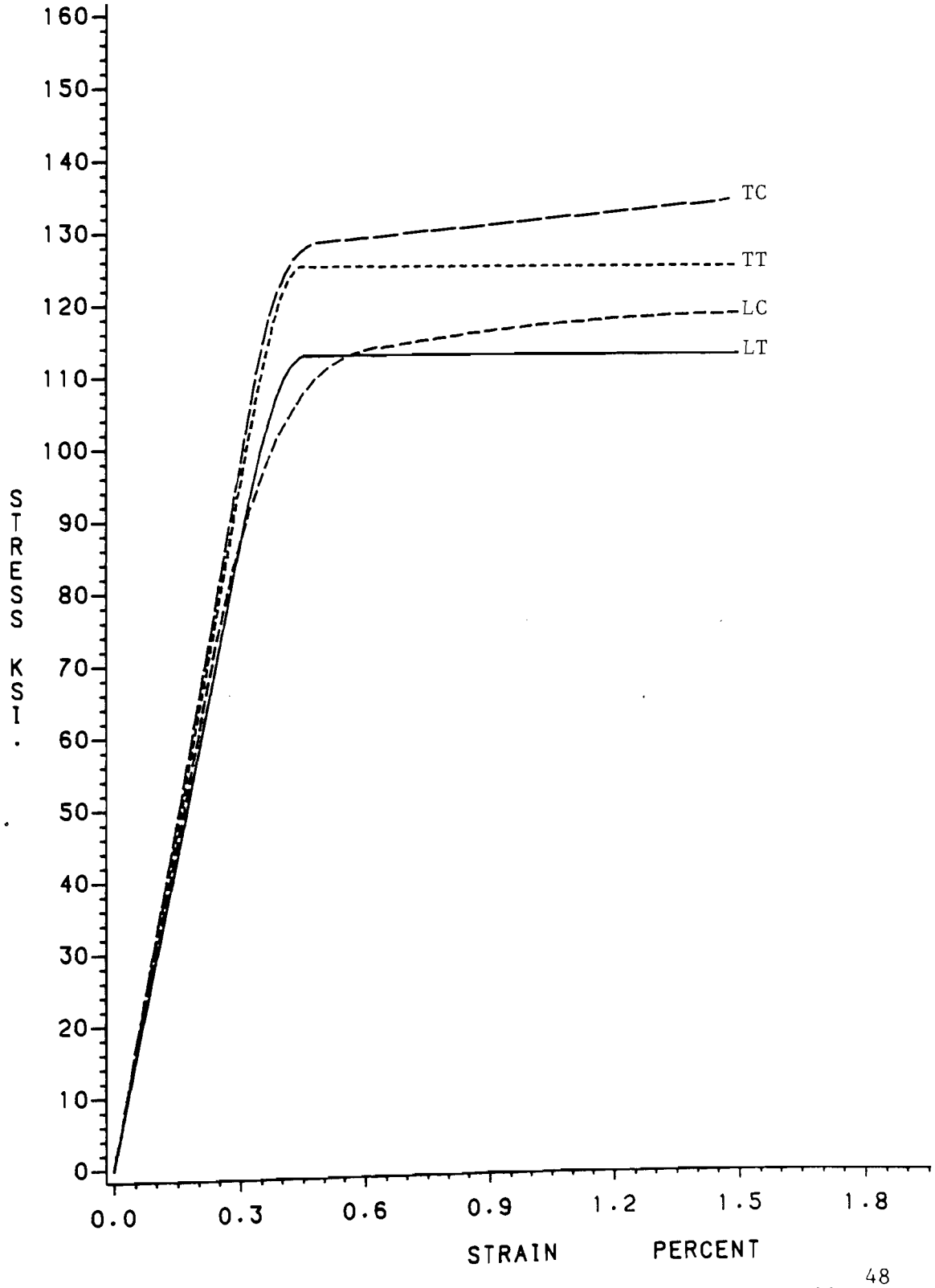

Fig. 3.30 Comparison of Various Tests for 100XF[48]

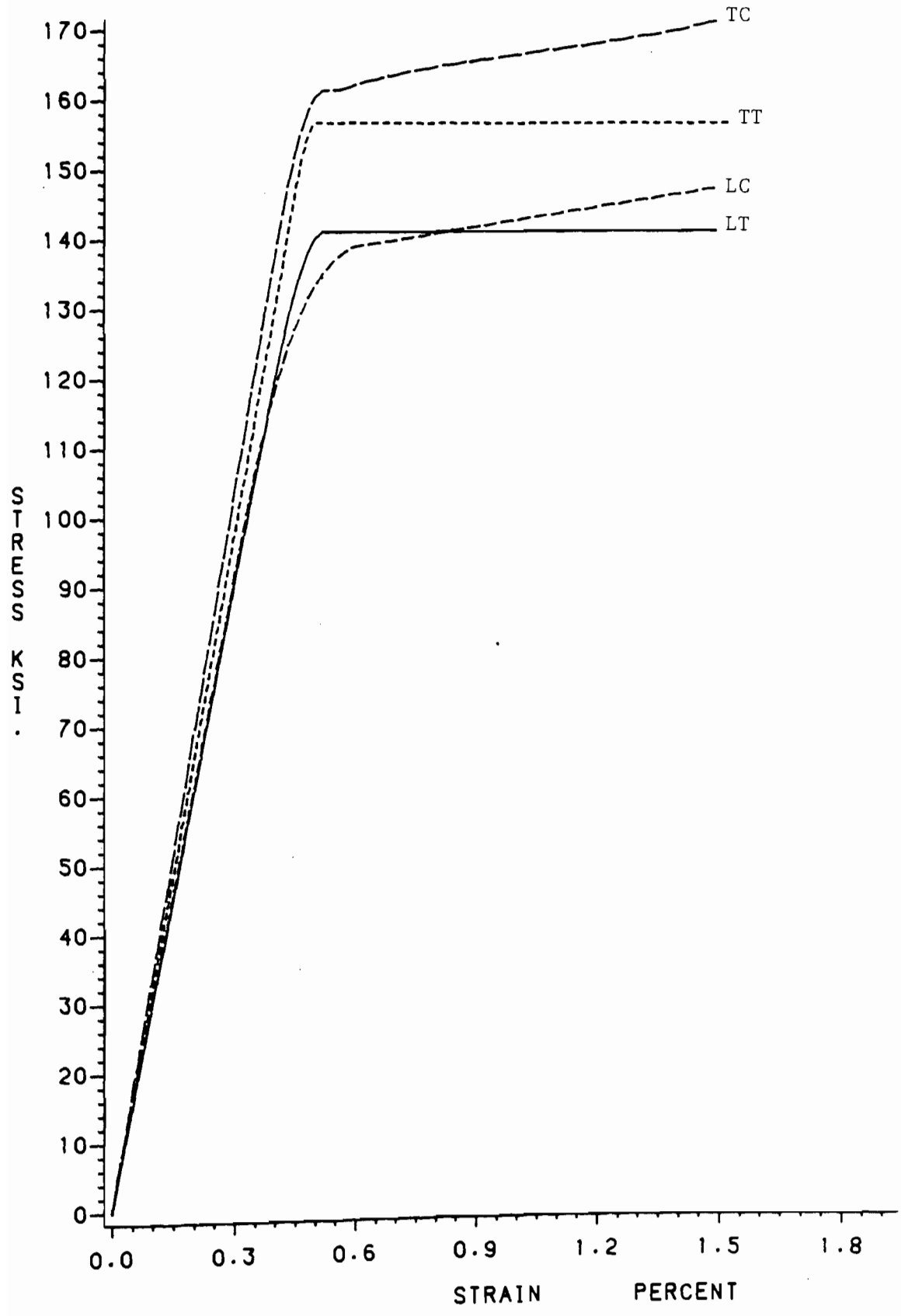

Fig. 3.31 Comparison of Various Tests for 140XF[48]

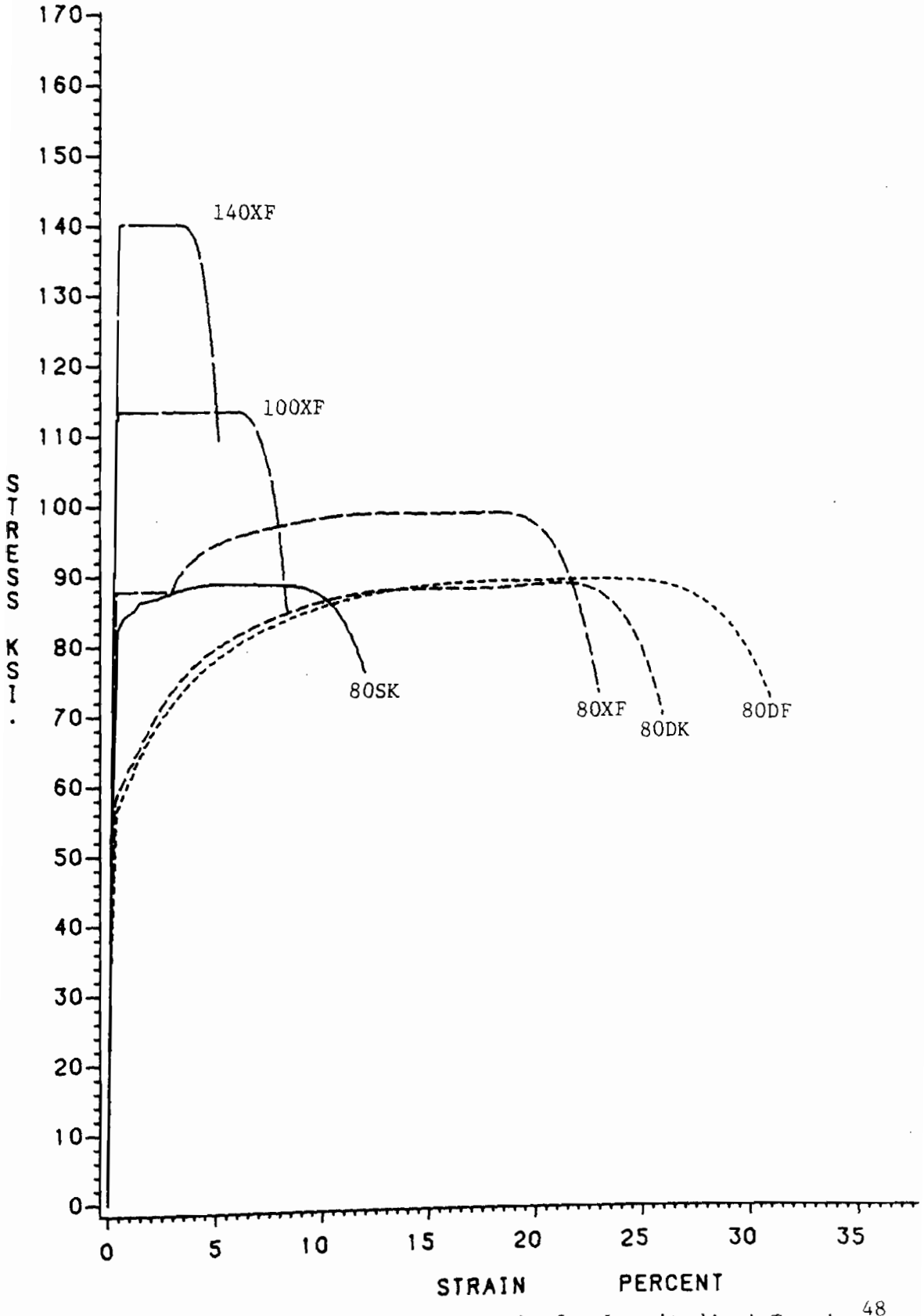

Fig. 3.32 Comparison of Six Sheet Steels for Longitudinal Tension[48]

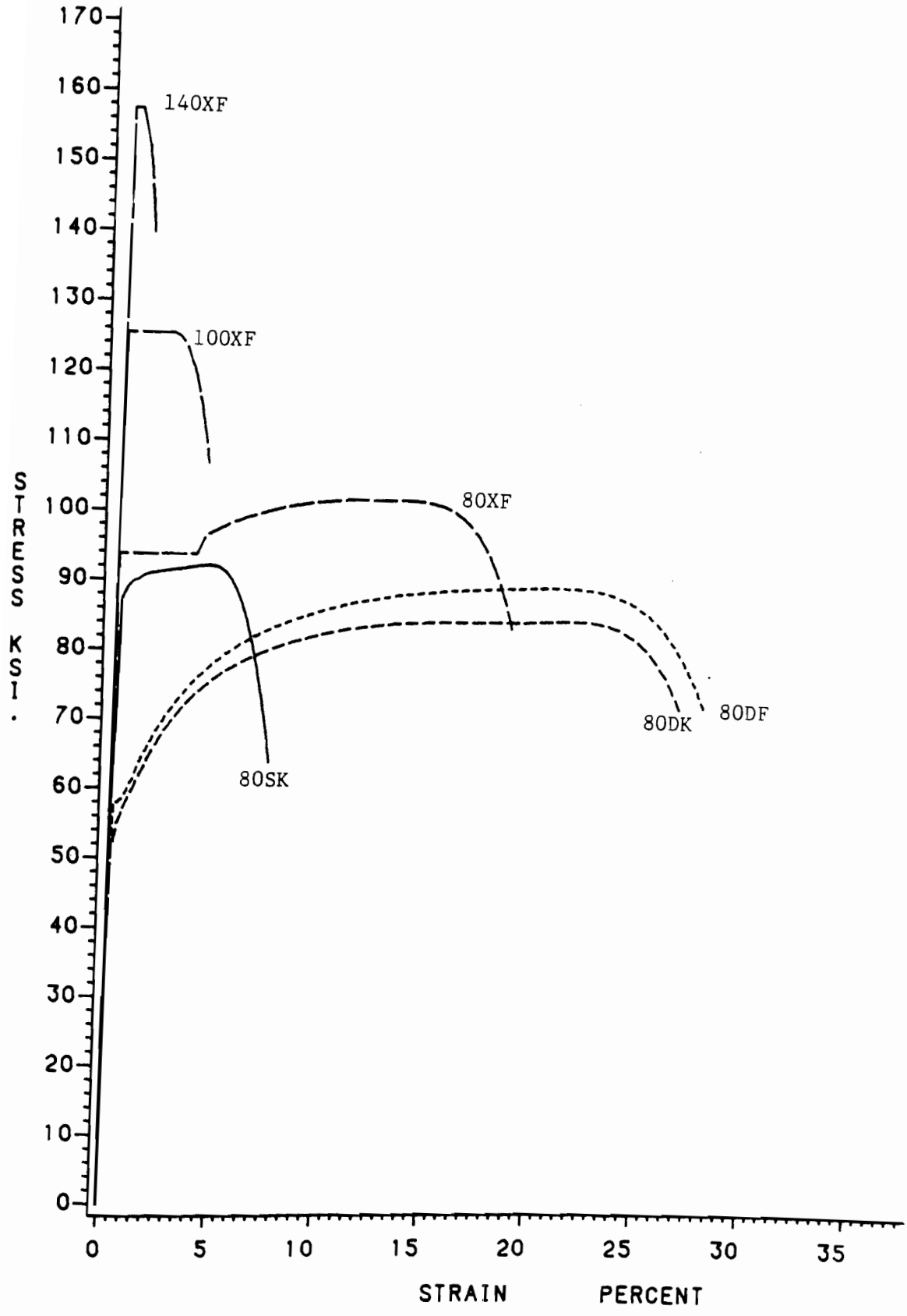

Fig. 3.33 Comparison of Six Sheet Steels for Transverse Tension[48]

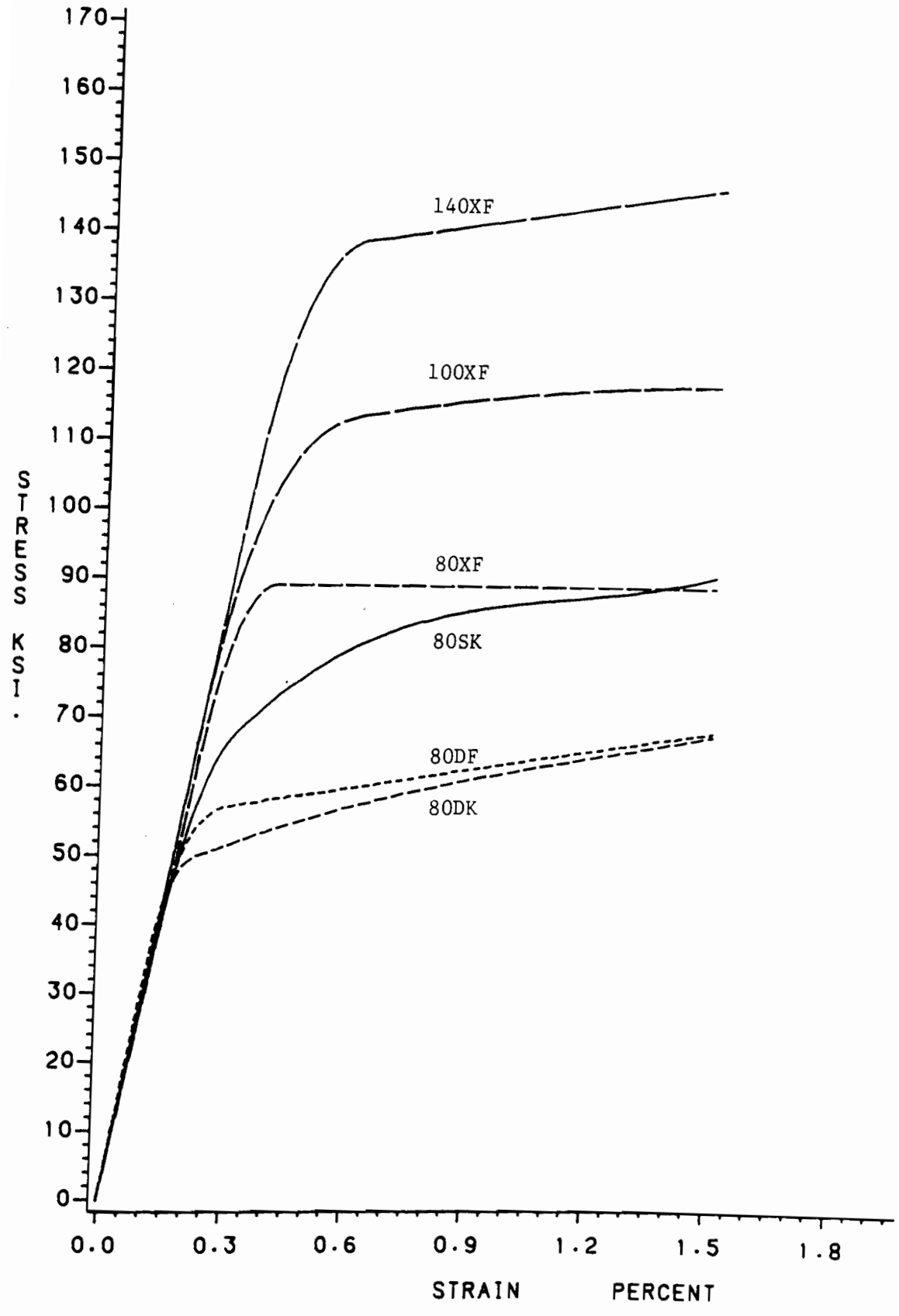

Fig. 3.34 Comparison of Six Sheet Steels for Longitudinal Compression[48]

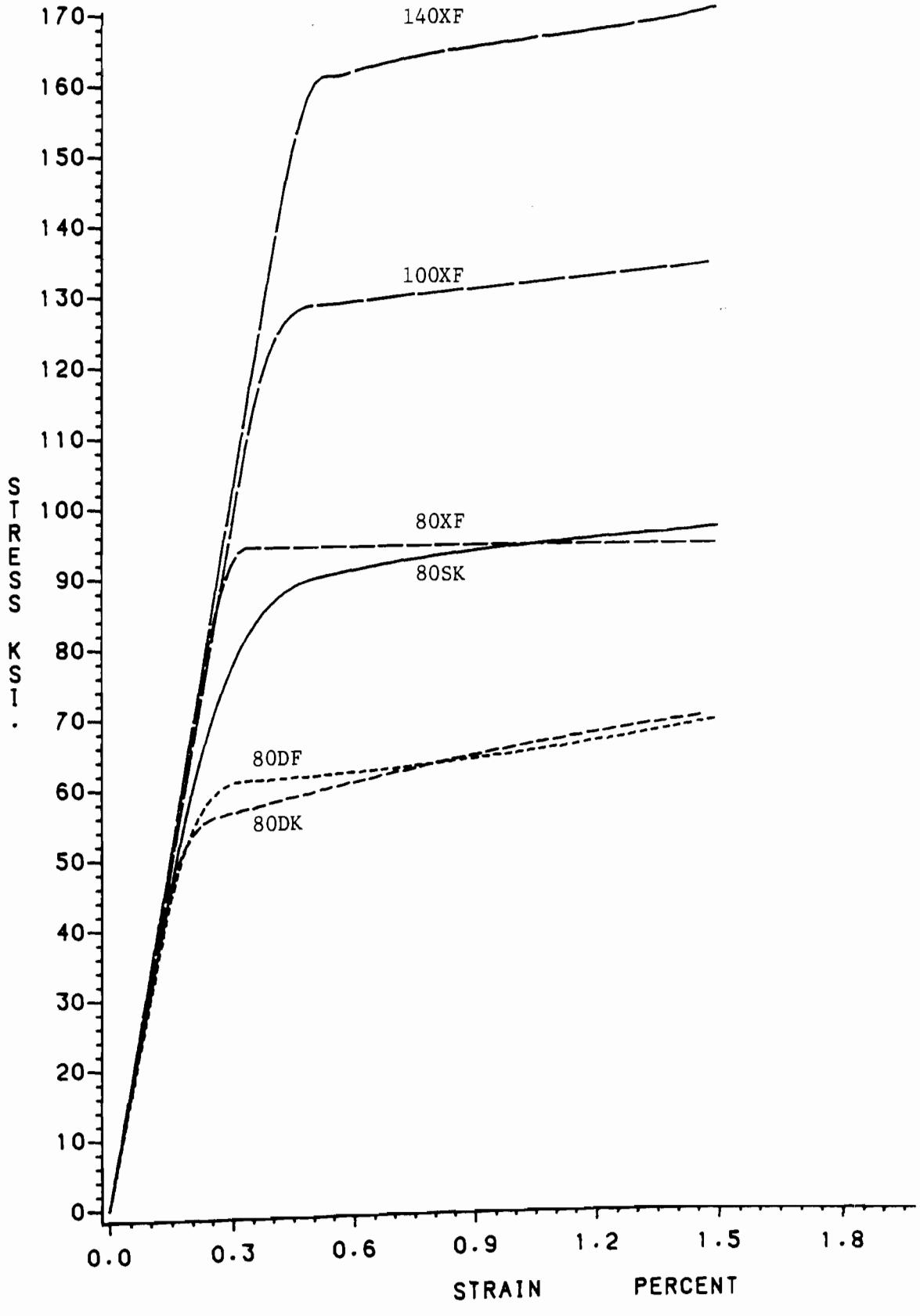

Fig. 3.35 Comparison of Six Sheet Steels for Transverse Compression[48]

2. Mechanical Properties. Included in Sections III.D.2.a through III.D.2.e is a detailed description of the procedures employed to determine the mechanical properties of each sheet steel for each type of test (i.e. LT, TT, LC, TC). The mechanical properties so determined are the modulus of elasticity, proportional limit, yield point, tensile strength and ductility. These properties are presented in Tables 3.4 through 3.9 for each individual test as well as for the representative curves. The average mechanical properties for each type of sheet steel are summarized in Table 3.10. These tables were originally presented in Reference 48.

a. Modulus of Elasticity. The modulus of elasticity is an important property in the design of cold-formed, sheet steel components since their load carrying capacity is often limited by buckling or other stiffness considerations[56].

In a recent study published by Venkataramaiah et al.[56] on the modulus of elasticity of ASTM-A446 galvanized sheet steel, the mean value of modulus of elasticity for 63 specimens was found to be 30,071 ksi with a standard deviation of 658 ksi and a coefficient of variation of 0.022. The tested A446 steel was of Grades A, B, C, or D and ranged in thickness from 8 to 30 gauge.

In this study, values of modulus of elasticity were determined for the six different sheet steels by extracting a portion of the original stress-strain data that was obviously in the elastic range of the material and then using the SAS system (described in Section III.C.2) to fit a straight line to this data. The slope of this line is, by definition, the modulus of elasticity. The range of the extracted

Table 3.4a

Tested Mechanical Properties of 80SK Sheet Steel
Longitudinal Tension

Test No.	$(F_{pr})_1$ (ksi)	$(F_{pr})_2$ (ksi)	F_y (ksi)	$\frac{(F_{pr})_1}{F_y}$	$\frac{(F_{pr})_2}{F_y}$	F_u (ksi)	Elongation in 2-in. Gage Length (percent)	Modulus of Elasticity (ksi)	Type of Stress-Strain Curve*
LT-1	55.9	62.6	80.9	0.69	0.77	87.6	12.6	26,347	G.Y.
LT-2	58.8	67.1	82.7	0.71	0.81	88.7	12.3	27,595	G.Y.
LT-3	53.9	63.7	83.0	0.65	0.77	89.2	13.7	27,550	G.Y.
LT-4	54.9	64.0	82.3	0.67	0.78	89.7	12.3	27,006	G.Y.
Ave. Value	55.9	64.4	82.2	0.68	0.78	88.8	12.7	27,131	N/A
Representative Curve	55.2	64.2	82.0	0.67	0.78	88.7	12.3	27,131	G.Y.

Table 3.4b

Tested Mechanical Properties of 80SK Sheet Steel
Transverse Tension

Test No.	$(F_{pr})_1$ (ksi)	$(F_{pr})_2$ (ksi)	F_y (ksi)	$\frac{(F_{pr})_1}{F_y}$	$\frac{(F_{pr})_2}{F_y}$	F_u (ksi)	Elongation in 2-in. Gage Length (percent)	Modulus of Elasticity (ksi)	Type of Stress-Strain Curve*
TT-1	56.7	67.0	87.0	0.65	0.77	91.6	6.0	29,457	G.Y.
TT-2	60.6	69.8	87.2	0.69	0.80	92.7	7.5	31,067	G.Y.
TT-3	53.3	64.3	87.0	0.61	0.74	92.0	7.4	32,327	G.Y.
TT-4	55.2	64.8	87.0	0.63	0.74	92.1	8.4	27,902	G.Y.
Ave. Value	56.5	66.5	87.1	0.65	0.76	92.1	7.3	30,188	N/A
Representative Curve	54.1	65.1	87.0	0.62	0.75	92.0	7.4	30,188	G.Y.

* G.Y. = Gradual Yielding

Table 3.4c

Tested Mechanical Properties of 80SK Sheet Steel
Longitudinal Compression

Test No.	$(F_{pr})_1$ (ksi)	$(F_{pr})_2$ (ksi)	F_y (ksi)	$\frac{(F_{pr})_1}{F_y}$	$\frac{(F_{pr})_2}{F_y}$	Modulus of Elasticity (ksi)	Type of Stress-Strain Curve*
LC-1	43.2	52.9	76.2	0.57	0.69	29,885	G.Y.
LC-2	41.8	51.5	75.0	0.56	0.69	28,570	G.Y.
LC-3	43.0	53.5	76.7	0.56	0.70	27,481	G.Y.
LC-4	45.8	54.2	73.7	0.62	0.74	29,988	G.Y.
Ave. Value	43.5	53.0	75.4	0.58	0.70	28,981	N/A
Representative Curve	41.8	52.5	75.6	0.55	0.69	28,981	G.Y.

Table 3.4d

Tested Mechanical Properties of 80SK Sheet Steel
Transverse Compression

Test No.	$(F_{pr})_1$ (ksi)	$(F_{pr})_2$ (ksi)	F_y (ksi)	$\frac{(F_{pr})_1}{F_y}$	$\frac{(F_{pr})_2}{F_y}$	Modulus of Elasticity (ksi)	Type of Stress-Strain Curve*
TC-1	51.7	63.1	90.0	0.57	0.70	30,888	G.Y.
TC-2	50.5	61.9	90.2	0.56	0.69	31,691	G.Y.
TC-3	53.4	64.3	89.5	0.60	0.72	32,000	G.Y.
TC-4	54.9	65.7	89.2	0.62	0.74	29,459	G.Y.
Ave. Value	52.6	63.8	89.7	0.59	0.71	31,010	N/A
Representative Curve	52.2	63.3	89.9	0.58	0.70	31,010	G.Y.

*G.Y. = Gradual Yielding

Table 3.5a

Tested Mechanical Properties of 80DF Sheet Steel
Longitudinal Tension

Test No.	$(F_{pr})_1$ (ksi)	$(F_{pr})_2$ (ksi)	F_y (ksi)	$\frac{(F_{pr})_1}{F_y}$	$\frac{(F_{pr})_2}{F_y}$	F_u (ksi)	Elongation in 2-in. Gage Length (percent)	Modulus of Elasticity (ksi)	Type of Stress-Strain Curve*
LT-1	38.3	46.9	55.2	0.69	0.85	89.0	33.3	27,146	S.Y.
LT-2	38.7	47.2	56.5	0.68	0.84	87.9	30.8	28,695	S.Y.
LT-3	35.2	43.4	56.8	0.62	0.76	88.6	31.3	23,670**	S.Y.
LT-4	36.0	44.1	54.8	0.66	0.80	89.8	30.1	28,079	S.Y.
Ave. Value	37.1	45.4	55.8	0.66	0.81	88.8	31.4	27,973	N/A
Representative Curve	36.5	44.4	55.8	0.65	0.80	88.6	31.3	27,973	S.Y.

Table 3.5b

Tested Mechanical Properties of 80DF Sheet Steel
Transverse Tension

Test No.	$(F_{pr})_1$ (ksi)	$(F_{pr})_2$ (ksi)	F_y (ksi)	$\frac{(F_{pr})_1}{F_y}$	$\frac{(F_{pr})_2}{F_y}$	F_u (ksi)	Elongation in 2-in. Gage Length (percent)	Modulus of Elasticity (ksi)	Type of Stress-Strain Curve*
TT-1	37.6	46.2	58.0	0.65	0.80	88.8	28.1	29,156	S.Y.
TT-2	37.2	46.5	57.1	0.65	0.81	88.6	28.8	29,599	S.Y.
TT-3	36.3	44.8	57.1	0.64	0.78	89.3	27.1	27,587	S.Y.
TT-4	37.7	46.8	57.3	0.66	0.82	89.0	28.3	27,789	S.Y.
Ave. Value	37.2	46.1	57.4	0.65	0.80	88.9	28.1	28,532	N/A
Representative Curve	36.3	45.7	57.3	0.63	0.80	88.8	28.1	28,532	S.Y.

* S.Y. = Sharp Yielding ** This value was not used in the calculation of the average value.

Table 3.5c

Tested Mechanical Properties of 80DF Sheet Steel
Longitudinal Compression

Test No.	$(F_{pr})_1$ (ksi)	$(F_{pr})_2$ (ksi)	F_y (ksi)	$\frac{(F_{pr})_1}{F_y}$	$\frac{(F_{pr})_2}{F_y}$	Modulus of Elasticity (ksi)	Type of Stress-Strain Curve*
LC-1	32.2	42.6	58.3	0.55	0.73	32,505	G.Y.
LC-2	34.9	44.0	58.8	0.59	0.75	31,493	G.Y.
LC-3	32.9	42.9	57.3	0.57	0.75	33,627	G.Y.
LC-4	33.9	43.9	57.3	0.59	0.77	31,872	G.Y.
Ave. Value	33.5	43.4	57.9	0.58	0.75	32,374	N/A
Representative Curve	35.4	43.4	58.0	0.61	0.75	32,374	G.Y.

Table 3.5d

Tested Mechanical Properties of 80DF Sheet Steel
Transverse Compression

Test No.	$(F_{pr})_1$ (ksi)	$(F_{pr})_2$ (ksi)	F_y (ksi)	$\frac{(F_{pr})_1}{F_y}$	$\frac{(F_{pr})_2}{F_y}$	Modulus of Elasticity (ksi)	Type of Stress-Strain Curve*
TC-1	43.0	51.5	60.4	0.71	0.85	29,517	G.Y.
TC-2	40.2	50.0	61.4	0.65	0.81	31,781	G.Y.
TC-3	43.8	52.5	64.2	0.68	0.82	31,395	G.Y.
TC-4	38.0	46.9	59.9	0.63	0.78	28,611	G.Y.
Ave. Value	41.3	50.2	61.5	0.67	0.82	30,326	N/A
Representative Curve	42.2	50.3	61.3	0.69	0.82	30,326	G.Y.

* G.Y. = Gradual Yielding

Table 3.6a

Tested Mechanical Properties of 80DK Sheet Steel
Longitudinal Tension

Test No.	$(F_{pr})_1$ (ksi)	$(F_{pr})_2$ (ksi)	F_y (ksi)	$\frac{(F_{pr})_1}{F_y}$	$\frac{(F_{pr})_2}{F_y}$	F_u (ksi)	Elongation in 2-in. Gage Length (percent)	Modulus of Elasticity (ksi)	Type of Stress-Strain Curve*
LT-1	37.2	45.0	57.8	0.64	0.78	87.5	24.8	26,229	G.Y.
LT-2	37.9	46.2	58.2	0.65	0.79	87.6	26.5	25,365	G.Y.
LT-3	38.7	47.1	58.8	0.66	0.80	87.8	25.5	24,227	G.Y.
LT-4	37.4	45.7	58.0	0.64	0.79	87.5	26.0	27.104	G.Y.
Ave. Value	37.8	46.0	58.2	0.65	0.79	87.6	25.7	25,731	N/A
Representative Curve	38.4	46.0	58.1	0.66	0.79	87.8	25.5	25,731	G.Y.

Table 3.6b

Tested Mechanical Properties of 80DK Sheet Steel
Transverse Tension

Test No.	$(F_{pr})_1$ (ksi)	$(F_{pr})_2$ (ksi)	F_y (ksi)	$\frac{(F_{pr})_1}{F_y}$	$\frac{(F_{pr})_2}{F_y}$	F_u (ksi)	Elongation in 2-in. Gage Length (percent)	Modulus of Elasticity (ksi)	Type of Stress-Strain Curve*
TT-1	34.0	41.1	50.0	0.68	0.82	81.8	24.2	29,610	G.Y.
TT-2	32.3	38.9	49.2	0.66	0.79	80.9	25.2	25,129	G.Y.
TT-3	33.1	41.4	53.3	0.62	0.78	84.4	27.1	27,612	G.Y.
TT-4	36.7	44.3	55.3	0.66	0.80	88.0	26.6	33,685**	G.Y.
Ave. Value	34.0	41.4	52.0	0.66	0.80	83.8	25.8	27,450	N/A
Representative Curve	33.4	41.4	52.6	0.63	0.79	84.4	27.1	27,450	G.Y.

* G.Y. = Gradual Yielding ** This value was not used in the calculation of the average value.

Table 3.6c

Tested Mechanical Properties of 80DK Sheet Steel
Longitudinal Compression

Test No.	$(F_{pr})_1$ (ksi)	$(F_{pr})_2$ (ksi)	F_y (ksi)	$\frac{(F_{pr})_1}{F_y}$	$\frac{(F_{pr})_2}{F_y}$	Modulus of Elasticity (ksi)	Type of Stress-Strain Curve*
LC-1	40.7	46.9	56.5	0.72	0.83	28,098	G.Y.
LC-2	40.1	45.9	53.1	0.76	0.86	30,530	G.Y.
LC-3	37.3	44.0	53.2	0.70	0.83	32,173	G.Y.
LC-4	41.1	46.6	53.5	0.77	0.87	30,405	G.Y.
Ave. Value	39.8	45.9	54.1	0.74	0.85	30,302	N/A
Representative Curve	41.1	46.1	53.5	0.77	0.86	30,302	G.Y.

Table 3.6d

Tested Mechanical Properties of 80DK Sheet Steel
Transverse Compression

Test No.	$(F_{pr})_1$ (ksi)	$(F_{pr})_2$ (ksi)	F_y (ksi)	$\frac{(F_{pr})_1}{F_y}$	$\frac{(F_{pr})_2}{F_y}$	Modulus of Elasticity (ksi)	Type of Stress-Strain Curve*
TC-1	41.2	48.4	59.5	0.69	0.81	31,836	G.Y.
TC-2	38.5	45.6	56.9	0.68	0.80	29,657	G.Y.
TC-3	43.6	49.8	56.7	0.77	0.88	32,131	G.Y.
TC-4	46.8	52.7	58.9	0.79	0.89	31,821	G.Y.
Ave. Value	42.5	49.1	58.0	0.73	0.85	31,361	N/A
Representative Curve	43.5	49.3	57.8	0.75	0.85	31,361	G.Y.

* G.Y. = Gradual Yielding

Table 3.7a

Tested Mechanical Properties of 80XF Sheet Steel
Longitudinal Tension

Test No.	$(F_{pr})_1$ (ksi)	$(F_{pr})_2$ (ksi)	F_y (ksi)	$\frac{(F_{pr})_1}{F_y}$	$\frac{(F_{pr})_2}{F_y}$	F_u (ksi)	Elongation in 2-in. Gage Length(percent)	Modulus of Elasticity (ksi)	Type of Stress-Strain Curve*
LT-1	84.9	87.7	88.6	0.96	0.99	98.5	22.4	26,375	S.Y.
LT-2	79.7	85.5	89.1	0.89	0.96	99.1	24.2	26,325	S.Y.
LT-3	76.9	83.6	87.7	0.88	0.95	98.3	21.9	25,089	S.Y.
LT-4	77.3	83.6	87.9	0.88	0.95	98.7	22.6	27,284	S.Y.
Ave. Value	79.7	85.1	88.3	0.90	0.96	98.7	22.8	26,268	N/A
Representative Curve	79.4	84.9	88.3	0.90	0.96	98.7	22.6	26,268	S.Y.

Table 3.7b

Tested Mechanical Properties of 80XF Sheet Steel
Transverse Tension

Test No.	$(F_{pr})_1$ (ksi)	$(F_{pr})_2$ (ksi)	F_y (ksi)	$\frac{(F_{pr})_1}{F_y}$	$\frac{(F_{pr})_2}{F_y}$	F_u (ksi)	Elongation in 2-in. Gage Length(percent)	Modulus of Elasticity (ksi)	Type of Stress-Strain Curve*
TT-1	88.1	92.2	93.6	0.94	0.99	100.8	19.3	31,091	S.Y.
TT-2	86.7	92.7	93.7	0.93	0.99	101.7	18.9	30,162	S.Y.
TT-3	85.1	92.1	94.1	0.90	0.98	101.6	18.3	30,899	S.Y.
TT-4	90.6	93.5	93.5	0.97	1.00	101.5	20.0	29,041	S.Y.
Ave. Value	87.6	92.6	93.7	0.94	0.99	101.4	19.1	30,298	N/A
Representative Curve	86.8	92.7	93.7	0.93	0.99	101.7	18.9	30,298	S.Y.

* S.Y. = Sharp Yielding

Table 3.7c

Tested Mechanical Properties of 80XF Sheet Steel
Longitudinal Compression

Test No.	$(F_{pr})_1$ (ksi)	$(F_{pr})_2$ (ksi)	F_y (ksi)	$\frac{(F_{pr})_1}{F_y}$	$\frac{(F_{pr})_2}{F_y}$	Modulus of Elasticity (ksi)	Type of Stress-Strain Curve*
LC-1	70.6	78.1	88.5	0.80	0.88	29,254	S.Y.
LC-2	64.2	75.2	89.8	0.71	0.84	29,761	S.Y.
LC-3	66.7	78.2	90.1	0.74	0.87	27,986	S.Y.
LC-4	67.9	76.8	89.0	0.76	0.86	28,917	S.Y.
Ave. Value	67.4	77.1	89.4	0.75	0.86	28,980	N/A
Representative Curve	67.4	77.0	89.4	0.75	0.86	28,980	S.Y.

Table 3.7d

Tested Mechanical Properties of 80XF Sheet Steel
Transverse Compression

Test No.	$(F_{pr})_1$ (ksi)	$(F_{pr})_2$ (ksi)	F_y (ksi)	$\frac{(F_{pr})_1}{F_y}$	$\frac{(F_{pr})_2}{F_y}$	Modulus of Elasticity (ksi)	Type of Stress-Strain Curve*
TC-1	74.1	86.4	94.6	0.78	0.91	33,942	S.Y.
TC-2	69.1	84.2	94.9	0.73	0.89	34,699	S.Y.
TC-3	73.4	86.5	93.8	0.78	0.92	33,077	S.Y.
TC-4	71.8	84.9	94.3	0.76	0.90	34,371	S.Y.
Ave. Value	72.1	85.5	94.4	0.76	0.91	34,022	N/A
Representative Curve	77.8	87.5	94.4	0.82	0.93	34,022	S.Y.

* S.Y. = Sharp Yielding

Table 3.8a

Tested Mechanical Properties of 100XF Sheet Steel
Longitudinal Tension

Test No.	$(F_{pr})_1$ (ksi)	$(F_{pr})_2$ (ksi)	F_y (ksi)	$\frac{(F_{pr})_1}{F_y}$	$\frac{(F_{pr})_2}{F_y}$	F_u (ksi)	Elongation in 2-in. Gage Length(percent)	Modulus of Elasticity (ksi)	Type of Stress-Strain Curve*
LT-1	92.3	101.5	113.5	0.81	0.89	113.5	8.3	30,984	S.Y.
LT-2	101.9	110.2	114.4	0.89	0.96	114.4	9.0	27,843	S.Y.
LT-3	96.0	103.9	113.6	0.85	0.91	113.6	7.4	30,143	S.Y.
LT-4	92.9	101.8	110.8	0.84	0.92	110.8	7.5	27,679	S.Y.
Ave. Value	95.8	104.4	113.1	0.85	0.92	113.1	8.1	29,163	N/A
Representative Curve	95.2	104.4	113.1	0.84	0.92	113.5	8.3	29,163	S.Y.

Table 3.8b

Tested Mechanical Properties of 100XF Sheet Steel
Transverse Tension

Test No.	$(F_{pr})_1$ (ksi)	$(F_{pr})_2$ (ksi)	F_y (ksi)	$\frac{(F_{pr})_1}{F_y}$	$\frac{(F_{pr})_2}{F_y}$	F_u (ksi)	Elongation in 2-in. Gage Length(percent)	Modulus of Elasticity (ksi)	Type of Stress-Strain Curve*
TT-1	105.8	115.5	123.2	0.86	0.94	123.2	4.8	32,145	S.Y.
TT-2	106.7	119.6	126.6	0.84	0.94	126.6	3.5	30,881	S.Y.
TT-3	107.1	116.2	126.3	0.85	0.92	126.3	4.2	32,028	S.Y.
TT-4	104.3	114.3	125.4	0.83	0.91	125.4	4.3	33,108	S.Y.
Ave. Value	106.0	116.4	125.4	0.85	0.93	125.4	4.2	32,040	N/A
Representative Curve	108.1	118.2	125.4	0.86	0.94	125.4	4.3	32,040	S.Y.

* S.Y. = Sharp Yielding

Table 3.8c

Tested Mechanical Properties of 100XF Sheet Steel
Longitudinal Compression

Test	$(F_{pr})_1$ (ksi)	$(F_{pr})_2$ (ksi)	F_y (ksi)	$\frac{(F_{pr})_1}{F_y}$	$\frac{(F_{pr})_2}{F_y}$	Modulus of Elasticity (ksi)	Type of Stress-Strain Curve*
LC-1	72.2	85.5	113.8	0.63	0.75	31,238	G.Y.
LC-2	73.0	85.9	112.3	0.65	0.76	30,318	G.Y.
LC-3	72.1	84.0	111.9	0.64	0.75	30,545	G.Y.
LC-4	70.8	83.8	113.5	0.62	0.74	30,319	G.Y.
Ave. Value	72.0	84.8	112.9	0.64	0.75	30,605	N/A
Representative Curve	74.1	84.5	113.3	0.65	0.75	30,605	G.Y.

Table 3.8d

Tested Mechanical Properties of 100XF Sheet Steel
Transverse Compression

Test No.	$(F_{pr})_1$ (ksi)	$(F_{pr})_2$ (ksi)	F_y (ksi)	$\frac{(F_{pr})_1}{F_y}$	$\frac{(F_{pr})_2}{F_y}$	Modulus of Elasticity (ksi)	Type of Stress-Strain Curve*
TC-1	109.9	118.2	130.6	0.84	0.91	32,450	G.Y.
TC-2	109.8	116.9	130.7	0.84	0.89	33,727	G.Y.
TC-3	115.8	121.0	128.0	0.90	0.95	32,296	G.Y.
TC-4	110.3	117.9	127.0	0.87	0.93	32,628	G.Y.
Ave. Value	111.5	118.5	129.1	0.86	0.92	33,025	N/A
Representative Curve	112.0	119.8	129.5	0.86	0.93	33,025	G.Y.

*G.Y. = Gradual Yielding

Table 3.9a

Tested Mechanical Properties of 140XF Sheet Steel
Longitudinal Tension

Test No.	$(F_{pr})_1$ (ksi)	$(F_{pr})_2$ (ksi)	F_y (ksi)	$\frac{(F_{pr})_1}{F_y}$	$\frac{(F_{pr})_2}{F_y}$	F_u (ksi)	Elongation in 2-in. Gage Length (percent	Modulus of Elasticity (ksi)	Type of Stress-Strain Curve*
LT-1	116.3	130.3	140.6	0.83	0.93	140.6	5.1	30,597	S.Y.
LT-2	123.5	132.7	140.2	0.88	0.94	140.2	4.4	30,007	S.Y.
LT-3	114.7	138.1	141.6	0.94	0.97	141.6	3.8	29,452	S.Y.
LT-4	124.2	134.7	142.5	0.87	0.94	142.5	3.9	30,472	S.Y.
Ave. Value	119.7	133.9	141.2	0.88	0.94	141.2	4.3	30,132	N/A
Representative Curve	122.1	133.3	141.2	0.86	0.94	140.2	4.4	30,132	S.Y.

Table 3.9b

Tested Mechanical Properties of 140XF Sheet Steel
Transverse Tension

Test No.	$(F_{pr})_1$ (ksi)	$(F_{pr})_2$ (ksi)	F_y (ksi)	$\frac{(F_{pr})_1}{F_y}$	$\frac{(F_{pr})_2}{F_y}$	F_u (ksi)	Elongation in 2-in. Gage Length (percent)	Modulus of Elasticity (ksi)	Type of Stress-Strain Curve*
TT-1	144.9	153.4	156.4	0.93	0.98	156.4	1.5	31,885	S.Y.
TT-2	140.9	151.8	157.5	0.89	0.96	157.5	1.5	32,286	S.Y.
TT-3	143.2	151.3	155.5	0.92	0.97	155.5	1.5	32,694	S.Y.
TT-4	143.6	153.8	158.3	0.91	0.97	158.3	1.6	33,473	S.Y.
Ave. Value	143.2	152.6	156.9	0.91	0.97	156.9	1.5	32,584	N/A
Representative Curve	150.8	155.8	156.9	0.96	0.99	157.5	1.5	32,584	S.Y.

* S.Y. = Sharp Yielding

Table 3.9c

Tested Mechanical Properties of 140XF Sheet Steel
Longitudinal Compression

Test No.	$(F_{pr})_1$ (ksi)	$(F_{pr})_2$ (ksi)	F_y (ksi)	$\frac{(F_{pr})_1}{F_y}$	$\frac{(F_{pr})_2}{F_y}$	Modulus of Elasticity (ksi)	Type of Stress-Strain Curve*
LC-1	100.5	113.0	139.7	0.72	0.81	29,844	G.Y.
LC-2	105.8	115.6	139.9	0.76	0.83	32,028	G.Y.
LC-3	108.2	117.4	136.2	0.79	0.86	30,490	G.Y.
LC-4	108.3	119.8	141.6	0.76	0.85	29,978	G.Y.
Ave. Value	105.7	116.5	139.4	0.76	0.84	30,585	N/A
Representative Curve	106.2	116.7	139.8	0.76	0.83	30,585	G.Y.

Table 3.9d

Tested Mechanical Properties of 140XF Sheet Steel
Transverse Compression

Test No.	$(F_{pr})_1$ (ksi)	$(F_{pr})_2$ (ksi)	F_y (ksi)	$\frac{(F_{pr})_1}{F_y}$	$\frac{(F_{pr})_2}{F_y}$	Modulus of Elasticity (ksi)	Type of Stress-Strain Curve*
TC-1	139.9	152.5	162.6	0.86	0.94	35,093	G.Y.
TC-2	147.2	156.7	162.3	0.91	0.97	34,697	G.Y.
TC-3	141.4	153.6	163.8	0.86	0.94	34,083	G.Y.
TC-4	146.8	156.2	164.3	0.89	0.95	34,619	G.Y.
Ave. Value	143.8	154.8	163.3	0.88	0.95	34,623	N/A
Representative Curve	141.5	152.8	163.1	0.87	0.94	34,623	G.Y.

*G.Y. = Gradual Yielding

Table 3.10

Summary of the Tested Mechanical Properties of Six Different Sheet Steels Based on Tables 3.4 Through 3.9[48]

Type of Sheet Steel	Type of Stress*	Ave. F_{pr}** (ksi)	Ave. F_y (ksi)	Ave. F_u (ksi)	F_{pr}/F_y	F_u/F_y	Elongation in 2-in Gage Length (percent)	Modulus of Elasticity (ksi)
80 SK (cold-rolled)	LT	64.4	82.2	88.8	0.78	1.08	12.7	27,131
	TT	66.5	87.1	92.1	0.76	1.06	7.3	30,188
	LC	53.0	75.4	--	0.70	--	--	28,981
	TC	63.8	89.7	--	0.71	--	--	31,010
80DF (hot-rolled)	LT	45.4	55.8	88.8	0.81	1.59	31.4	27,973
	TT	46.1	57.4	88.9	0.80	1.55	28.1	28,532
	LC	43.4	57.9	--	0.75	--	--	32,374
	TC	50.2	61.5	--	0.82	--	--	30,326
80DK (cold-rolled)	LT	46.0	58.2	87.6	0.79	1.51	25.7	25,731
	TT	41.4	52.0	83.8	0.80	1.61	25.8	27,450
	LC	45.9	54.1	--	0.85	--	--	30,302
	TC	49.1	58.0	--	0.85	--	--	31,361
80XF (hot-rolled)	LT	85.1	88.3	98.7	0.96	1.12	22.8	26,268
	TT	92.6	93.7	101.4	0.99	1.08	19.1	30,298
	LC	77.1	89.4	--	0.86	--	--	28,980
	TC	85.5	94.4	--	0.91	--	--	34,022

Table 3.10 (continued)

Summary of the Tested Mechanical Properties of Six Different Sheet Steels Based on Tables 3.4 Through 3.9[48]

Type of Sheet Steel	Type of Stress*	Ave. F_{pr}** (ksi)	Ave. F_y (ksi)	Ave. F_u (ksi)	F_{pr}/F_y	F_u/F_y	Elongation in 2-in. Gage Length (percent)	Modulus of Elasticity (ksi)
100XF (cold-rolled)	LT	104.4	113.1	113.1	0.92	1.00	8.1	29,163
	TT	116.4	125.4	125.4	0.93	1.00	4.2	32,040
	LC	84.8	112.9	--	0.75	--	--	30,605
	TC	118.5	129.1	--	0.92	--	--	33,025
140XF (cold-rolled)	LT	133.9	141.2	141.2	0.94	1.00	4.3	30,132
	TT	152.6	156.9	156.9	0.97	1.00	1.5	32,584
	LC	116.5	139.4	--	0.84	--	--	30,585
	TC	154.8	163.3	--	0.95	--	--	34,623

* LT = Longitudinal tension, TT = Transverse tension, LC = Longitudinal compression
TC = Transverse compression

** Based on the 0.01 percent offset method

stress-strain data typically ran from approximately 10 ksi to the point where the stress-strain curve became nonlinear. The reason for starting at 10 ksi (as opposed to zero) was to minimize the effects of any slippage that might have occured at the start of the tests.

Inspection of Tables 3.4 through 3.9 shows that the modulus of elasticity for the tested sheet steels vary as shown below:

Longitudinal tension:	24,227 - 30,989 ksi
Transverse tension:	25,129 - 33,473 ksi
Longitudinal compression:	27,481 - 33,627 ksi
Transverse compression:	28,611 - 35,093 ksi

Since the elastic modulus values were lower than expected, particularly for the 80SK, 80DK, and 80XF longitudinal tension tests, some concern over the accuracy of the extensometer used in these tests was expressed. In order to verify the accuracy of the extensometer, strain gages were attached to a few of the tension specimens and the tests were run with both the extensometer and strain gage simultaneously measuring the strain. The stress-strain curve determined in this manner for the 80DF longitudinal tension test is shown in Figure 3.36[48]. The solid line represents the stess-strain curve for the strain gage while the dotted line is for the extensometer. As can be seen from Figure 3.36, the stress-strain curves are practically identical. Thus it was decided that the extensometer used in the tension tests was providing sufficiently accurate results.

b. Proportional Limit, F_{pr}. The proportional limit is usually defined as the point along the stress-strain curve where the relationship between stress and strain becomes nonlinear. Since it is

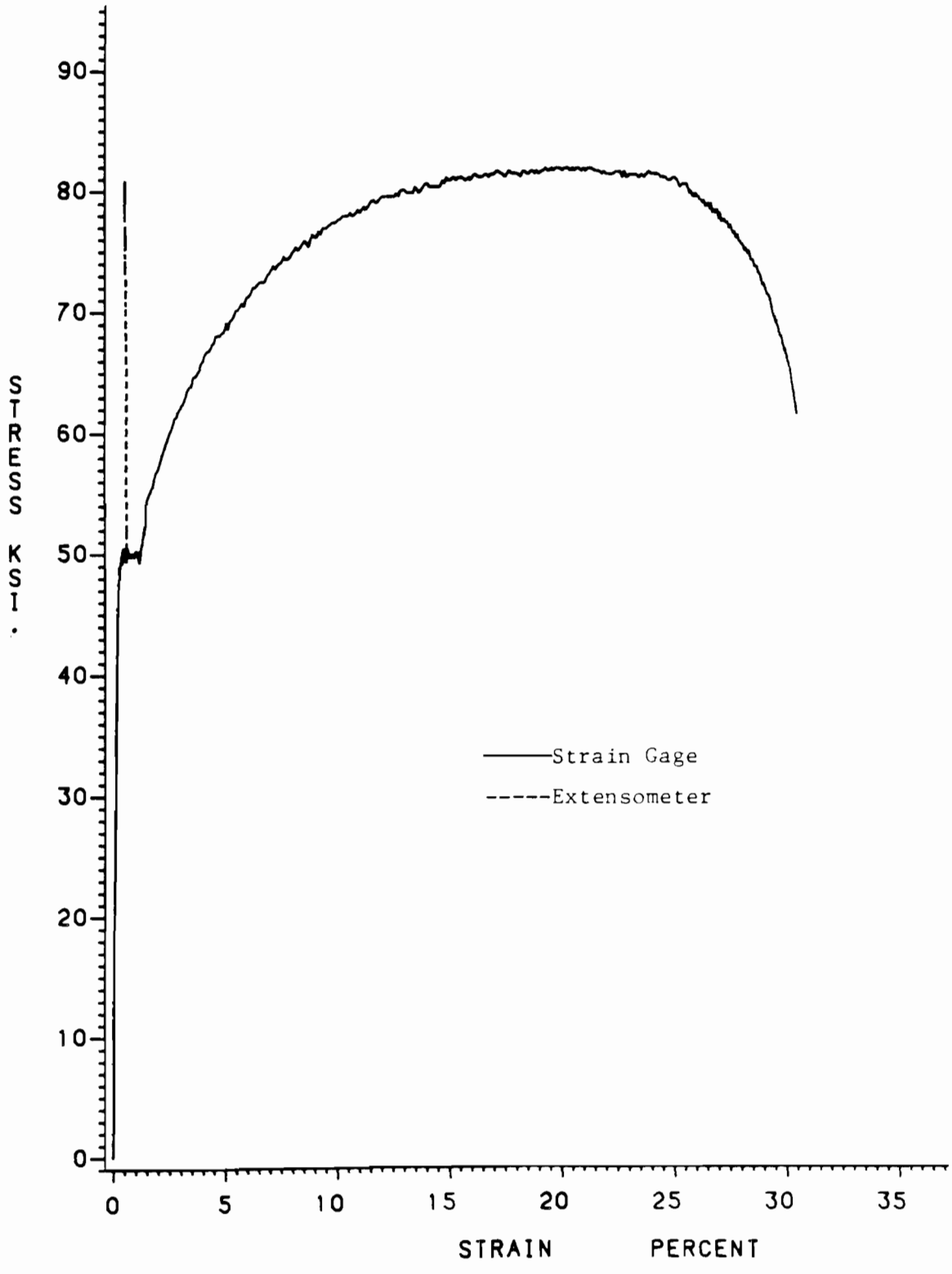

Fig. 3.36 Comparison of Stress-Strain Curves for 80DF-LT Using Strain Gage and Extensometer

often difficult to pinpoint the exact location of the true proportional limit, standard methods are normally used so that comparable values of proportional limit may be determined by different researchers. One such method that is commonly used for aircraft structures[57] and also for cold-formed stainless steel members[58,59] is the 0.01 percent offset method. For this method a straight line with a slope equal to the modulus of elasticity is drawn parallel to the stress-strain curve and offset such that it intersects the strain axis at 0.01 percent strain. The intersection of this line with the stress-strain curve is defined as the proportional limit.

In this study, the proportional limit was determined by two methods[48]. The first proportional limit, $(F_{pr})_1$, was determined by plotting a straight line with a slope equal to the modulus of elasticity directly on top of the stress-strain curve as shown by Curve A in Figure 3.37. The point where the stress-strain curve appeared to depart from curve A was taken as $(F_{pr})_1$. The second value of the proportional limit, $(F_{pr})_2$, was determined by the 0.01 percent offset method which was just discussed. The 0.01 percent offset method gives the value of the proportional limit as the intersection of the stress-strain curve and the straight line B as shown in Figure 3.37.

Inspection of Tables 3.4 through 3.9 shows that the $(F_{pr})_1/F_y$ ratios range from 0.55 to 0.99 while the $(F_{pr})_2/F_y$ ratios range from 0.69 to 1.00. As shown in these tables, the two methods for determining the proportional limit do not necessarily give comparable results.

c. Yield Strength or Yield Point, F_y. The method commonly used to determine the yield point of high strength sheet steels depends on

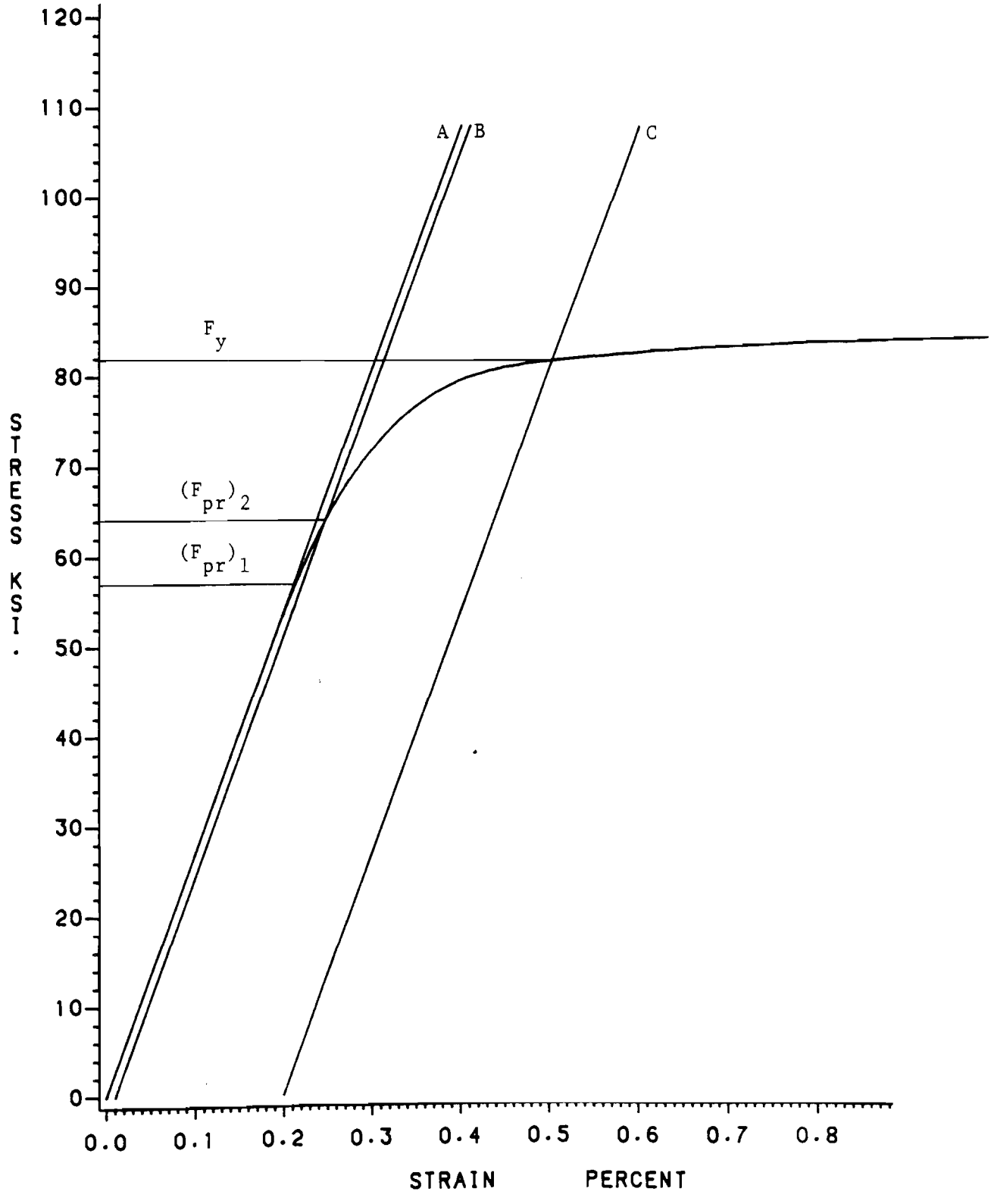

Fig. 3.37 Stress-Strain Curve for Determination of Mechanical Properties of 80SK-LT

whether the stress-strain curve is of the gradual or sharp yielding type. Each type has been previously defined in Section II.A of the literature review. As a general rule, the cold rolled sheet steels are gradual yielding while the hot rolled sheet steels tend to be sharp yielding. The type of stress-strain curve of each individual test is given in the far right column of Tables 3.4 through 3.9. In this study, the terms yield strength and yield point are synonomous.

For the gradual yielding steels, such as the 80SK-LT stress-strain curve shown in Figure 3.37, the yield point is defined by the intersection of a straight line (curve C, Figure 3.37), drawn parallel to the elastic portion of the stress-strain curve at an offset of 0.2 percent, and the stress-strain curve.

The yield point of the sharp yielding steels is defined as the stress where the stress-strain curve becomes horizontal. A typical sharp yielding stress-strain curve is shown in Figure 3.23(b). The upper yield point of the sharp yielding steels was neglected in all cases.

The range of yield points for the six different sheet steels may be obtained from Tables 3.4 through 3.9 as follows:

Longitudinal tension:	54.8 - 142.5 ksi
Transverse tension:	49.2 - 158.3 ksi
Longitudinal compression:	53.1 - 141.6 ksi
Transverse compression:	56.7 - 164.3 ksi

d. Ultimate Tensile Strength, F_u. The ultimate tensile strength was determined from each of the tension tests as the maximum stress that the given sheet steel could withstand before fracture. Since the compression tests were only performed to 1.5 percent strain, it was impossible to determine the ultimate strength in compression.

The range of ultimate tensile strengths, as taken from Tables 3.4 through 3.9, are as follows:

Longitudinal tension: 87.5 - 142.5 ksi

Transverse tension: 80.9 - 158.3 ksi

e. Ductility. Ductility is a very important property of high strength sheet steels since, without adequate ductility, it is impossible to cold-form the sheet steel into the desired structural shape. Ample ductility is also necessary for structural considerations where the plastic strength of bending members is taken into account.

In this study, ductility is measured by two methods. The first method expresses ductility as the ratio of F_u / F_y. Based on Table 3.10 the range of the average F_u/F_y ratios is as follows:

Longitudinal tension: 1.00 - 1.51

Transverse tension: 1.00 - 1.61

The other method usually employed to measure ductility is given by the total elongation in a 2-in. gage length. For this method, the maximum strain recorded by the computer before fracture was taken as the ductility. The maximum elongation was also verified by placing the fractured ends of the specimen together and measuring the distance between the gage marks. The range of percent elongation taken from Tables 3.4 through 3.9 is as follows:

Longitudinal tension: 3.8 - 33.3 percent

Transverse tension: 1.5 - 28.8 percent

It was impossible to determine the ductility in compression since these tests were only carried to 1.5 percent.

IV. DISCUSSION

Included in Section IV.A is a general review of the results presented in Section III.D. Particular emphasis is placed on the anisotropic nature of high strength sheet steels. Section IV.B presents a brief discussion of the cold work effects on the strength properties of sheet steels. In Sections IV.C and IV.D the information gained through the literature review on strain rate and fatigue is applied to the 80XF longitudinal test data.

A. EVALUATION OF RESULTS

1. Stress-Strain Curves. It was stated earlier that, as a general rule, hot rolled sheet steels tended to produce sharp yielding stress-strain curves while cold rolled sheet steels produced gradual yielding stress-strain curves. Looking at Table 3.10, this "general rule" seems to apply rather well to the 80 ksi yield strength steels (especially for the tension tests). However, the 100XF and 140XF steels exhibit sharp yielding behavior in tension even though they are cold rolled. Thus, it is apparent that the type of stress-strain curve depends not only on the rolling procedure but also other factors such as the processing technique used to develop the sheet steel and the sheet steel's chemical composition.

Also, it is worth noting that for all the tested sheet steels, except the 80XF steel, the compression stress-strain curve was gradual yielding even if the corresponding tension stress-strain curve was sharp yielding.

2. Mechanical Properties. Practically every mechanical property determined in this study was significantly affected by the anisotropy that was found to be typical of high strength sheet steels. Table 4.1 illustrates the anisotropic nature of these sheet steels by presenting the ratios of the tranverse to longitudinal mechanical properties for each type of test (compression or tension) and each steel. In Table 4.2, the effect of the type of test on the mechanical properties of the sheet steels is given by the ratio of the compression-to-tension mechanical properties of each steel for a given test direction. Each material property presented in Tables 4.1 and 4.2 is discussed in some detail in the following sections.

a. Modulus of Elasticity, E. Table 4.1 shows that the modulus of elasticity in the transverse direction is greater than the corresponding value in the longitudinal direction for each sheet steel tested except for the compression tests of 80DF sheet steel where, for some unknown reason, just the opposite seems to be true. At first it was thought that perhaps the two directions could have been incorrectly marked on the specimens. However, Table 4.1 shows that the yield strengths obtained from the transverse tests of the 80DF sheet steels are higher than the longitudinal tests which tends to disregard that assumption.

No conclusions can be drawn from Table 4.1 regarding whether or not the E values are more sensitive to test direction in tension or compression since the transverse-to-longitudinal E values are largest in compression for the 80XF and 140XF steels while the tension ratios are largest for the 80SK, 80DF, 80DK, and 100XF sheet steels.

Table 4.1

Ratios of Transverse to Longitudinal Mechanical Properties
For Analysis of Anisotropic Behavior of the Six Sheet Steels
Based on Table 3.10

Type of Sheet Steel	Type of Stress*	Ave. F_{pr}** (ksi)	Ave. F_y (ksi)	Ave. F_u (ksi)	F_{pr}/F_y	F_u/F_y	Elongation in 2-in. Gage Length (percent)	Modulus of Elasticity (ksi)
80SK	T	1.03	1.06	1.04	0.97	0.98	0.57	1.11
(cold-rolled)	C	1.20	1.19	--	1.01	--	--	1.07
80DF	T	1.02	1.03	1.00	0.99	0.97	0.89	1.02
(hot-rolled)	C	1.16	1.06	--	1.09	--	--	0.94
80DK	T	0.90	0.89	0.96	1.01	1.07	1.00	1.07
(cold-rolled)	C	1.07	1.07	--	1.00	--	--	1.03
80XF	T	1.09	1.06	1.03	1.03	0.96	0.84	1.15
(hot-rolled)	C	1.11	1.06	--	1.06	--	--	1.17
100XF	T	1.11	1.10	1.11	1.01	1.00	0.52	1.10
(cold-rolled)	C	1.40	1.14	--	1.23	--	--	1.08
140XF	T	1.14	1.11	1.11	1.03	1.00	0.35	1.08
(cold-rolled)	C	1.33	1.17	--	1.13	--	--	1.13

* T = Tension, C = Compression

** Based on 0.01 percent offset method

Table 4.2

Ratios of Compression to Tension Mechanical Properties
Based on Table 3.10

Type of Sheet Steel	Testing Direction*	Ave. F_{pr}** (ksi)	Ave. F_y (ksi)	F_{pr}/F_y	Modulus of Elasticity (ksi)
80SK (cold-rolled)	L	0.82	0.92	0.90	1.07
	TR	0.96	1.03	0.93	1.03
80DF (hot-rolled)	L	0.96	1.04	0.93	1.16
	TR	1.09	1.07	1.03	1.06
80DK (cold-rolled)	L	1.00	0.93	1.08	1.18
	TR	1.19	1.12	1.06	1.03
80XF (hot-rolled)	L	0.91	1.01	0.90	1.10
	TR	0.92	1.01	0.92	1.12
100XF (cold-rolled)	L	0.81	1.00	0.82	1.05
	TR	1.02	1.03	0.99	1.03
140XF (cold-rolled)	L	0.87	0.99	0.89	1.02
	TR	1.01	1.04	0.98	1.06

* L = Longitudinal TR = Transverse
** Based on 0.01 percent offset method

The ratio of transverse-to-longitudinal E values presented in Table 4.1 are as follows:

Tension tests: 1.02 - 1.15

Compression tests: 0.94 - 1.17

Table 4.2 illustrates the effect of the type of test (compression or tension) on the average modulus of elasticity values. It can be seen from Table 4.2 that the E values are greater in compression than tension for each type of sheet steel tested. No obvious trend as to whether or not one testing direction was any more sensitive to the test type than another was observed. The range of compression-to-tension E values shown in Table 4.2 are as follows:

Longitudinal tests: 1.02 - 1.18

Transverse tests: 1.03 - 1.12

b. Proportional Limit, F_{pr}. From the ratios of the transverse-to-longitudinal average proportional limits shown in Table 4.1, it can be seen that, for every material except the tension tests of 80DK sheet steel, the transverse-to-longitudinal F_{pr} ratio is greater in compression than tension for each material. The range of transverse-to-longitudinal F_{pr} is as follows:

Tension tests: 0.90 -1.14

Compression tests: 1.07 -1.40

Table 4.2 shows that the F_{pr} determined in the longitudinal direction was either equal to or greater in tension than compression for every material. However, for four out of the six sheet steels, the transverse F_{pr} was greater in compression than tension. The range of the compression-to-tension proportional limits is shown below:

Longitudinal tests: 0.82 - 1.00

Transverse tests: 0.92 - 1.19

c. Yield Strength or Yield Point, F_y. The yield strength is greater in the transverse direction than the longitudinal direction in every steel except the tension tests of 80DK sheet steels where, for some unknown reason, the longitudinal F_y values in compression are consistently equal to or greater than the tension values. These observations are based on the information presented in Table 4.1. The range of transverse-to-longitudinal average F_y values are as follows:

Tension tests: 0.89 - 1.11

Compression tests: 1.06 - 1.19

From Table 4.2 it can be seen that the longitudinal F_y values seem to be relatively independent of the type of test since the compression-to-tension F_y ratios are all fairly close to 1.0 for the longitudinal direction. The transverse compression tests produced higher F_y ratios than the longitudinal compression tests for a given steel. Also, it can be seen that for each steel the compression-to-tension ratio is greater in the transverse direction than the longitudinal direction which seems to indicate that the transverse F_y is more sensitive to the type of test than the longitudinal F_y. The range of compression-to-tension average F_y values are as follows:

Longitudinal tests: 0.92 - 1.04

Transverse tests: 1.01 - 1.12

d. Ultimate Tensile Strength, F_u. The average F_u values for the 80 ksi yield strength steels seem to be relatively insensitive to the test direction. However, the 100XF and 140XF sheet steels exhibited

transverse F_u values in their respective longitudinal directions. The range of the transverse-to-longitudinal F_u values shown in Table 4.1 are as follows:

Tension tests: 0.96 -1.11

Compression tests: not applicable

Since the compression tests were not performed to failure of the specimen, no comparison of F_u is possible in Table 4.2.

e. Ductility. Table 4.1 shows that the F_u/F_y ratio is practically independent of the tested direction since it only ranges from 0.97 to 1.07. However, the total elongation in a 2-in. gage length of each material except the 80DK sheet steel was significantly affected by the test direction. The range of transverse-to-longitudinal average elongations are as follows:

Tension tests: 0.57 - 1.00

Compression tests: not applicable

Again, since the compression tests were not carried to failure it is impossible to compare the F_u/F_y ratios and elongations in Table 4.2.

It is interesting to note that, as shown in Table 3.10, the two most ductile steels of the six sheet steels tested are the 80DF and 80DK sheet steels. This should come as no surprise since back in the material designation descriptions presented in Section III.A.1 the "dual phase" sheet steels (denoted by the "D" in their material designation) were said to exhibit better formability than the XF steels. Also, the second letter in their material designation represents the deoxidation practice. The "K" represents steel that has been killed

while the "F" represents steel that has been killed in addition to sulfide inclusion control which is added specifically to improve formability. Thus the 80DF steel should be more ductile than the 80DK steel. The results shown in Table 3.10 show that the 80DF steel is indeed slightly more ductile than the 80DK steel. Therefore the 80DF and 80DK sheet steels performed exactly as predicted by their material designations.

3. Summary. From the information presented in Tables 4.1 and 4.2 and in the descriptions in Sections IV.A.2.a through IV.A.2.e, it can be seen that high strength sheet steels are quite anisotropic. Table 4.1 shows that, with a few minor exceptions, the strength properties such as F_{pr}, F_y, F_u, and E are greater in the transverse than in the longitudinal direction while the elongation, as might be expected, was lowest in the transverse direction.

Table 4.2 shows that, without exception, the modulus of elasticity values are greater in compression than in tension regardless of the test direction. The proportional limit and yield strength values showed mixed responses to the test type.

B. EFFECT OF COLD-FORMING ON THE MECHANICAL PROPERTIES OF SHEET STEELS

Once the sheet steel is cold-formed into the desired structural shape the strength of the resulting cross-section varies depending on the location in the cross-section with the highest strength material occurring in the formed corners. However, this strength increase is

normally accompanied by a loss of ductility. According to Karen[1], the three phenomena responsible for the change in mechanical properties caused by cold-forming are strain hardening, strain aging, and the Bauschinger Effect. These three phenomena were originally described in Section II.A of the literature review. The effects of strain hardening and strain aging on a typical stress-strain curve may be seen in Figure 2.3[4].

The following sections discuss the applicability of the information gained in the literature review to the results obtained in this study.

1. Strain Hardening. The effect of strain hardening on the strength of a cold-formed cross-section is illustrated in Figure 4.1[50] for a typical hot-rolled semi-killed section. Since the average strength of the formed cross-section is obviously greater than the virgin material, it is desirable to take advantage of this increase in strength. The 1980 Edition of the AISI Specification[49] for buildings suggests that an average yield strength, F_{ya}, can be computed for compact cold-formed cross-sections based on the following equation[49]:

$$F_{ya} = CF_{yc} + (1-C)F_{yf} \qquad (4.1)$$

where:

C = ratio of the total corner area to the total cross-sectional area of the full section

$F_{yc} = B_c F_y/(R/t)^m$ = yield strength of the corner material, ksi

F_{yf} = weighted average tensile portions of the flat portions established in accordance with Section 6.4.2 of the Specification or virgin yield point if tests are not made

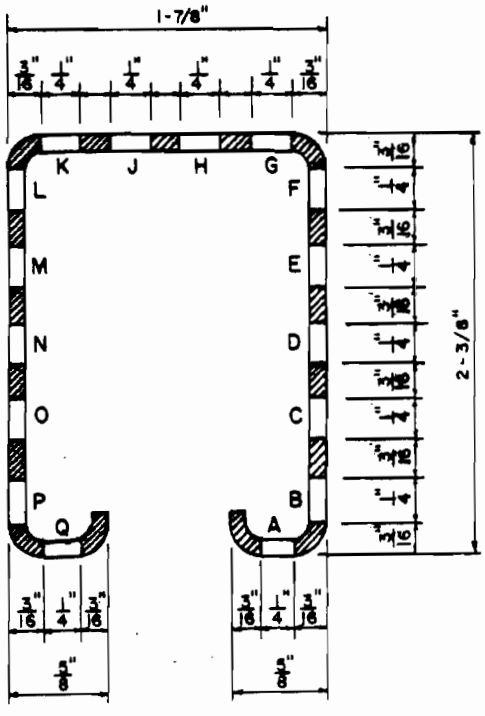

(a) Location of Test Specimens

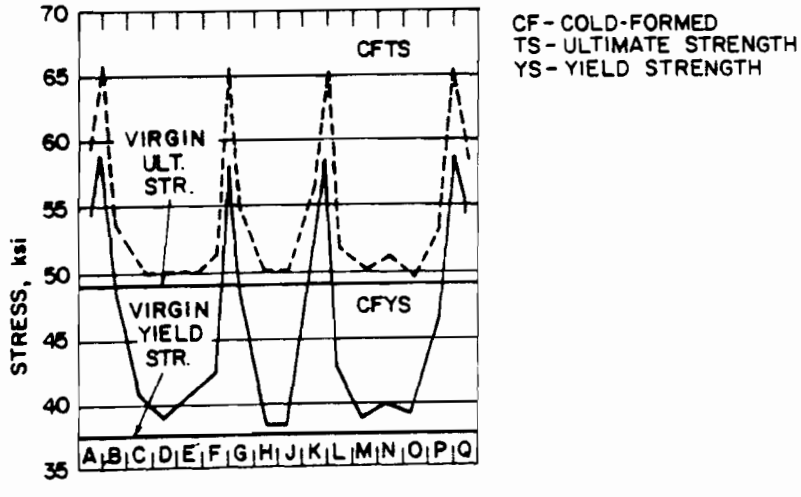

(b) Effect of Cold-Forming at Various Locations in Cross-Section

Fig. 4.1 Tensile Stress-Strain Characteristics of Roll-Formed Hot-Rolled Semi-Killed Section[50]

$$B_c = 3.69(F_u/F_y) - 0.819(F_u/F_y)^2 - 1.79$$

$$m = 0.192(F_u/F_y) - 0.068$$

R = inside bend radius, in.

t = thickness, in.

Equation 4.1 does not apply where F_u/F_y is less than 1.2, R/t exceeds 7, and/or maximum included angle exceeds 120°.

The amount of yield strength increase caused by strain hardening can be seen from Equation 4.1 to be a function of R/t and F_u/F_y. Inspection of the average test results presented in Table 3.10 shows that only the dual phase steels (80DF and 80DK) with F_u/F_y ratios from 1.51 to 1.61 possess the potential for significant strength increase upon cold working. Also, as can be seen in Figure 4.2, the dual phase steels exhibit relatively small plateaus in their stress-strain curves after yielding; therefore, once these materials have yielded, very little additional strain is required to produce appreciable increases in stress. It is because of the small plateau region and their high F_u/F_y ratios that the dual phase sheet steels may be classified at a higher yield strength than that determined by standard methods. For example, the average longitudinal tension yield strength for the 80DF sheet steel was determined to be only 55.8 ksi even though this material is classified as an 80 ksi yield strength sheet steel. The relatively large spread between the yield point, F_y, and the ultimate tensile strength, F_u, may be seen in Figure 4.2[48] for the original stress-strain curves of the 80DF sheet steel tested in longitudinal tension.

2. Strain Aging. Although specific design criteria for predicting the strength increase caused by strain aging are not available, it is

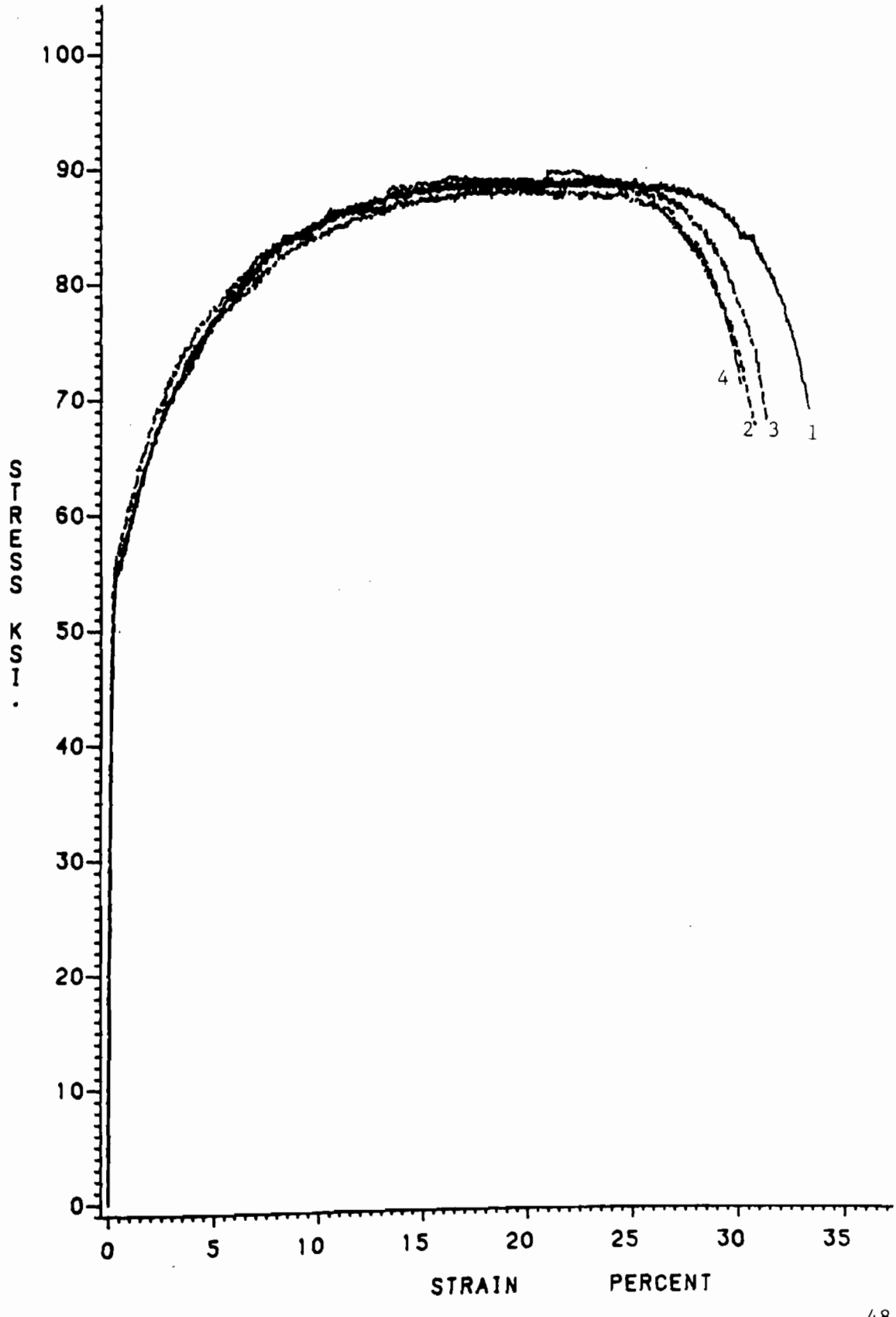

Fig. 4.2 Individual Stress-Strain Curve for 80DF-LT[48]

believed that the general effects of strain aging would be to further increase the yield strength over the cross-section with the proportionate increase between points on the cross-section much the same as caused by strain hardening. The time required for strain aging may be decreased from several days to a matter of hours if the formed materials are subjected to aging temperatures in the 300°F range[19].

3. Bauschinger Effect. Table 4.2 shows that the cold rolled 80 ksi yield strength sheet steels did exhibit Bauschinger Effects as shown by the longitudinal compression-to-tension yield point ratios of less than 1.0. Also, for these steels the transverse compression-to-tension yield point ratios are greater than 1.0 which is as predicted by the Inverse Bauschinger Effect. However, the cold rolled 100 and 140 ksi yield strength sheet steels, as shown in Table 4.2, were practically unaffected by the Bauschinger Effects.

C. EFFECT OF STRAIN RATE ON 80XF SHEET STEEL

Originally a brief experimental investigation into the effects of strain rate on the stress-strain relationship was planned for a couple of the sheet steels that were previously tested statically. However, the testing equipment used for the static tests was found to be incapable of providing an adequate range of strain rates to establish any reliable relationships between strain rate and stress flow. Consequently, the strain rate effects on the 80XF-LT sheet steel will be estimated in this section using the empirical results determined by Chatfield and Rote[10] and the original stress-strain data determined as described in Section III.D.1.

As reported in the literature review (Section II.B), for a given strain, ε, and temperature, the true stress flow, σ, for two different strain rates, $\dot{\varepsilon}$, may be related by a strain rate sensitivity exponent, m, as

$$\sigma_1 = \sigma_2(\dot{\varepsilon}_1/\dot{\varepsilon}_2)^m . \tag{4.2}$$

Also, Equation 2.8 relates the true stress, σ, to the engineering stress, f, at a given strain, ε, as

$$\sigma = f(1 + \varepsilon). \tag{4.3}$$

Although the literature review expresses Equation 4.2 in terms of true stress, it is believed that Equation 4.3 could be used to express Equation 4.2 in terms of engineering stress as follows:

$$\frac{\sigma_1}{\sigma_2} = \frac{f_1(1 + \varepsilon)}{f_2(1 + \varepsilon)} = \frac{f_1}{f_2} = (\dot{\varepsilon}_1/\dot{\varepsilon}_2)^m \tag{4.4}$$

The term $(1 + \varepsilon)$ cancels since σ_1 and σ_2 are defined as true stresses at the same strain. Equation 4.4 can then be directly used to show the strain rate effect on the engineering stress.

In the study published by Chatfield and Rote[10] they reported values of 0.018 and 0.020 for two hot rolled, low alloy sheet steels with yield points of 80 ksi. These values were presented earlier in Table 2.1. Since the 80XF sheet steel chosen for testing in this study is also a hot rolled, low alloy steel, it was assumed that the m values for the 80XF steel would be approximately 0.02. The accuracy of this assumption could only be verified by testing.

Figure 4.3 shows the stress-strain curves resulting from application of Equation 4.4 to the original stress-strain data for the

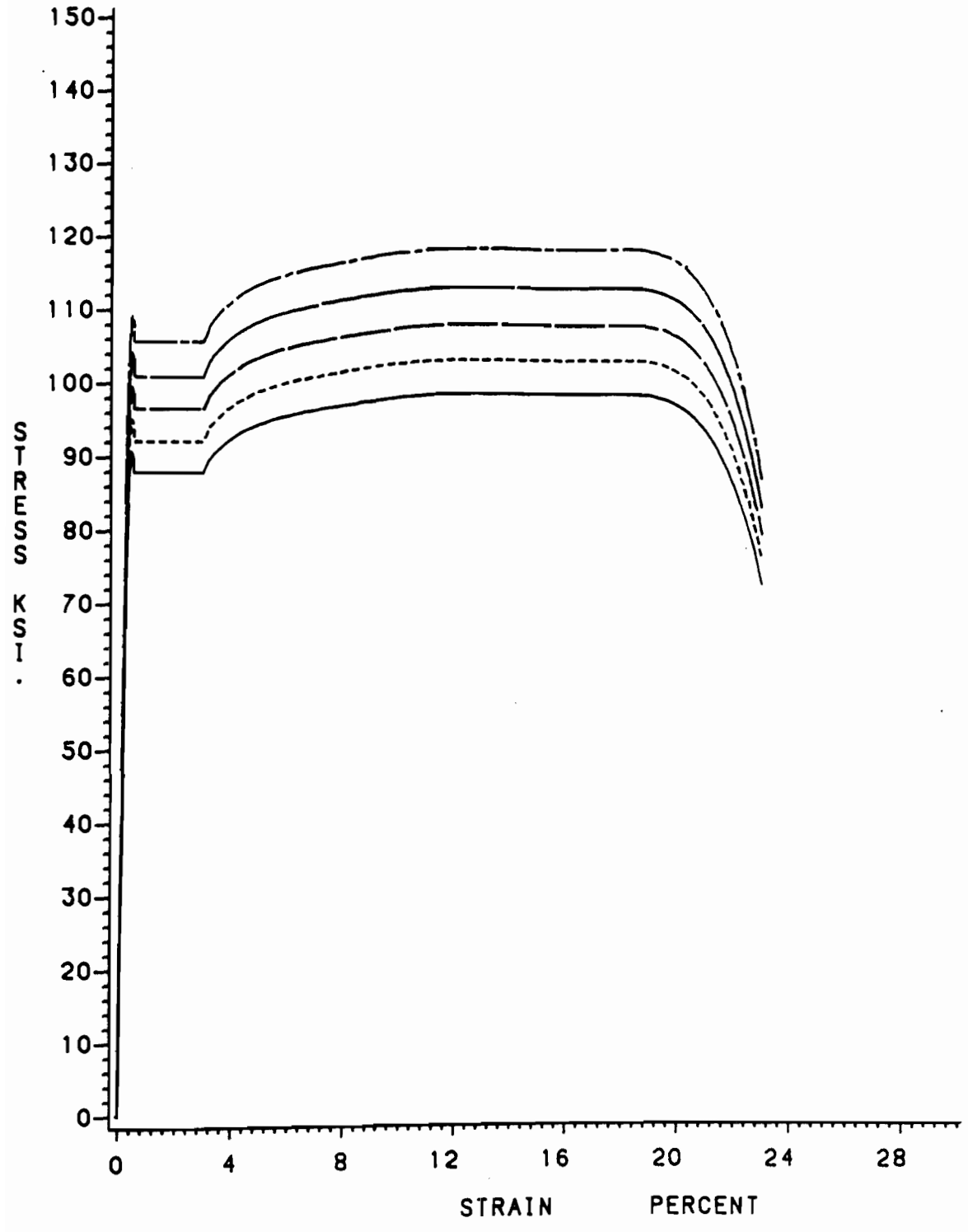

Strain Rate Ratios (New Strain Rate/Original Strain Rate)

1 = ——— 10 = ------- 100 = — — 1000 = ——— 10000 = —·—

Fig. 4.3 Strain Rate Effects on Stress-Strain Curve for 80XF-LT

representative 80XF longitudinal tension tests. The base values of f_1 and $\dot{\varepsilon}_1$ are those stresses obtained as described in Section III.A.1. The $\dot{\varepsilon}_1$ value is roughly 0.03 in./in./min.up until the yield point and 0.3 in./in./min. from the yield point to fracture. The fact that the strain rates change during the course of the tests does not affect Equation 4.4 since, in effect, each stress is increased by a common factor. For example, if the effect of increasing the strain rate by a factor of 10 over the original strain rate is desired, then the effective initial strain rate is 0.3 in./in./min. while the second strain rate is 3.0 in./in./min.

The strain rate effect on the 80XF yield stress can be seen in Table 4.3. Again these values are based on the assumption that m = 0.02.

Table 4.3
Strain Rate Effect on Yield Stress of 80XF
Tested in Longitudinal Tension

Initial Strain Rate (in./in./min.)	$(\dot{\varepsilon}_1/\dot{\varepsilon}_2)^m$	Yield Stress (ksi)
0.03	1.0	88.3
0.3	1.047	92.5
3.0	1.096	96.8
30.0	1.148	101.4
300.0	1.202	106.1

The curves shown in Figure 4.3 and the yield stresses presented in Table 4.3 are given only to show the general effects of strain rate and should not, in any way, be taken as exact vaules.

It is interesting to note that Equation 4.4 produces a uniform increase in stress throughout the stress-strain curve while Reference 13 (in Figure 2.7) showed that, for structural steel, the yield stress was more sensitive to strain rate than the ultimate strength.

D. ESTIMATED FATIGUE STRENGTH OF 80SK SHEET STEEL

The purpose of this section is to estimate the fatigue life characteristics of the 80XF sheet steel tested in longitudinal tension. The selection of the 80XF material was purely random. There is nothing special or unique about the 80XF sheet steel that makes the fatigue life prediction any more or less accurate than for any other type of sheet steel.

The following fatigue life prediction is based on the strain-life approach as discussed previously in Section II.C.3.b. Equation 2.33 presented the basic relationship between the total strain amplitude, $\Delta\varepsilon'/2$ or ε'_a, and the number of reversals to failure, $2N_f$. For convenience, Equation 2.33 is repeated below.

$$\varepsilon'_a = \Delta\varepsilon'/2 = \sigma'_f(2N_f)^b + \varepsilon''_f(2N_f)^c$$

The coefficients and exponents of Equation 2.33 may be determined according to the following procedure which is based on information presented in the Fatigue Design Handbook[21].

The fatigue strength coefficient, σ_f, may be approximated as

$$\sigma'_f \approx F_u + 50 \text{ ksi} = 98.7 + 50 + 148.7 \text{ ksi} \qquad (4.5)$$

for steels with a Brinell hardness less than 500 Bhn. The 80XF sheet steel is assumed to meet this requirement.

The fatigue ductility coefficient, ε_f'', may be approximated by the true fracture ductility, ε_f', as

$$\varepsilon_f'' \simeq \varepsilon_f' = \ln(100/(100-\%RA)). \tag{4.6a}$$

The percent reduction in area (%RA) is based on the average reduced area at fracture, A_f, of the four individual longitudinal tension tests for the 80XF sheet steel.

$$\%RA = ((A_o - A_f)/A_o)*100 =$$

$$((0.04118-0.0178)/0.04118)*100 = 57\% \tag{4.6b}$$

$$\text{thus } \varepsilon_f'' = \ln(100/(100-57)) = 0.84 \tag{4.6c}$$

Deiter[19] notes that "the determination of the reduction of area in thin sheets is difficult, and for this reason it is not measured in this type of specimen." However, since Equation 2.33 is used just to give the designer a rough estimate of the fatigue strength of a given steel and since the measured values of A_o and A_f were practically identical for all the 80XF-LT specimens, it is believed that the %RA can be measured accurately enough for this purpose.

The fatigue strength exponent, b, may be approximated as

$$b \simeq -(1/6)\log(2\sigma_f'/F_u). \tag{4.7}$$

The true fracture strength, σ_f', is determined by converting the representative stress-strain data for the 80XF-LT sheet steel from engineering to true stress using Equation 2.8 and then picking the maximum true stress from the resulting data. For the 80XF-LT material

$$\sigma_f' = 116.947 \text{ ksi};$$

$$\text{therefore, } b \simeq -(1/6)\log(2(116.947)/98.7) = -0.062. \tag{4.8}$$

According to Reference 21, a representative value of the fatigue ductility exponent, c, may be taken as -0.60.

Substituting the values of σ_f', b, ε_f'', and c and assuming E = 29,500 ksi, Equation 2.33 gives

$$\varepsilon_a' = 148.7(2N_f)^{-0.062}/29{,}500 + (0.84)(2N_f)^{-0.60} ,$$

ε_a' is plotted versus $2N_f$ in Figure 4.4.

It is important to keep in mind that fatigue life predictions based on Figure 4.4 will be, at best, rough estimates. If accurate life predictions are required, it is highly recommended that fatigue testing be performed on the material in question.

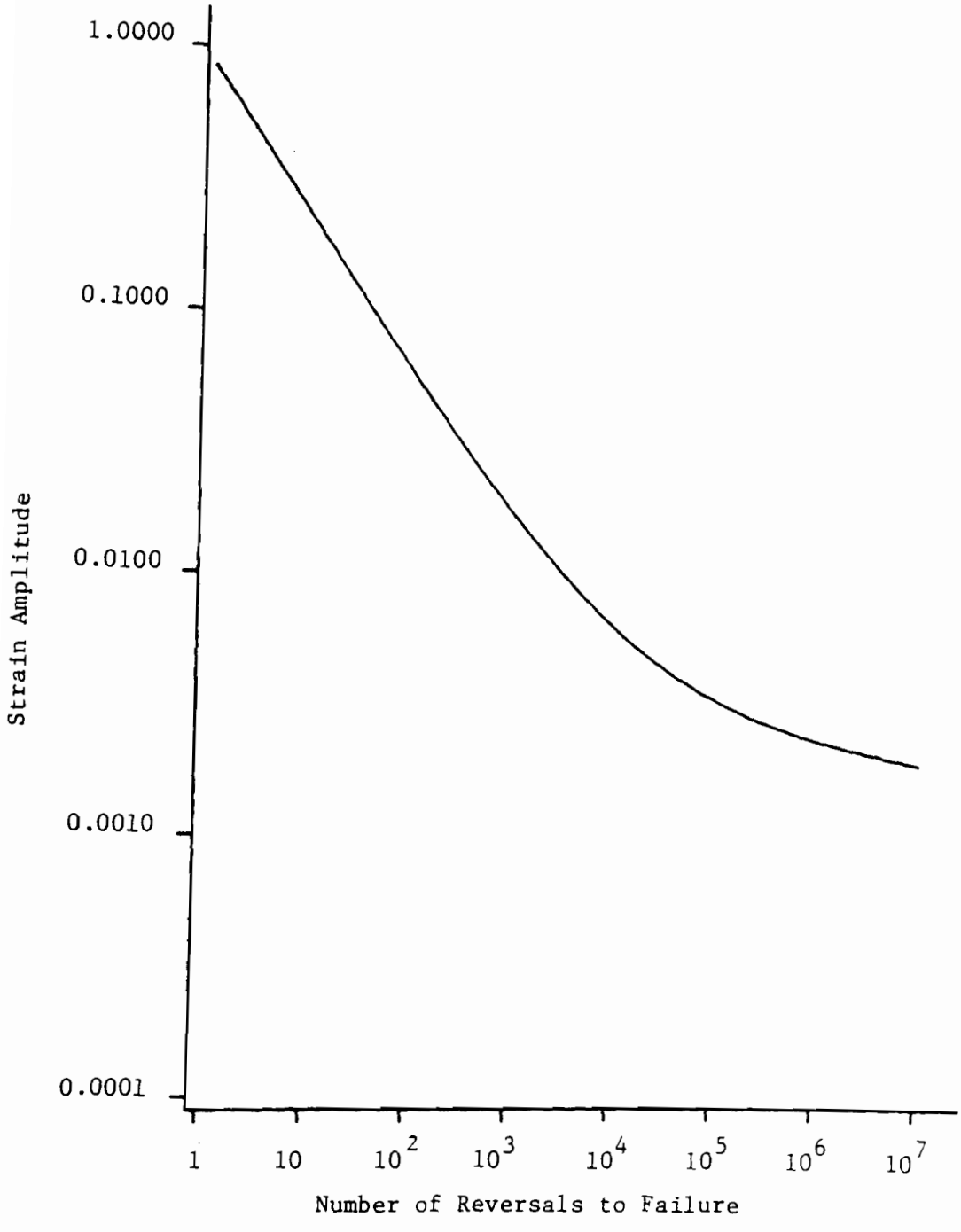

Fig. 4.4 Estimated Fatigue Life at 80XF-LT for Fully Reversed Loading

V. CONCLUSIONS

With the increasing demand for safer and more fuel efficient automobiles the automotive engineer is being forced to consider design alternatives. One such alternative is the substitution of the relatively new high strength sheet steels for traditional materials of low to moderate strength in automotive structural components. In many cases this substitution can provide substantial weight savings at competitive costs with no loss in total strength or performance. However, since the high strength sheet steels have only been available for a few years, there is a limited amount of published information on their structural analysis and design[3]. Consequently, a three phase research project began in early 1982 at the University of Missouri-Rolla under the sponsorship of the American Iron and Steel Institute. The primary goals of this project are to establish the applicability of existing design criteria[3] and develop the necessary new criteria to produce a comprehensive design specification for high strength sheet steels used in the automobile industry. This thesis dealt with the mechanical properties of high strength sheet steels to be used for automotive structural components. The experimental portion of this thesis was based mainly on the information obtained from Phase I of the three phase UMR research project. Also included in this thesis was a review of the literature on the determination of the various mechanical properties as well as on the effects of strain rate and fatigue on the design of high strength sheet steels.

The literature review of the classical methods required to obtain both engineering and true stress-strain curves and also the mechanical properties was discussed in Section II.A. In Section II.B, the strain rate effects on the mechanical properties of high strength sheet steels were reviewed. As a general rule, increasing strain rates were found to increase the yield point and ultimate tensile strength while decreasing the ductility. The modulus of elasticity is unaffected by strain rate.

Section II.C presented a brief history of the fatigue analysis and design procedures along with the current fatigue design methods used by the automobile industry. It was found that the two basic approaches currently used to predict fatigue behavior are the stress-life and strain-life approaches. Although both methods are presently used by the automobile industry it is generally believed that the strain-life method will eventually dominate because it can describe more accurately the actual cyclic stress-strain behavior. However, a recent comparison[25] of the strain-life predictions of fatigue life to actual fatigue lives showed ratios of predicted-to-actual fatigue lives as high as 160 for some sheet steels used in the automobile industry. Thus it is obvious that there is still much room for improvement in the prediction of fatigue failure.

The experimental program used to determine the typical stress-strain curves and material properties of the six high strength sheet steels was described in Section III. The mechanical properties of each of the 96 tests were presented in Tables 3.4 through 3.9. Table 3.10 summarizes the average mechanical properties of each type of sheet steel. Also typical stress-strain curves were illustrated in Section III.C.

From the evaluation of the results presented in Section IV, it was found that high strength sheet steels are quite anisotropic as shown in Table 4.1. The strength properties of proportional limit, yield strength, ultimate tensile strength, and modulus of elasticity were higher in the transverse direction than the longitudinal direction for practically all the tested sheet steels. As might be expected, the transverse ductility was generally lower than the longitudinal ductility. These sheet steels were also found to be slightly sensitive to the Bauschinger Effects as shown in Table 4.2. This Table also shows that the modulus of elasticity values were greater in compression than tension for each of the tested sheet steels.

The representative mechanical properties and stress-strain curves determined in this study will be utilized in future phases of this research project for the analysis of automotive structural components using these sheet steels as well as the development of design criteria for the automobile industry.

BIBLIOGRAPHY

1. American Iron and Steel Institute, "The Materials Decision," SG-834.

2. American Iron and Steel Institute, "Automotive Steels: They Still Do It Better," SG-937.

3. American Iron and Steel Institute, "Guide for Preliminary Design of Sheet Steel Automotive Structural Components," 1981 Edition.

4. Yu, W. W., Cold-Formed Steel Structures. New York: McGraw-Hill Book Company, Inc., (1973), 36-52.

5. Hosford, W.F. and Caddel, R.M., Metal Forming- Mechanics and Metallurgy . Englewood Cliffs, N.J.: Prentice Hall, Inc., 1983, 80-84.

6. Timoshenko, S., Strength of Material-Part II. Princeton, N.J.: D. Van Nostrand Company, Inc., (1956), 400-428.

7. Malvern, L.E., Introduction to the Mechanics of a Continuous Medium. Englewood Cliffs, N.J.: Prentice Hall, Inc. (1969) 327-333.

8. Juvinall, R.C., Stress, Strain and Strength. New York: McGraw-Hill Book Company, (1967), 96-100.

9. American Iron and Steel Institute," Cost-Effective Weight Reduction with Sheet Steel," SG-631 R.

10. Chatfield, D.A. and Rote, R.R., "Strain Rate Effects on the Properties of High Strength, Low Alloy Steels," Paper 740177, SAE Automotive Engineering Congress, Detroit, February 1974.

11. Manjoine, M.J., "Influence of Strain and Temperature on Yield Stresses of Mild Steel," Journal of Applied Mechanics, ASME Transactions, 66 (1944), A-211-218.

12. Nadai, A., Theory of Flow and Fracture of Solids. Volume I, 2nd ed., New York: McGraw-Hill Book Company, Inc., 1950, p.24.

13. Norris, C.H., Hansen, R.J., Holley, M.J. Jr., Biggs, J.M., Namyet, S., and Minami, J.K., Structural Design for Dynamic Loads. New York: McGraw-Hill Book Company, Inc., 1959, 3-12.

14. Campbell, J.D., "Dynamic Plasticity: Macroscopic and Microscopic Aspects," Materials Science and Engineering, XII (1973), 3-21.

15. Green, S.J., Langan, J.J., Leasia, J.D., and Young, W.H., "Material Properies, Including Strain Rate Effects, as Related to Sheet Metal Forming," Matallurgical Transactions, II (1971), 1813-1820.

16. Leslie, W.C., Sober, R.J., Babcock, S.G., and Green, S.J., "Plastic Flow in Binary Substitutional Alloys of BCC Iron-Effects of Strain Rate, Temperature and Alloy Content". Transaction of ASM, LXII, (1969), 690-710.

17. Harding, J., "Effects of High Strain Rate on the Room Temperature Strength and Ductility of Fine Alloy Steels," Journal of Iron and Steel Institute, CCX, (1972), 435-432.

18. Atkins, A.G., "Consequences of High Strain Rates in Cold Working," Journal of Institute of Metals, XCVII (1969), 289-298.

19. Dieter, G.E., Mechanical Metallurgy. New York: McGraw-Hill Book Company, (1961), 237-295.

20. American Iron and Steel Institute, "Sheet Steel Properties and Fatigue Design."

21. Fatigue Design Handbook. Graham, J.A., ed., Society of Automotive Engineers, IV, 1968.

22. Neville, R.J., "Corrosion and Its Prevention in the Automobile," Report on AISI Project No. 1201-409, DOFASCO, Hamilton, Ontario, Canada, October, 1977.

23. Hiam, J.R., and Pietrowski, R., "The Influence of Forming and Corrosion on the Fatigue Behavior of Automotive Steels," SAE Paper No. 780040, 1978.

24. Lorai, E.A., and Bush, G.W., "Fatigue Properties of Galvanic Steel and Hot Rolled Steel Before and After Exposure to Salt Spray," SAE Paper No. 740034, 1974.

25. Barsom, J.M., Klippstein, K.H., and Shoemaker, A.K., "Fatigue Behavior of Sheet Steels for Automotive Applications," Washington D.C.: American Iron and Steel Institute, SG-80-2, (February 1980).

26. Libertini, G.Z., Topper, T.H., and Leis, B.N., "The Effect of Large Prestrains on Fatigue," Experimental Mechanics, February, 1977.

27. Aichbhaumik, D., "Steel Variability Effects on Low Cycle Fatigue Behavior of a Single Grade of High Strength Low Alloy Steel," Metallurgical Transactions A, X(A), March, 1979, 269-278.

28. Holt, J.M. and Stewart, B.K., "Variatiability of Strain-Controlled Fatigue Properties of USS Dual Phase 80," SAE Paper No. 801400, 1980.

29. Pietrowski, R. "The Effect of Forming on the Fatugue Properties of Dofascoloys 50F, 50W, and 50Z," Dominion Foundries and Steel, Limited, Hamilton, Ontario, November, 1977.

30. Krause, A.R., Landgraf, R.W., and Crandall, B.T., "Fatigue Properties of Cold-Rolled Sheet steels," SAE Paper No. 790461, 1979.

31. Sherman, A.M., "Fatigue Properties of High Strength-Low Alloy Steels," Metallurgical Transactions A, VI(A), May 1975.

32. Nueber, H., "Theory of Stress Concentration for Stress-Strain Prismatical Bodies with Arbitriary Nonlinear Stress-Strain Law," Journal of Applied Mechanics, Trans. ASME, XXVIII,(December,1961), 544-550.

33. Peterson, R.E., Stress Concentration Design Factors. New York: John Wiley & Sons, Inc., 1953.

34. Peterson, R.E., "Analytical Approach of Stress Concentration Effect in Fatigue of Aircraft Material," Proceedings of Symposium on Fatigue of Aircraft Structures, WADC Technical Report 59-507, (August, 1959),273-299.

35. Topper, T.H., Wetzel, R.M., and Morrow, J., Journal of Materials, JMCSA, (March, 1969), 200-209.

36. Bhat, S.P., "Notch Fatigue Strengths of Several High-Strength Low-Alloy Sheet Steels," SAE Paper No. 830174.

37. Dowling, N.E., Rose, W.R. and Wilson, W.K., "Notched Member Fatigue Life Predictions by the Local Strain Approach," Fatigue Under Complex Loading, ed. R.M. Wetzel, Warrandale, PA: Society of Automotive Engineers, Inc., 1977, 55-84.

38. Tsai, P.J., "Design Analysis for Stress and Fatigue," Modern Automotive Structural Analysis, ed. M.M. Kamal and J.A. Wolf, Jr., New York: Van Nostrand Reinhold Company, 1982, 280-315.

39. Miner, M.A., "Cummulative Damage in Fatigue," Journal of Applied Mechanics, XII, 1942.

40. Weibull, W., Fatigue Testing and Analysis of Results. New York: Pergammon Press, 1961.

41. American Society of Testing and Materials, A Tentative Guide for Fatigue Testing and the Statistical Analysis of Fatigue Data, Philadelphia, Pa: ASTM Special Technical Publication No. 91-A, 1958, 16-21.

42. Marin, J., Mechanical Properties of Material and Design. New York: McGraw-Hill Book Company, Inc., (1942), 116-150.

43. Rolfe, S.T. and Barsom, J.M., Fracture and Fatigue Control in Structures-Application of Fracture Mechanics. Englewood Cliffs, N.J.: Prentice-Hall Inc., 1977.

44. Coffin, T.F., Jr., Fatigue of High Temperatures. ASTM STP 520, American Society of Testing and Materials, 1973, 5-34.

45. Morrow, J. and Millan, J.F. (eds.), "Influence of Residual Stress on Fatigue of Steel," SAE J783, Handbook Supplement TR-198, New York: SAE, July, 1961.

46. Klippstein, K.H., "Fatigue of Fabricated Steel-Sheet Details," SAE Paper No. 810436, 1981.

47. American Iron and Steel Institute, "High Strength Sheet Steel Source Guide," SG-603D.

48. Yu, W.W., Santaputra, C. and Parks, M.B., "Design of Automobile Structural Components Using High Strength Sheet Steels," Civil Engineering Study 83-1, University of Missouri-Rolla, Rolla, MO, 1983.

49. American Iron and Steel Institute, "Specification for the Design of Cold-Formed Steel Members," 1980 Edition.

50. American Iron and Steel Institute, "Commentary on the September 3, 1980 Edition of the Specification for the Design of Cold-Formed Steel Structural Members," Report SG 81-1, 1983.

51. American Iron and Steel Institute, "Specification for the Design of Light Gage Steel Structural Members," 1946 Edition.

52. American Iron and Steel Institute, "Specification for the Design of Cold-Formed Steel Sructural Members," 1974.

53. American Iron and Steel Institute, "Specification for the Design of Cold-Formed Stainless Steel Structural Members," 1974 Edition.

54. American Iron and Steel Institute, "Specification for the Design of Light Gage Cold-Formed Stainless Steel Structural Members," 1968 Edition.

55. Helwig, J.T., Council, K.,A., ed., SAS User's Guide, SAS Institute Inc., 1979, 237-244.

56. Venkataramaih, K.R., Roorda, J. and Srinivasaih, K.R., "Elastic Modulus of Cold-Formed Sheet Steel," Proceedings of the Fifth International Speciality Conference on Cold-Formed Steel Structures, University of Missouri-Rolla, November 18-19,1980.

57. Niles, A.S., and Newell, J.S., Airplane Structures, New York: John Wiley and Sons, Inc., Fourth Edition, 1954.

58. Johnson, A.L., "The Structural Performance of Austentic Stainless Steel Members," Department of Structural Engineering Report No. 327, Cornell University, November 1966.

59. Wang, S.J., "Cold-Rolled Austentic Stainless Steel Material Properties and Structural Performance," Department of Structural Engineering Report No. 334, Cornell University, July 1969.

APPENDIX

CLASSIFICATION AND CALIBRATION OF THE EXTENSOMETER AND COMPRESSOMETER

This section presents a summary of the calibration procedures along with the information necessary to classify both the Tinius Olsen No. 90828 extensometer and the Saytec PC-5M compressometer.

These strain measuring devices were calibrated by applying known amounts of strain with a Tinius Olsen Linear Motion Calibrator Model CAL-60 No. 128890-2 and recording the corresponding voltage values for each strain level. A straight line was then fitted to the resulting strain-voltage points. The slope of this line is the strain calibration factor with units of strain divided by voltage. Therefore, the strain may be obtained for a given load as the voltage multiplied by the strain calibration factor.

In order to classify these strain measuring devices, Table A.1 and A.2 present the apparent or measured strain obtained from these devices along with the actual strain (labeled as "Strain") from the calibrator at several strain values. The difference between the "apparent" and actual strain is given in these tables in the "Error" column.

The ASTM E83 Specification lists the following classification requirements for extensometers:

Class	Maximum Error of Indicated Strain
A	0.00001
B-1	0.0001
B-2	0.0002
C	0.001
D	0.01
E	0.1

From Table A.1, it can be seen that the recorded errors for the extensometer lie between the Class B-1 and B-2 classifications with the exception of one point where the error is 0.000201313.

The maximum error of the compressometer was -0.00011430 as shown in Table A.2. Therefore, the compressometer is also between the B-1 and B-2 classifications although it is considerably more accurate than the extensometer.

Table A.1 Classification of Tinius Olsen No. 90828 Extensometer

Obs	Strain	Volts	Apparent	Error
1	0.00000	4.5950	0.000000000	0.000000000
2	0.00005	4.5950	0.000000000	-0.000050000
3	0.00010	4.5925	0.000087527	-0.000012473
4	0.00015	4.5900	0.000175055	0.000025055
5	0.00020	4.5900	0.000175055	-0.000024945
6	0.00025	4.5875	0.000262582	0.000012582
7	0.00030	4.5855	0.000332604	0.000032604
8	0.00035	4.5850	0.000350109	0.000000109
9	0.00040	4.5840	0.000385120	-0.000014880
10	0.00045	4.5820	0.000455142	0.000005142
11	0.00050	4.5800	0.000525164	0.000025164
12	0.00055	4.5780	0.000595186	0.000045186
13	0.00060	4.5750	0.000700219	0.000100219
14	0.00065	4.5750	0.000700219	0.000050219
15	0.00070	4.5750	0.000700219	0.000000219
16	0.00075	4.5750	0.000700219	-0.000049781
17	0.00080	4.5710	0.000840263	0.000040263
18	0.00085	4.5700	0.000875274	0.000025274
19	0.00090	4.5700	0.000875274	-0.000024726
20	0.00095	4.5675	0.000962801	0.000012801
21	0.00100	4.5650	0.00105033	0.000050328
22	0.00105	4.5650	0.00105033	0.000000328

Table A.1 (Cont.) Classification of
Tinius Olsen No. 90828 Extensometer

Obs	Strain	Volts	Apparent	Error
23	0.00110	4.5613	0.00117987	0.000079869
24	0.00115	4.5600	0.00122538	0.000075383
25	0.00120	4.5600	0.00122538	0.000025383
26	0.00125	4.5580	0.00129540	0.000045405
27	0.00130	4.5550	0.00140044	0.000100438
28	0.00135	4.5550	0.00140044	0.000050438
29	0.00140	4.5535	0.00145295	0.000052954
30	0.00145	4.5505	0.00155799	0.000107987
31	0.00150	4.5500	0.00157549	0.000075492
32	0.00155	4.5490	0.00161050	0.000060503
33	0.00160	4.5450	0.00175055	0.000150547
34	0.00165	4.5450	0.00175055	0.000100547
35	0.00170	4.5440	0.00178556	0.000085558
36	0.00175	4.5415	0.00187309	0.000123085
37	0.00180	4.5400	0.00192560	0.000125602
38	0.00185	4.5395	0.00194311	0.000093107
39	0.00190	4.5365	0.00204814	0.000148140
40	0.00195	4.5355	0.00208315	0.000133151
41	0.00200	4.5350	0.00210066	0.000100656
42	0.00205	4.5350	0.00210066	0.000050656
43	0.00210	4.5340	0.00213567	0.000035667
44	0.00215	4.5300	0.00227571	0.000125711
45	0.00220	4.5300	0.00227571	0.000075711
46	0.00225	4.5280	0.00234573	0.000095733
47	0.00230	4.5250	0.00245077	0.000150766
48	0.00235	4.5250	0.00245077	0.000100766
49	0.00240	4.5245	0.00246827	0.000068271
50	0.00245	4.5215	0.00257330	0.000123304
51	0.00250	4.5200	0.00262582	0.000125821
52	0.00255	4.5190	0.00266083	0.000110832
53	0.00260	4.5160	0.00276586	0.000165864
54	0.00265	4.5150	0.00280088	0.000150875
55	0.00270	4.5150	0.00280088	0.000100875
56	0.00275	4.5135	0.00285339	0.000103392
57	0.00280	4.5100	0.00297593	0.000175930
58	0.00285	4.5100	0.00297593	0.000125930
59	0.00290	4.5100	0.00297593	0.000075930
60	0.00295	4.5065	0.00309847	0.000148468
61	0.00300	4.505	0.00315098	0.000150985
62	0.00325	4.498	0.00339606	0.000146061
63	0.00350	4.490	0.00367615	0.000176149
64	0.00375	4.485	0.00385120	0.000101203
65	0.00400	4.475	0.00420131	0.000201313
66	0.00450	4.464	0.00458643	0.000086433
67	0.00500	4.450	0.00507659	0.000076586

Table A.2 Classification of PC-5M Compressometer

Obs	Strain	Volts	Apparent	Error
1	0.00000	3.1750	0.000000000	0.000000000
2	0.00005	3.1750	0.000000000	-0.000050000
3	0.00010	3.1700	0.000070892	-0.000029108
4	0.00015	3.1690	0.000085071	-0.000064929
5	0.00020	3.1650	0.000141785	-0.000058215
6	0.00025	3.1600	0.000212677	-0.000037323
7	0.00030	3.1550	0.000283570	-0.000016430
8	0.00035	3.1540	0.000297748	-0.000052252
9	0.00040	3.1500	0.000354462	-0.000045538
10	0.00045	3.1450	0.000425355	-0.000024645
11	0.00050	3.1415	0.000474980	-0.000025020
12	0.00055	3.1400	0.000496247	-0.000053753
13	0.00060	3.1350	0.000567140	-0.000032860
14	0.00065	3.1345	0.000574229	-0.000075771
15	0.00070	3.1300	0.000638032	-0.000061968
16	0.00075	3.1250	0.000708925	-0.000041075
17	0.00080	3.1225	0.000744371	-0.000055629
18	0.00085	3.1200	0.000779817	-0.000070183
19	0.00090	3.1150	0.000850710	-0.000049290
20	0.00095	3.1105	0.000914513	-0.000035487
21	0.00100	3.1100	0.00092160	-0.000078398
22	0.00105	3.1050	0.00099249	-0.000057505
23	0.00110	3.1000	0.00106339	-0.000036613
24	0.00115	3.0960	0.00112010	-0.000029899
25	0.00120	3.0950	0.00113428	-0.000065720
26	0.00125	3.0900	0.00120517	-0.000044828
27	0.00130	3.0880	0.00123353	-0.000066471
28	0.00135	3.0850	0.00127606	-0.000073935
29	0.00140	3.0800	0.00134696	-0.000053043
30	0.00145	3.0760	0.00140367	-0.000046329
31	0.00150	3.0750	0.00141785	-0.000082150
32	0.00155	3.0700	0.00148874	-0.000061258
33	0.00160	3.0650	0.00155963	-0.000040365
34	0.00165	3.0625	0.00159508	-0.000054919
35	0.00170	3.0595	0.00163762	-0.000062383
36	0.00175	3.0565	0.00168015	-0.000069848
37	0.00180	3.0540	0.00171560	-0.000084402
38	0.00185	3.0500	0.00177231	-0.000077688
39	0.00190	3.0450	0.00184320	-0.000056795
40	0.00195	3.0425	0.00187865	-0.000071349
41	0.00200	3.0400	0.00191410	-0.00008590
42	0.00205	3.0350	0.00198499	-0.00006501
43	0.00210	3.0320	0.00202753	-0.00007247
44	0.00215	3.0300	0.00205588	-0.00009412
45	0.00220	3.0250	0.00212677	-0.00007323

Table A.2 (Cont.) Classification of PC-5M Compressometer

Obs	Strain	Volts	Apparent	Error
46	0.00225	3.0200	0.00219767	-0.00005233
47	0.00230	3.0155	0.00226147	-0.00003853
48	0.00235	3.0150	0.00226856	-0.00008144
49	0.00240	3.0110	0.00232527	-0.00007473
50	0.00245	3.0100	0.00233945	-0.00011055
51	0.00250	3.0050	0.00241034	-0.00008966
52	0.00255	3.0000	0.00248124	-0.00006876
53	0.00260	2.9955	0.00254504	-0.00005496
54	0.00265	2.9950	0.00255213	-0.00009787
55	0.00270	2.9900	0.00262302	-0.00007698
56	0.00275	2.9850	0.00269391	-0.00005609
57	0.00280	2.9825	0.00272936	-0.00007064
58	0.00285	2.9800	0.00276481	-0.00008519
59	0.00290	2.9750	0.00283570	-0.00006430
60	0.00295	2.9750	0.00283570	-0.00011430
61	0.00300	2.970	0.00290659	-0.00009341
62	0.00325	2.950	0.00319016	-0.00005984
63	0.00350	2.935	0.00340284	-0.00009716
64	0.00375	2.915	0.00368641	-0.00006359
65	0.00400	2.900	0.00389909	-0.00010091
66	0.00450	2.865	0.00439533	-0.00010467
67	0.00500	2.830	0.00489158	-0.00010842